



Kent Academic Repository

Serrano Sanchez, Angela (2022) *Understanding antimicrobial activity in live cells*. Master of Science by Research (MScRes) thesis, University of Kent,.

Downloaded from

<https://kar.kent.ac.uk/97707/> The University of Kent's Academic Repository KAR

The version of record is available from

<https://doi.org/10.22024/UniKent/01.02.97707>

This document version

UNSPECIFIED

DOI for this version

Licence for this version

UNSPECIFIED

Additional information

Versions of research works

Versions of Record

If this version is the version of record, it is the same as the published version available on the publisher's web site. Cite as the published version.

Author Accepted Manuscripts

If this document is identified as the Author Accepted Manuscript it is the version after peer review but before type setting, copy editing or publisher branding. Cite as Surname, Initial. (Year) 'Title of article'. To be published in *Title of Journal*, Volume and issue numbers [peer-reviewed accepted version]. Available at: DOI or URL (Accessed: date).

Enquiries

If you have questions about this document contact ResearchSupport@kent.ac.uk. Please include the URL of the record in KAR. If you believe that your, or a third party's rights have been compromised through this document please see our [Take Down policy](https://www.kent.ac.uk/guides/kar-the-kent-academic-repository#policies) (available from <https://www.kent.ac.uk/guides/kar-the-kent-academic-repository#policies>).



School of Biosciences

Understanding antimicrobial activity in live cells

The critical rise of antimicrobial resistance (AMR) requires the discovery of new antibiotics, particularly against Gram-negative bacteria. The permeability barrier of bacteria is a vital property to consider within the drug development process. In this work, we describe a new NMR method to assess membrane permeability and membrane interaction affinity of a new family of antimicrobial compounds exploiting the enhanced paramagnetic relaxation enhancement (PRE) effect induced by solvent paramagnetic agents in non-permeable drugs mixed with lipid vesicles. The results exhibited differences in the permeability rate and membrane interaction affinity of drugs among membranes with different lipid composition, confirming that our method is applicable to any type of cell/bacterial membrane. In addition, we have expanded this assay to live cells making use of a NMR-coupled bioreactor. With this setup, we have been able to measure NMR metabolomics to simultaneously monitor membrane permeation, membrane affinity and changes in the bacterial metabolism as a result of the addition of antimicrobial agents, providing evidence on their mechanism of action at the metabolite level. In general, our study introduces a new method for assessing drug permeability in lipid vesicles or live cells that will allow the design of more efficacious drugs and antimicrobial agents in a standard chemistry lab environment.

Ángela Serrano Sánchez

MScR - 2021/2022

146 pages

Declaration

No part of this thesis has been submitted in support of an application for any degree or other qualification of the University of Kent, or any other University or Institutions of learning.

Acknowledgements

I could not have undertaken this project without the support of the following people. I wish to express my first appreciation to my supervisor Dr. Jose Ortega Roldan for his continued patience and an endless supply of fascinating projects; I am grateful for this year working with him. Many thanks for offering his advice and encouragement with a perfect combination of insight and humour. I would like to thank my lab mates Encarni, Vicky, and Joe for their company every day and for making my research both productive and enjoyable. Also, Dr. Gary Thompson taught me the knowledge of NMR spectroscopy and gave me great feedback throughout this project. I am fortunate to have been part of this lab group. Special thanks to Lorena for her valuable guidance and help inside and outside the University.

Last but not least, I am extremely grateful to my friends in Canterbury, especially, Carla, Cristina, and Paula who kept me motivated and confident since my first day. Many thanks to my family, boyfriend, and friends for their unconditional and loving support from Spain whenever I needed them.

Table of Contents

Acknowledgements	2
List of Figures.....	7
List of Tables	13
1. Abstract	14
2. Introduction.....	15
2.1. Antimicrobial resistance and tolerance.....	15
2.1.1. Mechanisms of antibiotic resistance.....	16
2.1.2. Designing drugs for overcoming antimicrobial resistance.....	19
2.1.2.1. Composition of bacterial membrane.....	19
2.1.2.2. Di-anionic self-associating supramolecular amphiphiles as antimicrobial agents	21
2.2. Drug's membrane permeability	22
2.2.1. Drug transport mechanisms	23
2.3. An introduction to NMR spectroscopy	25
2.3.1. Small molecule drug discovery and role of NMR spectroscopy	27
2.3.2. Paramagnetic effect	28
2.3.3. CPMG pulse sequence.....	31
2.4. In-cell NMR.....	33
2.4.1. NMR-coupled bioreactor	35
2.5. NMR-based metabolomics	38
2.5.1. Metabolic investigation of live cells using NMR spectroscopy	38
2.5.2. NMR-based metabolomics for drug discovery.....	41
2.5.3. Analysing different metabolomics approaches.....	45

3. Aims	47
PART I: <i>IN VITRO</i> ASSAY ON MEMBRANE PERMEABILITY	
4. Methods.....	48
4.1. Bacteria and growth conditions	48
4.2. Preparation of Inner Membrane Vesicles	48
4.3. Preparation of stock solutions	49
4.4. NMR sample preparation	49
4.5. NMR acquisition	50
4.6. Lipid quantification	51
4.7. NMR Data Collection and Processing	51
4.8. Calculation of permeability and membrane interaction parameters	52
5. Results	53
5.1. Comparison of CPMG experiments at different PRE reagent concentrations.....	54
5.2. Variation of T1 and T2 relaxation times in controls.....	60
5.3. Quantification of permeability <i>in vitro</i>	66
5.4. Quantification of membrane interaction <i>in vitro</i>	68
5.5. Permeability and membrane interaction of SSA compounds in cancer membrane vesicles.....	70
6. Discussion	74
6.1. Measuring permeability, interaction and self-association of compounds.....	74
6.2. Relaxation modification for detection of ligand binding.....	76
PART II: <i>IN VIVO</i> ASSAY TO MONITOR DRUG INTERNALISATION.....	
7. Methods.....	78
7.1. Cultivation of <i>E. coli</i>	78

7.2.	Cultivation and encapsulation of <i>E. coli</i> cells in calcium alginate beads	78
7.3.	Viability assay of <i>E. coli</i> cells in calcium alginate beads	79
7.4.	Cytotoxic activity of PRE reagent effects.....	80
7.5.	Sample preparation for in-cell NMR	81
7.6.	Sample preparation for drug screening	81
7.7.	Setting up the perfusion system	82
7.8.	NMR acquisition.....	84
7.9.	Processing of targeted metabolic profile.....	85
7.10.	Analysis of metabolite concentration.....	85
8.	Results	86
8.1.	Measuring permeability and membrane interaction of SSA agents in live cells ...	86
8.2.	Cell viability of encapsulated cells	90
8.3.	Cytotoxic activity of PRE reagent effects.....	91
8.4.	NMR profile and metabolic alterations in standard conditions	93
8.5.	SSA60 induces broad metabolic perturbations in <i>E. coli</i>	98
9.	Discussion	107
9.1.	Evaluating SSAs permeation and membrane interaction in live cells	107
9.2.	Efficacy and viability of encapsulated cells in a bioreactor system	108
9.3.	Challenges on cell viability and metabolic effect evaluation using in-cell NMR	109
9.4.	Antimicrobial agents induce metabolic alterations in <i>E. coli</i>	112
9.5.	Prediction of mechanism of action using NMR metabolomics	113
10.	General discussion.....	116
11.	Future work and limitations.....	118
12.	Conclusions	120

13. References	121
14. Appendices	135
Appendix1. List of spectra of SSA agents in NMR conventional employing CPMG pulse sequence.....	135
Appendix2. Quantification of lipid composition of membrane vesicles from <i>E. coli</i>	142
Appendix3. Metabolomics analysis in control sample and sample including SSA60 at concentrations of 0.2 mM and 0.5 mM in in-cell NMR experiments.....	143

List of Figures

- Figure 1. Biological mechanisms of antibiotic resistance. (A) Antibiotic degradation chemically by enzymes. (B) Altered target. (C) Antibiotic efflux. (D) Receptor modification. 17
- Figure 2. Schematic representation of the different cell envelopes of Gram-positive and Gram-negative bacteria. 21
- Figure 3. Chemical structures of SSAs (TBA= tetrabutylammonium). 22
- Figure 4. Simplified layout of an NMR experiment. 26
- Figure 5. Schematic representation of the CPMG pulse sequence. 31
- Figure 6. Illustration of the CPMG experiment. Non-binding (blue) and binding (red) small molecules in the presence of lipid vesicles with their respective NMR signals. 32
- Figure 7. A) Schematic design of tube setup based on a sealed flow unit. B) Gel-encapsulated cells in porous matrix materials with growth media enable the continuous exchange of nutrients to sustain cellular viability and physiological energy metabolism. 37
- Figure 8. Schematic workflow for metabolomics investigations. 40
- Figure 9. Cellular processes targeted by conventional antibiotics. 43
- Figure 10. Schematic comparison between NMR permeation assays in presence or absence of a PRE agent. 55

Figure 11. A) Spectra of controls samples (indol and glucose) treated with different concentrations of manganese: 0 mM (orange); 0.5 mM (green); 2 mM (blue); 4 mM (magenta). B) Spectra of samples containing lipid vesicles and controls treated with different concentrations of manganese: 0 mM (orange); 0.5 mM (green); 2 mM (blue); 4 mM (magenta). C) Permeability rate of glucose (right) and indol (left) tested in lipid vesicles at the three different concentrations of Mn^{2+} and spin-lock times. 60

Figure 12. Variation of T1 in indol (A) and glucose (B) samples with their respective 1D 1H NMR spectra (A1 and B1 from vesicles in absence of Mn^{2+} , A2 and B2 from vesicles treated with Mn^{2+}). 63

Figure 13. Variation of T2 in indol (A) and glucose (B) samples with their respective 1D 1H NMR spectra (A1 and B1 from vesicles in absence of Mn^{2+} , A2 and B2 from vesicles treated with Mn^{2+}). 65

Figure 14. Schematic of cells encapsulation device. 79

Figure 15. NMR tube filled with encapsulated cells in alginate beads. 83

Figure 16. Stacked spectra showing the flow of 0.2 mM SSA48 + 0.5 mM Mn^{2+} at different points (0 min, 5 min, 15 min, 20 min and 30 min) after its injection in a sample containing cells encapsulated in beads. 87

Figure 17. Change in the formation of bacterial MTT formazan by reduction time. 91

Figure 18. Optical density measurements of bacteria at a wavelength of 600 nm for *E. coli* at different concentrations of Mn^{2+} . 92

Figure 19. 1D ^1H NMR spectrum of *E. coli* used for metabolite quantification. 94

Figure 20. Bar plots illustrating fold change (\log_2) in the relative concentration of individual metabolites and sub-pathways with respect to the $t = 0$ for *E. coli* at 5, 15, 30, 60 and 120. 97

Figure 21. Time course of the relative concentration of ATP at time 0 min obtained treating cells encapsulated in alginate beads with increasing concentrations of SSA60. 98

Figure 22. Bar plots illustrating fold change in the relative concentration of individual metabolites and sub-pathways with respect to the untreated sample for *E. coli* at 5, 15, 30, 60 and 120 min post antimicrobial SSA60 treatment at concentrations of 0.2 mM (green bar plots) and 0.5 mM (orange bar plots). 104

Figure 23. Hierarchical clustering of the metabolic profiling data at 0, 5, 15, 30, 60 and 120 min in controls and after SSA60 treatment at concentrations of 0.2 mM and 0.5 mM. 106

Figure 24. Comparison between the experimental set up of the CEC bioreactor (A) (Sharaf et al. 2010) and NMR-coupled bioreactor (B) used in this study. 110

Figure 25. Increasing concentrations of manganese from left to right (0 mM, 0.5 mM, and 4 mM) at different CPMG spin-lock times: 20 mS (orange), 50 ms (green) and 150 ms (purple). 135

Figure 26. Increasing concentrations of manganese from left to right (0 mM, 0.5 mM, and 2 mM) at different CPMG spin-lock times: 20 mS (orange), 50 ms (green) and 150 ms (purple). 136

Figure 27. Increasing concentrations of manganese from left to right (0 mM, 0.5 mM, and 4 mM) at different CPMG spin-lock times: 20 mS (orange), 50 ms (green) and 150 ms (purple). 137

Figure 28. Increasing concentrations of manganese from left to right (0 mM, 0.5 mM, and 2 mM) at different CPMG spin-lock times: 20 mS (orange), 50 ms (green) and 150 ms (purple). 137

Figure 29. Increasing concentrations of manganese from left to right (0 mM, 0.5 mM, and 4 mM) at different CPMG spin-lock times: 20 mS (orange), 50 ms (green) and 150 ms (purple). 138

Figure 30. Increasing concentrations of manganese from left to right (0 mM, 0.5 mM, and 2 mM) at different CPMG spin-lock times: 20 mS (orange), 50 ms (green) and 150 ms (purple). 138

Figure 31. Increasing concentrations of manganese from left to right (0 mM, 0.5 mM, and 4 mM) at different CPMG spin-lock times: 20 mS (orange), 50 ms (green) and 150 ms (purple). 139

Figure 32. Increasing concentrations of manganese from left to right (0 mM, 0.5 mM, and 2 mM) at different CPMG spin-lock times: 20 mS (orange), 50 ms (green) and 150 ms (purple). 139

Figure 33. Increasing concentrations of manganese from left to right (0 mM, 0.5 mM, and 4 mM) at different CPMG spin-lock times: 20 mS (orange), 50 ms (green) and 150 ms (purple). 140

Figure 34. Increasing concentrations of manganese from left to right (0 mM, 0.5 mM, and 2 mM) at different CPMG spin-lock times: 20 mS (orange), 50 ms (green) and 150 ms (purple). 140

Figure 35. Increasing concentrations of manganese from left to right (0 mM, 0.5 mM, and 4 mM) at different CPMG spin-lock times: 20 mS (orange), 50 ms (green) and 150 ms (purple). 141

Figure 36. Increasing concentrations of manganese from left to right (0 mM, 0.5 mM, and 2 mM) at different CPMG spin-lock times: 20 mS (orange), 50 ms (green) and 150 ms (purple). 141

Figure 37. ^1H - ^{31}P HSQC spectrum for quantification of lipid composition of membrane vesicles prepared from *E. coli*. Integration of the lipid peaks gave rise to a PE:PG ratio of 3:1. 142

Figure 38. At the top a diagram of one-way ANOVA analysis of control sample with a significant change of 2. At the bottom the two up-regulated significant metabolites: biotin and panthothenate. 143

Figure 39. Diagram of one-way ANOVA analysis of sample containing SSA60 0.2 mM with a significant change of 2. 144

Figure 40. Diagram of one-way ANOVA analysis of sample containing SSA60 0.5 mM with a significant change of 2. 145

List of Tables

Table 1. Predicted permeability for the set of control and SSA compounds at concentration of manganese 0.5 mM.	67
Table 2. Membrane interaction data for the set of control and SSA compounds.	69
Table 3. Self-association values for control and set of SSA compounds.	70
Table 4. Predicted permeability category for the set of SSA compounds at concentration of manganese 0.5 mM in two types of cancer membrane vesicles: resistant (green) and no resistant (yellow) cells.	72
Table 5. Membrane interaction category for SSA compounds in two types of cancer membrane vesicles: resistant (green) and no resistant (yellow) cells.	73
Table 6. Predicted permeability for SSA compounds at concentration of manganese 0.5 mM in live cells.	88
Table 7. Predicted membrane interaction for SSA compounds in live cells.	89
Table 8. Comparison of self-association values of SSA compounds in <i>in vitro</i> and <i>in vivo</i> assays.	89
Table 9. Fold change values log transformed for metabolites of cells treated with SSA60 0.2 mM.	146
Table 10. Fold change values log transformed for metabolites of cells treated with SSA60 0.5 mM.	146

1. Abstract

The critical rise of antimicrobial resistance (AMR) requires the discovery of new antibiotics, particularly against Gram-negative bacteria. The permeability barrier of bacteria is a vital property to consider within the drug development process. In this work, we describe a new NMR method to assess membrane permeability and membrane interaction affinity of a new family of antimicrobial compounds exploiting the enhanced paramagnetic relaxation enhancement (PRE) effect induced by solvent paramagnetic agents in non-permeable drugs mixed with lipid vesicles. The results exhibited differences in the permeability rate and membrane interaction affinity of drugs among membranes with different lipid composition, confirming that our method is applicable to any type of cell/bacterial membrane. In addition, we have expanded this assay to live cells making use of a NMR-coupled bioreactor. With this setup, we have been able to measure NMR metabolomics to simultaneously monitor membrane permeation, membrane affinity and changes in the bacterial metabolism as a result of the addition of antimicrobial agents, providing evidence on their mechanism of action at the metabolite level. In general, our study introduces a new method for assessing drug permeability in lipid vesicles or live cells that will allow the design of more efficacious drugs and antimicrobial agents in a standard chemistry lab environment.

2. Introduction

2.1. Antimicrobial resistance and tolerance

The discovery of penicillin by Alexander Fleming in 1928 gave rise to the transformation of medical practice. Since then, antibiotics provided extensive health benefits to human medicine, reducing the death rate of many infectious microbial diseases such as 60% for meningial and cerebral infections. However, 50-60 years afterwards, the success of medical science against pathogens has been decreasing as microorganisms began to develop resistance toward antibiotics (Dhingra et al. 2020).

Although AMR is considered as a natural phenomenon, the misuse and overuse of antimicrobials in veterinary and human medicine has increased the growth rate of this process (Dhingra et al. 2020; Ferri et al. 2017). As a result, AMR is a current severe threat for global public health. The measures proposed for responding to AMR challenges include designing more effective preventive measures to reduce the use of antimicrobial, the urgent development of novel antimicrobials and boosting the knowledge of the ecology of resistant bacteria and genes (Ferri et al. 2017).

It has been observed that bacteria could survive without genotypic variations under extensive antibiotic treatments. This phenomenon is called antibiotic tolerance and was first described by Tomasz *et al.* (Hibberd and Leedale 1970) who showed that *Streptococcus pneumoniae* could protect from lysis by penicillin with a deficient autolytic system (Y. Liu et al. 2020).

As of today, it has been estimated that drug resistant infections will kill more people than cancer by 2050. However, pharmaceuticals are giving up antibiotic discovery due to the extreme costs associated (Ferreira and Kasson 2019; Makowski et al. 2020). Since 1999, the drop in industry research on novel antibacterial agents is caused by the large number of pharmaceutical companies giving up or reducing their antibiotic research programs (Projan and Shlaes 2004). One of the main problems that affect the efficacy of antibiotics is the introduction of a new antibiotic that results in resistance to it at any given moment. Thus, the rate of discovery and development of new antibiotics delay the emergence of resistance mechanism among bacteria, which responds quickly to selective pressure (Ferri et al. 2017).

2.1.1. Mechanisms of antibiotic resistance

AMR is considered as an ability of microorganisms to counteract drugs by developing mechanisms for resisting to their effects and for transferring of resistant genetic properties to the group (Ferri et al. 2017).

In general, there are five types of resistance mechanisms (Figure 1) (Ferri et al. 2017; Cox and Wright 2013):

1. Reduction of drug accumulation by a drop in outer membrane permeability or a rise in active efflux of the drug across the cell surface.
2. Drug inactivation or modification by production of enzymes that either alter or neutralize the antibiotics voiding their efficacy such as bacterial production of beta-lactamases.

3. Alteration of target or active binding sites of their receptors like ribosomal alterations.
4. Modification of metabolic pathways such as by synthesis of altered enzymes.
5. Changes in membrane permeability to antibiotics: OM of Gram-negative bacteria like *Escherichia coli* (*E. coli*) presents some impermeability to hydrophobic compounds such as beta-lactam antibiotics.

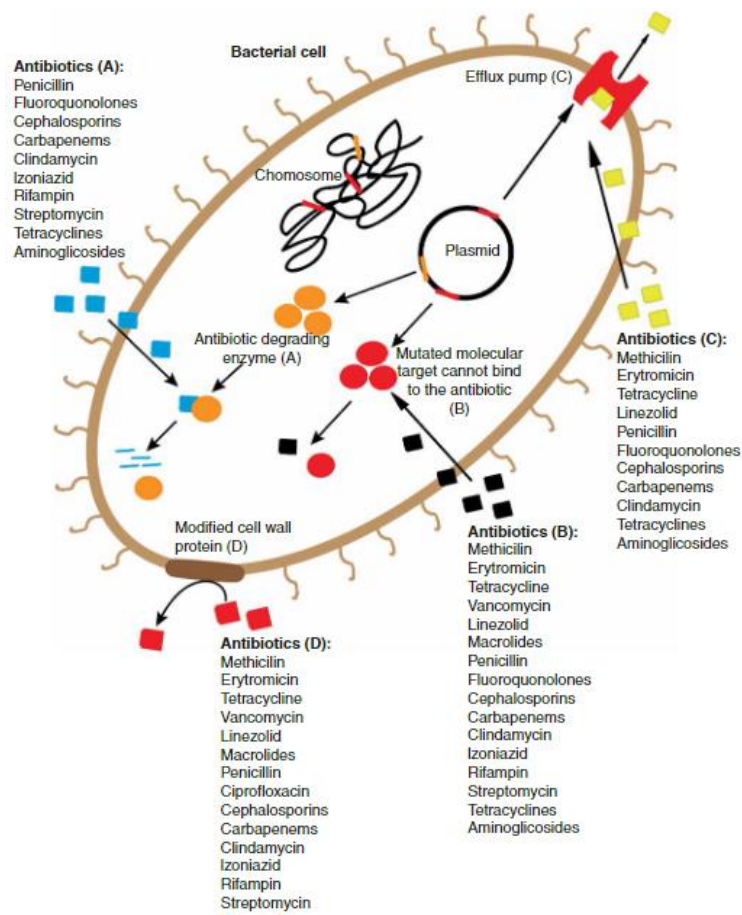


Figure 1. Biological mechanisms of antibiotic resistance. (A) Antibiotic degradation chemically by enzymes. (B) Altered target. (C) Antibiotic efflux. (D) Receptor modification (Penchovsky and Traykovska 2015).

In certain bacteria, referred to as “insensitive”, this resistant trait can be innate and intrinsically related to the general physiology or anatomy of the microorganisms and is not affected by misuse of antibiotics. Bacteria can acquire resistance through genetic changes such as mutations and uptake of genetic material by horizontal transfer mechanism both between and within species through exchange of plasmids (Alanis 2005).

Bacterial species seem to have acquired a preference for only a type of resistance mechanism over other. For instance, among Gram-negative bacteria, penicillin resistance is mainly moderated by beta-lactamase enzymes that destroy the antibiotic. However Gram-positive bacteria alter the penicillin-binding sites to render them penicillin resistant (Morrison and Zembower 2020).

Alternatively, bacterial species can develop resistance as well as more than one mechanism of resistance. They can be divided in three groups: multidrug resistant for bacteria that are resistant to at least one agent in three or more antibiotic classes, extensively-drug-resistant bacteria that are susceptible to only one or two antibiotic groups and pan drug resistant bacterial phenotypes that describes resistance to all agents in all antibiotic classes (Morrison and Zembower 2020). Some of multidrug resistant bacterial strains are known as “superbugs” such as *Salmonella Typhimurium* phage type DT104 (Ferri et al. 2017).

Among multidrug resistant bacteria, extensive genetic and metabolic studies reported of *E. coli* make it a suitable strain to investigate resistance pathways for new antimicrobial agents. *E. coli* is one of the most popular pathogenic bacteria employed in medical science and veterinary clinical infections studies as their infections are a huge threat to human

health. This bacteria is responsible of common infections and uses different processes for antibiotic resistance: random beneficial genetic mutations (rate of 2×10^{-9}), horizontal gene transfer and strengthening of the cell wall and basic defense systems (Aries and Cloninger 2020; Y. Lin et al. 2019).

2.1.2. Designing drugs for overcoming antimicrobial resistance

The emergence of antimicrobial resistance has driven an enthusiasm in the area of drug discovery. Novel agents with novel modes of action are required to address the problem. Although efficient inhibitors of the bacterial targets are discovered, it is considerably difficult to optimise such agents and discover drugs with elevated levels of antimicrobial activity. The main reason for the failure of these drug discovery projects is the inability of the products to penetrate to the organism and achieve their site of action. Their external permeability barrier supplies an essential protection against toxic compounds from the environment such as xenobiotics, particularly complex in Gram-negative bacteria, as well as selective uptake of nutrients and excretion of waste products. This barrier is the complex cell envelope which restricts movement molecules into the cytoplasm, resulting in inherent antibiotic resistance. For that reason, understanding the architecture of bacterial envelopes is critical to define if candidate antibacterial compounds can go across these proteo-lipid barriers (Benedetto Tiz, Kikelj, and Zidar 2018).

2.1.2.1. Composition of bacterial membrane

One of the biggest challenges in developing antibiotics against multi-drug resistant Gram-negative bacterial pathogens is their small-molecule uptake as their membranes differ

substantially from mammalian cells membranes. The plasma membranes of bacteria are surrounded by a cell envelope composed of peptidoglycan and between them there is the periplasmic space. There are several differences between Gram-positive and Gram-negative bacteria but the most important one is the presence of an additional outer membrane (OM) in Gram-negative bacteria (Figure 2). The OM provides a primary permeability barrier and several antibiotics make their effect in the periplasmic space. Thus, outer-membrane uptake of small molecules is a good target as an initial optimization for an effective uptake into Gram-negative bacteria (Benedetto Tiz, Kikelj, and Zidar 2018; Ferreira and Kasson 2019; Makowski et al. 2020).

The outer leaflet of the OM is composed of an asymmetric composition of phospholipids and mostly highly anionic glycolipid lipopolysaccharide (LPS). LPS is comprised of three regions: lipid A is a phosphorylated glucosaminidiasaccharide with four to six fatty acids, a core of oligosaccharides and the O-antigen made up of repetitive monosaccharide subunits. The negative charges, mostly provided by phosphate residues of lipid A, are stabilized by divalent cations such as Mg^{2+} , resulting impermeable for hydrophilic and hydrophobic molecules. In addition, other components of outer membrane are non-specific and specific outer membrane porins through which the majority of antibiotics and hydrophilic metabolites enter. Overall, the OM of Gram-negative bacteria represents a highly selective barrier due to the combined effects of the protecting hydrophobic lipid bilayer and porins with specific properties. The inner leaflet of the OM and the inner membrane (IM) are comprised of around 60-70% of the zwitterionic phosphatidylethanolamine (PE), 30-35% of anionic phosphatidylglycerol (PG) and 5% of cardiolipin (CL) with two negative charges

per molecule. The membrane is also comprised of some less important phospholipids. (Ferreira and Kasson 2019; Makowski et al. 2020; Benedetto Tiz, Kikelj, and Zidar 2018).

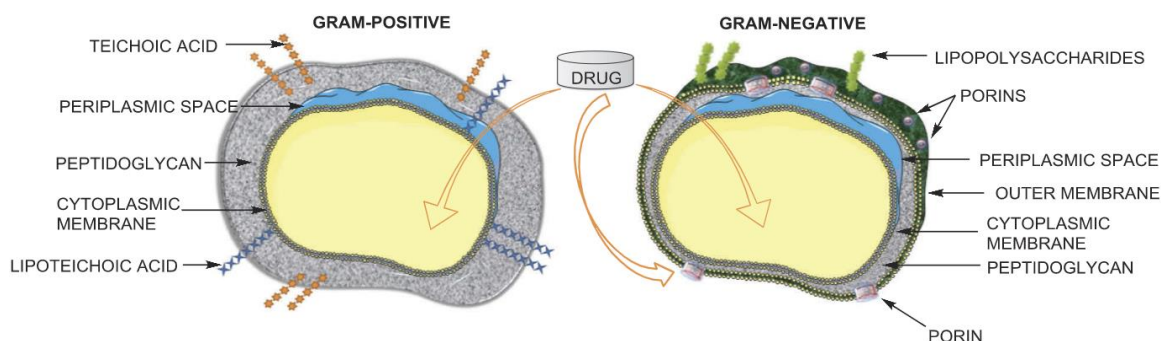


Figure 2. Schematic representation of the different cell envelopes of Gram-positive and Gram-negative bacteria (Penchovsky and Traykovska 2015).

2.1.2.2. Di-anionic self-associating supramolecular amphiphiles as antimicrobial agents

Since the 1950s novel strategies for the development of antimicrobial agents have been adopted, some of which have been inspired by supramolecular chemistry. Employing structures to enable selective host-guest complex systems formation capable of inserting into bacterial membranes and resulting in biological molecular machines (Allen et al. 2020; White et al. 2021).

On this topic, White and co-workers have developed a novel class of Supramolecular Self-associating Amphiphile (SSA) (Figure 3) considered as selective phospholipid membrane coordination agents. In addition, some of them have been shown to: exhibit antimicrobial

efficacy against both Gram-negative *E. coli* and Gram-positive Methicillin-Resistant *Staphylococcus aureus*, be also anticancer agents and have the potential to act as drug delivery molecules and therapeutic efficacy enhancement agents (White et al. 2021; Boles et al. 2022).

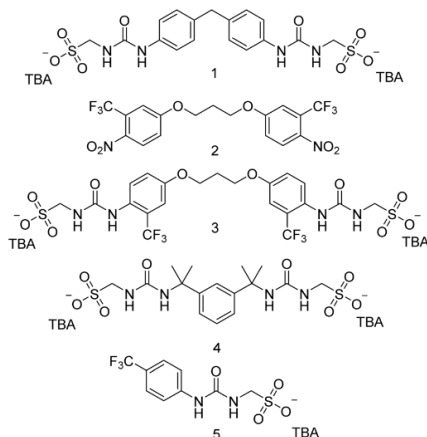


Figure 3. Chemical structures of SSAs (TBA= tetrabutylammonium) (White et al. 2021).

2.2. Drug's membrane permeability

The process of discovery, development and registration of a new drug requires a long, labor-intensive, and costly procedure. Currently, several *in vitro* experimental models provide an evaluation of the permeability and transport of pharmaceutical molecules across at least one cellular membrane to reach their target. There are currently high-throughput *in vitro* techniques based in artificial membranes, such as parallel artificial membrane permeability assay (PAMPA), the immobilized artificial membrane (IAM) method,

liposome chromatography (ILC) and systems based in cells such as Caco-2. These models are important in the initial stages of drug discovery as a decision-making tool for identifying successful drug candidates (Bennion et al. 2017; Cabrera-Pérez et al. 2016).

The PAMPA technique was developed by Kansy et al. (Kansy, Senner, and Gubernator 1998) in 1998 and predicts permeability of compounds passively absorbed by transcellular transport, useful to estimate absorption through the gastrointestinal tract and also used for other systems such as the blood brain barrier. However, this system only allows a simple classification of molecules: low, medium and high probability of absorption. This high-throughput methodology method is based on two compartments separated by a lipid artificial membrane that contains a variety of phospholipid mixtures. The compound tested permeates between the donor and the acceptor compartments through the membrane. (Bennion et al. 2017; Cabrera-Pérez et al. 2016).

Regarding the other two techniques, IAMs mimic the phospholipid component of the cellular membrane by using synthetic lipids attached to silica particles which are used as the packing material for liquid chromatography column. This artificial membrane method is employed to predict membrane permeability. On the other hand, ILC technique is used to investigate solute-membrane interactions by liposomes that can be composed of varied lipid composition and are covalently immobilized to gel beads (Bennion et al. 2017).

2.2.1. Drug transport mechanisms

A drug molecule interacts with the action site of its receptor or therapeutic target to exerting its pharmaceutical effects. To overcome the problems of low permeability of the

bacterial cell envelope to drugs, several approaches have been reported using carriers such as liposomes to enhance the intracellular delivery of antibacterial drugs (Benedetto Tiz, Kikelj, and Zidar 2018).

The absorption process involves semipermeable cell membranes composed of various protein channels which contribute to the equilibrium of accumulation of intracellular drugs and are related to the antibiotic susceptibility (Cabrera-Pérez et al. 2016; Bolla et al. 2011). In these barriers, there are two types of drug transport: paracellular (between cells) transport is size-restricted passive diffusion and transcellular (across the cell) transport includes passive diffusion, carrier-mediated transport (active or facilitated diffusion) and endocytosis (Cabrera-Pérez et al. 2016).

Hydrophilic molecules such as β -lactam antibiotics use primarily porins to enter the cell whereas hydrophobic compounds such as aminoglycosides can cross the OM by passive diffusion or self-promoted uptake which results in disorganization of the LPS by these polycationic antibiotics (Bolla et al. 2011; Chopra 1988).

In addition to these influx transport mechanism, the intrinsic production of efflux pumps in Gram-negative bacteria offers a way to export antibiotics reducing drug concentrations inside the cell which is contributing to antibiotic resistance. Efflux transporters can be divided into two groups depending on the source of energy needed for efflux: primary and secondary transporters. The first group is composed of ATP-binding cassette (ABC) superfamily that uses the energy of ATP binding and hydrolysis. Secondary transporters include the major facilitator superfamily (MFS), small multidrug resistance family (SMR),

resistance nodulation-division (RND) family and multidrug and toxic compound extrusion (MATE) family that employ the energy from the ion gradient (Blair, Richmond, and Piddock 2014; Benedetto Tiz, Kikelj, and Zidar 2018).

2.3. An introduction to NMR spectroscopy

NMR is a versatile tool for studying many kinds of biomolecules and is based on the interaction of magnetic moments of nuclei of different atoms with strong, static and homogeneous magnetic fields. The magnetic moment of nuclei is related to a nuclear spin. The basic feature of NMR is to detect the Larmor precession of individual nuclei (spins) which varies depends on the atomic, electronic and chemical environments (Emwas et al. 2020; Mlynárik 2017).

Firstly, the sample is placed in a magnetic field and exposed to and induced electromagnetic fields at radiofrequencies (RF pulses) which are applied transverse to the plane of the magnetic field. This bulk magnetization suffers an effective rotation and subsequently, preceding magnetization vectors induce a tiny fluctuating voltage in the NMR receiver coil. This latter voltage is represented as an analogue time domain signal which is amplified and converted to a frequency reading via Fourier transformation (Emwas et al. 2020).

Briefly, these resulting signals are recorded in response to the induced radio-wave pulses and represent the spectroscopic signature of the chemical and magnetic environment of the atom, offering wealthy and detailed atomic resolution information about the structure of the molecule, dynamics of the spins or conformational exchange (Figure 4). Thus, any change

in the environment of the associated spins, such as molecular binding, interactions or exchanges between conformations can be detected. The use of NMR for drug design research has increased in recent years since this analytical tool allow the study of several functional molecules: natural products, metabolites, saccharides, DNA and proteins (Emwas et al. 2020).

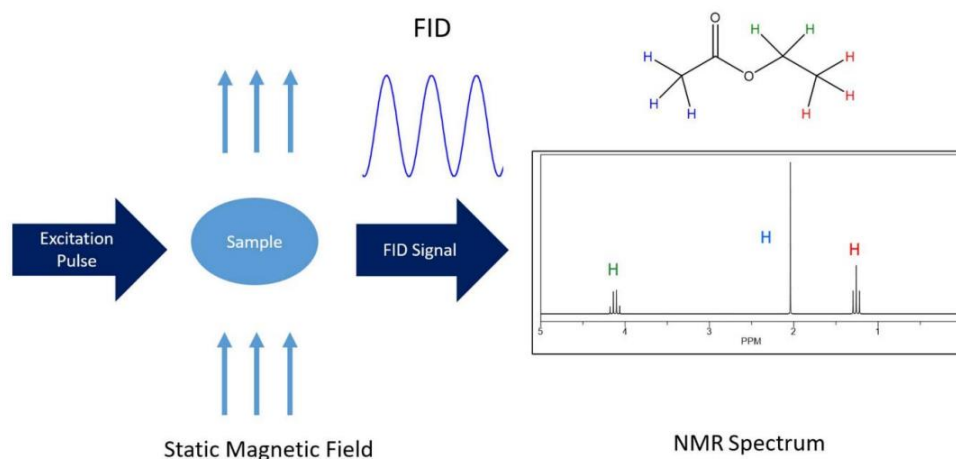


Figure 4. Simplified layout of an NMR experiment (Emwas et al. 2020).

In contrast to mass spectrometry coupled with high-performance liquid chromatography (HPLC), NMR presents unique advantages: intrinsically quantitative, non-destructive, non-invasive and highly reproducible allowing measurements under different experimental conditions, even while the sample is inside the magnet. In addition, because kinetic studies can be carried out, NMR provides dynamic information under physiological conditions. This helps in medical drug design as the interactions between an enzyme and its respective ligand(s) must be studied. Therefore, NMR offers information about binding affinity of

ligands, details of the binding site and associated structural alterations which are essential biophysical details for evaluating the efficacy of a drug (Emwas et al. 2020).

2.3.1. Small molecule drug discovery and role of NMR spectroscopy

Since the development of structural biology, NMR has been one of the techniques to provide structural information at atomic level detail of cellular components and unique for drug and vaccine design (Luchinat and Banci 2017).

Understanding the structure of biological macromolecules and how physiological processes are altered by changes in the molecular environment is essential to deduce their function and their mode of interaction. The relationship with their partners gives rise to and regulates biological activity (Luchinat and Banci 2017; Maldonado, Burz, and Shekhtman 2011).

Cryogenic electron microscopy (cryo-EM), X-ray crystallography and NMR are important technical developments for obtaining the structures of large macromolecular complexes at atomic resolution. In recent years, the rapid progress of cryo-EM has made it possible to decrease the molecular size limit and increase resolution to solve structures of many difficult targets and high molecular weight species such as ion channels and membrane-bound enzymes complexes. Solution NMR is also considered as a robust tool to inquire into protein-ligand and protein-protein interactions under solution conditions and at various temperatures. Despite of signal overlap and sensitivity from protein structures with high molecular mass, NMR spectroscopy has been employed in various research topics including protein chemistry and drug discovery with the development of magnets, pulses

programs and different protein-labeling strategies. Many structures of membrane proteins have been successfully characterized using solution and solid-state NMR spectroscopy (Luchinat and Banci 2017; Kang 2019).

With the correlation between structure and function of biomolecules resolved by such methods, the information obtained has to relate to that acquired from cell biology and biochemistry. Indeed, it is critical that the information of macromolecular structures is only determined under physiological conditions. For that reason, NMR is the most effective technique to reach those requirements (Kang 2019).

2.3.2. Paramagnetic effect

Even though NMR spectroscopy is a key analytical technique to determine and validate structure and dynamic of small molecules macromolecules both in solution and in solid state, NMR presents a lack of sensitivity due to small energy differences among the states of nuclear spins or low population differences. This disadvantage results in poor signal-to-noise ratios. NMR requires samples with high concentration between micro and millimolar range in order to boost the sensitivity. Another way to achieve high sensitivity of NMR spectra is through novel probe designs and the use of cryogenic probes that reduce noise levels. Furthermore, the alteration of relaxation properties of the nuclei by the introduction of paramagnetic probes provides an increase of NMR sensitivity (Kocman et al. 2019).

Firstly, relaxation is defined as a process by which the Boltzmann equilibrium of spin stated is restored after the perturbation of nuclear spins by radio-frequency pulses. This

phenomenon can be described simply by longitudinal (characterized by the time constant T1) and transverse (T2) relaxations (Bloch 1946).

In general, the paramagnetic NMR strategy for small molecule NMR is practical since no isotopic labelling is needed because only the NMR spectrum of the ligand is shown (Carneiro et al. 2017). In the relaxation processes of a paramagnetic system, the electronic relaxation times play a significant role as they are determined by the nature of the paramagnetic ion used, in addition to the proton effective correlation times when it deals with ^1H relaxation and the molecular rotational correlation time. It has been demonstrated that depending on the speed of rotating molecules, T1 and/or T2 can be affected. For fast molecules or part of them, the electronic relaxation times dominate which means that T2 is not altered but T1 is shortened. On the other hand, if the electronic relaxation times are longer than rotational correlation times of molecules, T2 are much shorter than T1 which can be observed in the NMR spectrum as a consequent line-broadening effects (Kocman et al. 2019; Cai et al. 2006).

In the last two decades, NMR of paramagnetic systems has enhanced their use in biological, biomedical investigations and in material sciences as remarkable developments in experimental NMR have made it easier and more useful. The NMR data related to shifts and relaxation rates collected by systems with a paramagnetic centre, contain relevant information on their structure and dynamics which could become important for the study of large or conformationally heterogeneous complexes (Parigi, Ravera, and Luchinat 2019).

Paramagnetism is caused by the presence of an unpaired electron in a chemical moiety. This effect offers an opportunity to further enhance and broaden the utility of NMR in drug discovery as well as novel approaches for screening of ligand binding poses and structural analysis (Softley et al. 2020). Paramagnetic NMR such as PRE increases the transverse relaxation rate by accelerating dipolar interaction with unpaired electrons from spin-label and paramagnetic agent (metal ion) when they approach to a macromolecule. The PRE depends on the distance (r^{-6}) between the nucleus of interest and the paramagnetic centre (Sugiki et al. 2018). Molecular tumbling gives rise to PRE effect which depends on the distance (r) between the electronic spins and the nucleus of interest to the inverse sixth power but not orientation (Softley et al. 2020). Hence, this effect provides the detection of ligand-binding by the decline in signal intensity of the drug (Sugiki et al. 2018). Paramagnetic nuclear relaxation is caused by dipole-dipole interaction between nuclear and electron spins and is calculated as the difference between paramagnetic and diamagnetic rates (Softley et al. 2020).

A PRE reagent reduces the T1 relaxation times for all nuclei in the sample as it presents unpaired electrons. An ideal PRE reagent shows high spin quantum number (unpaired electrons in the outer shell), faster water exchanges kinetics and a long longitudinal electronic relaxation time even at low concentrations. In order to reduce any specific associations with the solute, they are uncharged polar molecules. Also, the main functional action of the PRE reagent is shorten ^1H T1 and/or T2 relaxation times (Mulder, Tenori, and Luchinat 2019; Smeraldo, Netti, and Torino 2020).

2.3.3. CPMG pulse sequence

An NMR experiment involves a large number of pulses making it more sensitive to hardware restrictions and small miscalibrations of the pulses duration. Therefore, to diminish the unexpected effects by miscalibrations on the measurement of spin relaxation, Meiboom and Gill modified the previously employed Carr-Purcell sequence (Carr and Purcell 1954) by changing the phase of the applied 180° pulses from x to y axis (Emwas et al. 2020). The Carr-Purcell-Meiboom-Gill (CPMG) experiment is a technique that modifies relaxation times and hence, properties between the nuclei in biomacromolecules and in small molecules to analyse binding (Shi and Zhang 2021). This pulse sequence is composed of a 90° RF pulse and a spin-echo period (delay- 180° -delay block). Primarily, a 90° RF pulse applied creates a transverse (xy plane) magnetization. Subsequently, the spin-echo period generates a M_{xy} magnetization decay and this last period is repeated “ n ” times which is called CPMG block (Figure 5) (Emwas et al. 2020).

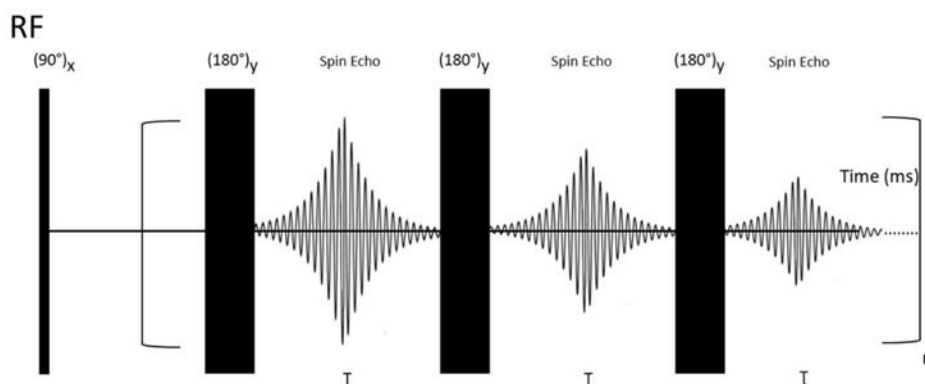


Figure 5. Schematic representation of the CPMG pulse sequence (Emwas et al. 2020).

This method can be employed to measure T2 relaxation times of all types of nuclei. T2 measurements of ligands are employed to determine the binding nature of small molecules. It is important to point out that small molecules and non-binding ligands display longer T2 values than those of bigger molecules and bound ligands. Mostly macromolecules have more elevated spin-spin diffusion rates, and because bound ligands interacting with the target adopt similar vibrational and rotational energies adopt similar T2 rates (Emwas et al. 2020). Small molecules present a slow relaxation which means sharp and well-defined peak. On the other hand, biomacromolecules and their bound ligands tend to relax rapidly and present broader signals (Figure 6) (Shi and Zhang 2021). If a ligand binds to the slowly relaxing macromolecule, it will result too in a broader peak.

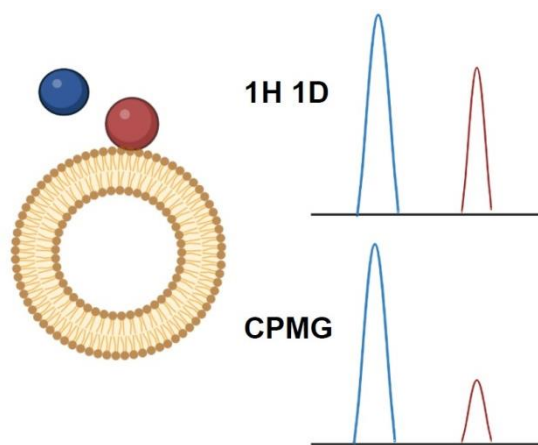


Figure 6. Illustration of the CPMG experiment. Non-binding (blue) and binding (red) small molecules in the presence of lipid vesicles with their respective NMR signals.

2.4. In-cell NMR

NMR spectroscopy has shown to be an excellent tool for the study of live cells that can be employed in monitoring their biochemical processes within a crowded intracellular environment in a non-invasive way (Carvalho et al. 2019). In In-cell NMR spectroscopy, active nuclei in biological macromolecules are extremely sensitive to alterations in the chemical environment: specific and non-specific binding interactions with ions, small effector ligands and macromolecules or changes because of biochemical modifications. This results in changes in the chemical shifts of these nuclei (Maldonado, Burz, and Shekhtman 2011).

Different cells such as bacteria, yeast, oocyte and mammalian cells can be employed for in-cell NMR studies. The application of mammalian cells makes it useful for target engagement in drug discovery when the targets are related to human diseases. As in-cell NMR maintain intact live cells containing the complete cellular component, the information is especially useful for probing protein and drug interaction in living cells, providing helpful information for medicinal area in order to improve the potency and understand the mode of action of the developed compounds (Kang 2019).

The first experiments using in-cell NMR were performed in *E. coli* cells by Serber and coworkers (Serber and Dötsch 2001), who reported that globular proteins overexpressed in these cells and isotopically labelled to a sufficient level could be detected above the other cellular components by heteronuclear NMR. Since then, bacteria have been shown to be a suitable organism for in-cell protein NMR analysis (Luchinat and Banci 2017).

In comparison with other *in vitro* viability assays, this technique presents several advantages as it is an unlimited-time assay as cell viability can be monitored in a real time before, after and even during the addition of the studied drug. In addition, the control of the duration of drug exposure is a favorable characteristic as well as study of cellular response after pharmacological compound removal upon its acute, short or long-term toxicological effects (Carvalho et al. 2019).

However, the experimental set up in-cell NMR presents several drawbacks. A high cell number is required for an in-cell NMR experiment to increase the signal-to-noise ratio to detect intracellular signals and for a more accurate quantification, due to the low sensitivity of this spectroscopy. These cells are suspended in simple buffer mixtures or pH-buffered nutrient-rich growth. The dense number of cells promotes rapid nutrition depletion, anaerobic environment, and accumulation of waste metabolic products inside the NMR tube. As a result of this, metabolic depletion may result in cell death or a state of metabolic hibernation and cell reprogramming which affects ATP-activities and functions or structures of proteins. These consequences hamper over-time acquisition and monitorization of NMR signals. In addition, one of the main problems is to maintain cell viability within the NMR tube over the NMR spectra acquisition. Even though sampling methods reduce the time required for multidimensional spectra acquisition using fresh samples each time, currently the development of bioreactor systems has been the principal solution (Carvalho et al. 2019; Siegal and Selenko 2019).

These devices are compatible with NMR magnets and keep a consistent cellular background with live and metabolically active cells for prolonged periods of time. There

are so far two types of bioreactor: an in-magnet bioreactor that allows cells to grow inside the NMR tube to a high density, and a perfusion system that flows fresh medium continuously into the cells while supplying nutrients and oxygen and removing metabolic waste when they are immobilized in an accurate matrix. These devices are designed to study metabolism, allowing the assessment of cell viability and metabolic state by monitoring the ATP levels (Burz, Breindel, and Shekhtman 2019; Carvalho et al. 2019; Sharaf et al. 2010).

2.4.1. NMR-coupled bioreactor

Over years, various research groups have developed different flow-probe bioreactor designs, inspired by earlier *in vivo* NMR set ups, available since 1990. The new generation of NMR bioreactors shares important concepts from the previous designs that have been explore to develop the modern bioreactors: a circulating encapsulated cells (CEC) bioreactor, a continuous-flow system that employs immobilized cells and a membrane perfusion system that provides a fresh medium for cell suspension (Burz, Breindel, and Shekhtman 2019; Luchinat, Cremonini, and Banci 2021; Siegal and Selenko 2019).

One challenge to overcome with bioreactors for cell cultures that grow in suspension is to guarantee that the fresh medium flows continuously and freely inside the NMR sample tube without removing cells and without clogging inlet and outlet channels. Therefore, cells can be embedded in porous matrix material through which fresh medium flows (Figure 7A). In 2008, Pielak group created the first device for protein in-cell NMR experiments of bacterial cells encapsulated in Ca^{2+} -alginate spheres, introducing the concept of CEC, although they

borrowed concepts from the stirred cellular suspension employed by Freyer *et al.* (Luchinat, Cremonini, and Banci 2021; Siegal and Selenko 2019; Freyer et al., 1990). CEC bioreactor does not operate in a continuous mode because only when the pump is active the cells embedded in alginate are pushed in the circulation chamber where the exchange of nutrients and oxygen occurs. However, bioreactors developed later for in-cell NMR present continuous operation and most of them are designed for a continuous perfusion of cells encapsulated in gel. In these devices, cells are encapsulated in different gel matrices and placed in the NMR tube where an uniform flow of fresh medium for exchange of nutrients, gases and waste products (Figure 7B) (Luchinat, Cremonini, and Banci 2021).

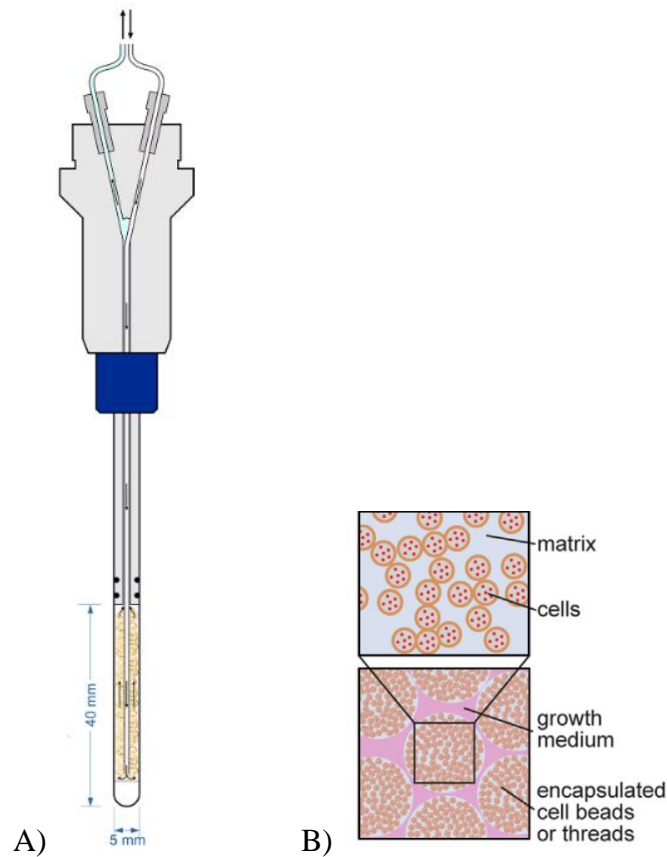


Figure 7. A) Schematic design of tube setup based on a sealed flow unit. (Luchinat, Cremonini, and Banci 2021). B) Gel-encapsulated cells in porous matrix materials with growth media enable the continuous exchange of nutrients to sustain cellular viability and physiological energy metabolism (Siegal and Selenko 2019).

The majority of bioreactors are composed of a complex framework requiring pumps to circulate the fresh medium and creating a closed system. The current design of bioreactors sustains high metabolic energy levels for up to 12-24 hours. Constant elevated levels of energy are required for maintaining full metabolic pathways which are essential for ATP-

dependent processes (Breindel, Burz, and Shekhtman 2020; Burz, Breindel, and Shekhtman 2019).

2.5. NMR-based metabolomics

2.5.1. Metabolic investigation of live cells using NMR spectroscopy

In recent years, metabolomics has become an increasing popular branch of systems biology methodology together with proteomics and genomics analysis, which study the cellular processes as well as their responses to specific antibiotic stimuli and potential targets (Y. Lin et al. 2019; Hoerr et al. 2016).

Ideally, metabolites represent downstream products, intermediates, and regulators of the most of biological processes that reflect physiological functions. The metabolic profile characteristic for bacteria is different when culture under antibiotic stress and in antibiotic resistant strains. Finding a non-destructive method to quantify metabolites from a test sample suggests that they can be used as a proxy to study or monitor these processes in an extensive range of biological systems, even live cell cultures. Some high-throughput metabolomics applications involve drug discovery, toxicology, biomass processing and production of vaccines in bioreactors (Y. Lin et al. 2019; Wang et al. 2021).

Regarding drug discovery, metabolomics may influence in all the steps of this process as it is able to identify therapeutic targets which provide novel knowledge of cellular physiology and disease progression. Furthermore, metabolic profiles arising from a disease state or drug-resistant aid detecting critical cellular or metabolic processes. In this way, proteins involve in these up- or down-regulated signalling pathways can be targeted as part of a

therapy as well as metabolic characterization can be employed to monitor that response (Bhinderwala and Powers 2019).

Metabolomics is a -omic science driven by technologic discipline. Currently, the most popular analytical technologies used in metabolomics include LC-MS, GC-MS and NMR spectroscopy which also provide information of the mechanism of action of antibiotics on various bacterial species (Y. Lin et al. 2019; Wang et al. 2021). Although MS-based methods are more sensitive and hence can detect more metabolites than NMR, this last technique is ideal for performing real-time metabolic profile and flux analysis of living cells because NMR experiments can be carried out easily and quickly without sample preparation procedures. In contrast, LC-MS and GC-MS techniques cannot be employed to analyse living samples due to their destructive nature (Emwas et al. 2019; Wang et al. 2021). In terms of bioreactor applications, flow NMR probes provide continuously sample measurements making it attractive for NMR metabolomics. Furthermore, Quantitative NMR metabolomics can be an additional tool for monitoring the molecules related to the reactor process (Wang et al. 2021).

High resolution NMR has been considered as a technique capable of characterise metabolically cells, extracts and biopsies (Figure 8). The analysis of rapid metabolic changes to cell responses requires challenges laborious as it is needed an efficient metabolism at time measurement. However, these hurdles can be solved by NMR measurement of intact cells in their inherent environment through control of cell-culture conditions (Hertig et al. 2021).

Metabolism adapts fast, between seconds to minutes, to environmental changes (Lippens et al. 2018). Hence, the major impediment during the entire in-cell NMR experiments is to maintain an active metabolism and high degree of cell viability as cell death occurs commonly during long-time experiments. Hence, controls are thoroughly applied to not give rise to signals from within intact cells. The introduction of bioreactors allows to establish favourable conditions for cell growth (Breindel, Burz, and Shekhtman 2020).

NMR experiment requires a long process for sample preparation including various stressful steps for the cells: centrifugation, changes of temperature or pH and oxygen availability during the measurement (Lippens et al. 2018).

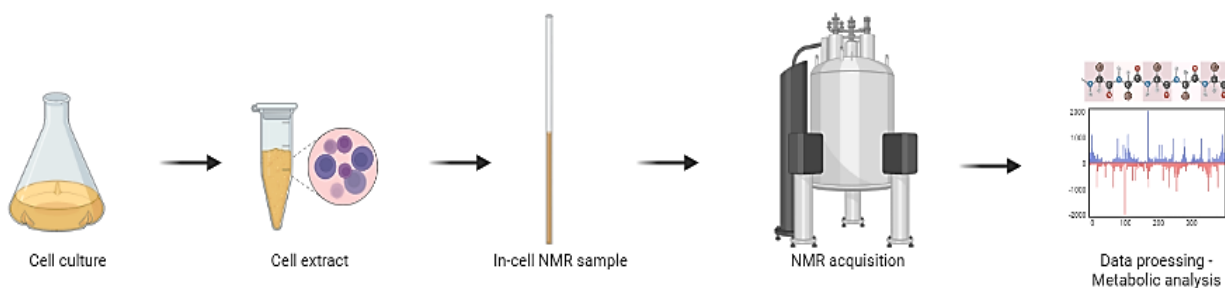


Figure 8. Schematic workflow for metabolomics investigations.

In vivo NMR provides to follow in real time biochemical reactions, the transformation of metabolites in a cellular environment. Although ^1H NMR has more sensitivity, it is not the common method due to its difficult water suppression and limited spectral window for the signals (Lippens et al. 2018). Even so, few studies using ^1H NMR have been performed for metabolomics investigations of living cells in bioreactor under controlled conditions (Hertig et al. 2021). ^1H is approximately 100% in natural abundance and is found in most

metabolites. Despite this, ^1H NMR requires good magnetic fields uniformity and longer measurements time because it suffers from a small chemical shift range. The substantial water signal must be attenuated in order to detect signals of metabolites in low concentrations (Majors, McLean, and Scholten 2008).

Alternatively, the majority of NMR investigations on living cells in bioreactor have employed ^{31}P NMR to study metabolism or ^{13}C NMR of labeled substrates to trace metabolic pathways and fluxes in real time (Hertig et al. 2021). In particular, ^{31}P NMR identified and quantified the phospho-metabolites such as ATP, ADP, NAD(P)H, and inorganic phosphate, which all of them offer insight into basal metabolism and energy level of the cells (Lippens et al. 2018; Luchinat, Cremonini, and Banci 2021). In addition to evaluation of metabolic changes, analysis of oxygen consumption is applied as a surrogate marker of aerobic energy production by mitochondrial oxidative phosphorylation (Hertig et al. 2021).

Particularly, recent metabolomics investigations offer studies of changes in the intracellular metabolism that occur in an organism in response to antibacterial compounds and even knowledge about their mode of action (Hoerr et al. 2016).

2.5.2. NMR-based metabolomics for drug discovery

For expanding drug efficacy, it is necessary understand how bacteria respond to antibiotics (Stokes et al. 2019). For many years, antibacterial drug-target interactions of the recent antibiotics have been deeply studied, showing their inhibitor effect on several essential cellular functions (Hoerr et al. 2016). Mostly of conventional antibiotics can be grouped

into cell envelope biogenesis, DNA replication, transcription and protein biosynthesis (Figure 9) (Stokes et al. 2019).

Microbial metabolomics has an essential biochemical importance for assessing metabolic changes in microorganisms (Q. Liu et al. 2017). In general, metabolism plays a principal role in cell regulation to unexpected environmental alterations. Even though various antibiotics are not involved directly in metabolism, existing evolutionary features in resistant bacteria are highly related to metabolic functions such as glycolysis, biosynthesis of amino acids, respirations and energy metabolism. Contributing to emergence of multidrug resistance, it has shown that carbon and nitrogen catabolism, redox balance, biosynthesis of triglycerides and ATP production participate in antibiotic tolerance. Although numerous high throughput studies have explained the mode of action of antibiotics, direct experimental evidence describes that rapid metabolic changes can be causal in regulating the bacterial response to those compounds (Zampieri et al. 2017).

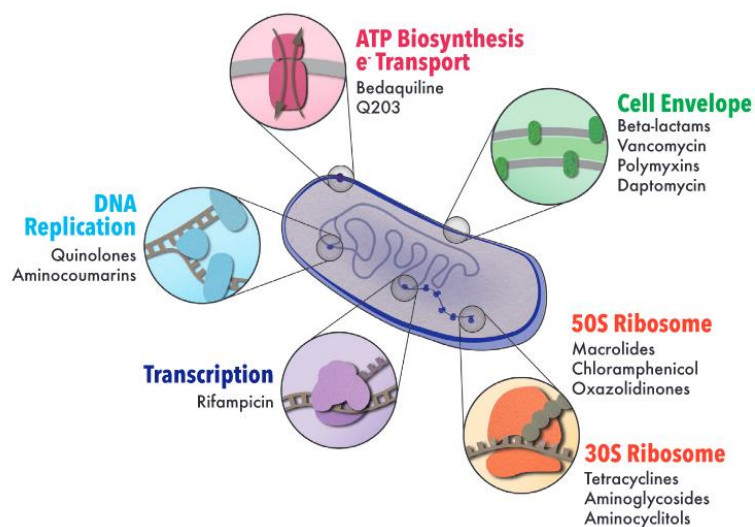


Figure 9. Cellular processes targeted by conventional antibiotics (Stokes et al. 2019).

In total, most of the metabolic yield of the cell is consumed by these processes. For that reason, it is highly possible that antibiotics can induce a significant perturbation of these energy-consuming processes which involves alterations on metabolic homeostasis. In this perspective, Stokes *et al.* (Stokes et al. 2019) defines the importance of antibiotic efficacy in terms of bacterial metabolism through three postulates: a consequence of antibiotic treatment is the alteration of the metabolic state of bacteria which may result in death or stasis; the metabolic state of bacteria impacts on susceptibility to antibiotics; and antibiotic efficacy can be improved by perturbation of the metabolic state of bacteria.

Although the development of new novel analogues of these existing antibiotics could compensate the resistance, the possible chemical modifications are finite. Therefore, the drug discovery process has changed from introducing structural variations in existing

compounds to target-based or whole cell-based high throughput screening (HTS) of massive chemical libraries to identify novel ‘hits’ (Hoerr et al. 2016). However, these drug developments procedures require to optimise the activity and determine the selectivity and toxicity of identified “hits” (Hoerr et al. 2016).

Over the last few years, proteomic, genomic and metabolomics approaches have been carried out to study the cellular processes as well as their responses to specific antibiotic stimuli and potential targets. In particular, metabolomics provides a unique methodology to identify changes in the metabolic profile in response to drugs and consequently, insights of their respective mode of action. Furthermore, various chemical methods such as mass spectrometry and NMR spectroscopy have already widened metabolic or whole-organism profiling of the microbial response to antibacterial compounds (Hoerr et al. 2016).

NMR-based metabolomics is very useful in drug discovery since it enables to characterise metabolite level perturbations and altered metabolomics pathways which helps identify protein targets for designing new drugs. Metabolic changes caused by a drug therapy may be related to the inhibition of the protein-target or as a consequence of unwanted off-target effects (Bhinderwala and Powers 2019).

The comparison between induced metabolic profile by a new drug and metabolic profiles for drugs with known mechanisms results in understanding the *in vivo* mode of action of this new chemical lead. Those compounds that share similar or same mechanisms of action may have similar impacts on the metabolome. Overall, mechanistic knowledge of *in vivo* and *in vitro* drug activity enhance the rate of the chemical lead design. Although

elucidating a mechanism of action is typically a challenge due to a time intensive task, technological improvements have decreased NMR analyses times to a few minutes per sample (Bhinderwala and Powers 2019).

Looking to the future, discovering drugs that target relevant biological processes performing a range of mechanism of action may also support disease control and combating the emergence of resistance (Bhinderwala and Powers 2019).

2.5.3. Analysing different metabolomics approaches

In terms of metabolome investigations, there are two distinct approaches: targeted and untargeted metabolomics. The first one is based on hypothetic changes that are produced in a specific or set of metabolites. In particular, this approach responds to a drug treatment, disease state, genetic changes or environmental perturbations to identify metabolites. In contrast, untargeted metabolomics follows unknown metabolites or metabolic pathways affected by these stress factors. This discovery-based metabolomics expects to monitor the entire metabolome to detect the altered metabolites or pathways. Regardless, the metabolome is compared before and after the addition of any stress factor (Powers 2014).

Both approaches should be carried out together to achieve an appropriate identification of metabolites. For those investigations, several analytical techniques can be employed for metabolomics although mass spectrometry and NMR spectroscopy are the two most commonly used methods (Nalbantoglu 2019; Powers 2014)

Other metabolomics hypothesis could be generated for screening the global composition of the intracellular metabolome (fingerprinting) or extracellular fluid metabolome

(footprinting). To date, the approaches in this field have focused on investigating alterations in the intracellular metabolism in response to these compounds. However, several studies have reported that the combination of metabolomics fingerprint and footprint analysis give rise to a more complete insights into mechanism of action of drugs. For instance, metabolic changes in *E. coli* and in the extracellular culture medium can be employed as a powerful classification tool due to different antibiotic treatments with distinct modes of action. As a result, clusters of antibiotics that target intracellular processes could be identified and separated in the fingerprint analysis (Hoerr et al. 2016; Nalsibantoglu 2019).

3. Aims

This project is based on the development of a new simple high-throughput method employing both conventional and in cell-NMR spectroscopy to assess the membrane permeability of drugs using PRE effect, firstly in lipid vesicles and subsequently in live cells. Additionally, we aim to employ a NMR-coupled bioreactor to study the mechanism of action of antimicrobials and monitor their metabolic effect. This new method would aid in the testing and design of more efficacious drugs and antimicrobial compounds in a standard chemistry/biochemistry laboratory.

PART I: *IN VITRO* ASSAY ON MEMBRANE PERMEABILITY

4. Methods

4.1. Bacteria and growth conditions

Experiments were performed on the Gram-negative bacterial strain of *E. coli* DH5 α containing CLIC1 plasmid that confers kanamycin resistance. An aliquot of these bacteria was inoculated in 10 mL of Luria broth medium and treated with 10 μ L kanamycin (50 mg/mL). The culture was incubated overnight at 37°C with shaking at 200 rpm. LB medium is comprised of 10 g/L of tryptone, 5 g/L of yeast extract and 10 g/L of NaCl in distilled water at pH 7.4. This starter culture was transferred into 1 L of fresh medium and incubated in the same previous conditions until the optical density at 600 nm was 1.6-1.8.

4.2. Preparation of Inner Membrane Vesicles

Culture was centrifuged for 10 min at 6000 rpm and 4 °C and the pellet was then resuspended into 25 mL of lysis buffer. Cells were lysed by sonication in 30 second intervals for 15 minutes. Supernatant was centrifuged at 70,000 rpm for 45 min and pellet was saved. Lipid extraction for organic solvent was applied following Folch method (Folch, Lees, and Sloane Stanely 1957). Firstly, the membrane extract was homogenized in water and then lipids were dissolved in a mixture of chloroform and methanol in a volumetric ratio of 2:1. The solution was vortexed and incubated for 1 h at room temperature in a shaker. Then phase separation was induced by adding water until getting a final volumetric ratio of chloroform, methanol and water 8:4:3. The mixture was left for 30

min at room temperature. Afterwards, the lower phase is collected. The resulting lipid film was created by drying the solvent with nitrogen or using a rotavapor, rehydrated with buffer and then sonicated for 1 h. Finally, multilamellar vesicles were extruded through a membrane with a pore size of 1000 nm to make empty unilamellar vesicles (Makowski et al. 2020).

For vesicles with glucose inside, the lipid film was rehydrated with glucose 200 mM solubilized in D₂O, sonicated for 1 h and followed by extrusion through a 100 nm pore-size membrane. Then, vesicles were precipitated at 13000 rpm for 30 min using a bench top ultracentrifuge and washed twice with D₂O.

4.3. Preparation of stock solutions

Approximately 400 µM of a stock solution was prepared for each antimicrobial compound to be tested by dissolving the required amount of the compound into 350 µL of DMSO-d₆. For SSA compounds, 400 µM of a stock solution 5 mM was prepared dissolving the required amount of the compound into HEPES buffer (10 mM HEPES and 10 mM NaCl) at 90 ° C by sonicating. As control samples, 400 µM of stock solution of glucose and indol were prepared as well as 400 µM of manganese stock for the titrations.

4.4. NMR sample preparation

Prior to use, tubes were washed with water and dried under a stream of nitrogen gas. Samples were brought to a total final volume of 600 µL or 300 µL was transferred to clean

6 mm tubes and 3 mm tubes, respectively, including 5% D₂O and 0.01 mM of DSS as internal standard reference.

Each assay measured permeability of the compound added to the lipids individually. With a long glass pipette, 30 μ L of the lipid vesicles were transferred to a 3 mm NMR tube for measurement. Negative control assay employed glucose at 4 mM. For positive assay, indol was added at 2 mM. For test assay, a wide range of two types of unspecified industry compounds was utilized.

The sample- for ¹H-³¹P NMR analysis was prepared dissolving approximately 10 mg in 300 μ L of a solvent mixture (75% CDCl₃, 25% MeOD, 0.315 mM TMP and 0.05 % TMS).

4.5. NMR acquisition

The 1D ¹H NMR and ¹H CPMG spectra were collected using a Bruker Avance III spectrometer at a proton frequency of 600 MHz and recorded at 298 K. This spectrometer is equipped with a QCIP cryoprobe with a standard 31P pre-amplifier without enhance sensitivity from cryogenic cooling. 1D ¹H NMR spectra were acquired using the standard zgpcpmg pulse sequence from the Bruker library, though it was modified with an excitation water suppression element (1D ¹H WATERGATE) to ensure elimination of water signal for all experiments. That was achieved with 3-9-19 watergate sequence using 1 ms pulses (Barbieri et al., 2016; Hoerr et al., 2016).

The following acquisition parameters were used: spectral width of 12 ppm, relaxation delay of 10 μ s and acquisition time of 1.02 s at a power of 7.9W. All data was collected

with 32768 points and receiver gain was set to 256 with an accumulation time of 32 scans and 8 dummy scans. The CPMG component had three different spin-lock times to reach differences between unbound, lightly and strong ligands to the membrane: 20 ms, 50 ms and 150 ms.

The CPMG element was collected at three different CPMG spin-lock times: 20 ms, 50 ms and 150 ms; after a selection process between 20 ms and 300 ms. The rest of parameters were the same as the 1D ^1H NMR experiment except the relaxation delay that was 1 ms and an acquisition time of 1.02 ms.

4.6. Lipid quantification

^1H - ^{31}P HSQC spectrum was collected using the pulse program na_hsqcctf3gpxy using 32 scans and 4 dummy scans and with an acquisition time of 0.04 s for F1 and 0.07 s for F2. Processing 1D ^{31}P skyline projection of the ^1H - ^{31}P HSQC spectra, quantity of lipids was calculated through integrals for TMP and each phospholipid peak using MestReNova (Mestrelab Research) software. The percentage of each type of phospholipid was estimated, PE and PG, using the ratio of each one integral over the sum of the integrals of all phospholipids (Appendix2, Figure 37).

4.7. NMR Data Collection and Processing

TOPSPIN (Bruker) software was used to obtain data in NMR spectroscopy. All spectra were automatically or manually corrected for phase and baseline distortions using a polynomial function and calibrated to the centre of DSS peak (at 0 ppm) using

MestReNova software. Also, 2D spectra were calibrated to the centre of TMP peak. In addition, this software was employed for overlaying spectra, peak picking and integrations in order to calculate composition proportions. While the 1D ^1H NMR and ^1H CPMG spectra were utilized for the permeability assays, 2D ^1H - ^{31}P HSQC spectra were used for the determination of lipid composition.

4.8. Calculation of permeability and membrane interaction parameters

Novel permeability and membrane interaction parameters for a set of compounds were determined in lipid vesicles using data of NMR spectroscopy.

For the statistical analysis, the average of the peak heights of each type of compound tested was used to calculate the effective drug permeability (P) parameter. The membrane permeability of controls and SSA compounds tested was calculated at each CPMG time from samples with and without vesicles as well as at each concentration of manganese using the following relation:

$$P = \frac{P_1}{P_2}$$

where P_1 is the result of dividing the peak intensity at each manganese concentration (0.5 mM, 2 mM or 4 mM) by the peak intensity in the absence of manganese from samples with vesicles and P_2 from samples without vesicles.

To assess membrane interaction, only data of samples without manganese was applied. The membrane interaction (MI) parameter was calculated as the division between each CPMG spin-lock time of the two type of samples for each compound:

$$MI = \frac{CPMG(X1)}{CPMG(X2)}$$

where X_1 and X_2 are the same CPMG spin-lock times for sample without and with vesicles respectively.

To examine if the membrane interaction data is a result of the actual interaction between the small molecule and the membrane or due to self-association of compounds, we estimated the self-association value (SA) taking the ratio between longest and shortest CPMG times according to the following equation:

$$SA = \frac{CPMG(20)}{CPMG(150)}$$

only taking the data of samples without vesicles and manganese.

5. Results

Crossing both the Gram-positive or negative bacterial membranes is a challenge in antibiotic development. The lack of new tools to predict permeability of small molecules in bacterial membranes drove us to develop a new approach to evaluate the membrane interaction and permeation of diverse compounds into vesicles with different lipid

composition. To determine these properties we made use of PRE effect and different CPMG spin-lock times and introduced two new parameters that enable the classification of compounds depending on their behaviour with lipid membranes.

5.1. Comparison of CPMG experiments at different PRE reagent concentrations

In this assay we tested whether the addition of manganese only to the buffer along with the lipid vesicles and a compound will display a distinct effect on the ^1H NMR peak intensities due to the different modulation of T1 and T2 values. This would mean that the solvent PRE reagent allows identifying different permeation rates. Furthermore, as the CPMG pulse sequence is a NMR T2 filtering technique, CPMG filter is able to suppress the resonances from molecules with long correlations times. Three different CPMG spin-lock times were used to maximise the PRE effect on T2 relaxation and to enhance the distinction between molecules with different permeation rates.

The addition to PRE reagents has demonstrated an enhancement of sensitivity in NMR experiments. Manganese as the PRE reagent used in this study was added to the control in different concentrations. It is important to point out that this ion cannot cross the membrane and causes broadening of all molecule signals in the exterior of the vesicle, so all the signals from molecules that can cross the bilayer will be less affected by manganese (Figure 10). The concentration of the PRE agent is tuneable so the appropriate amount needed to achieve the desired effect has to be determined.

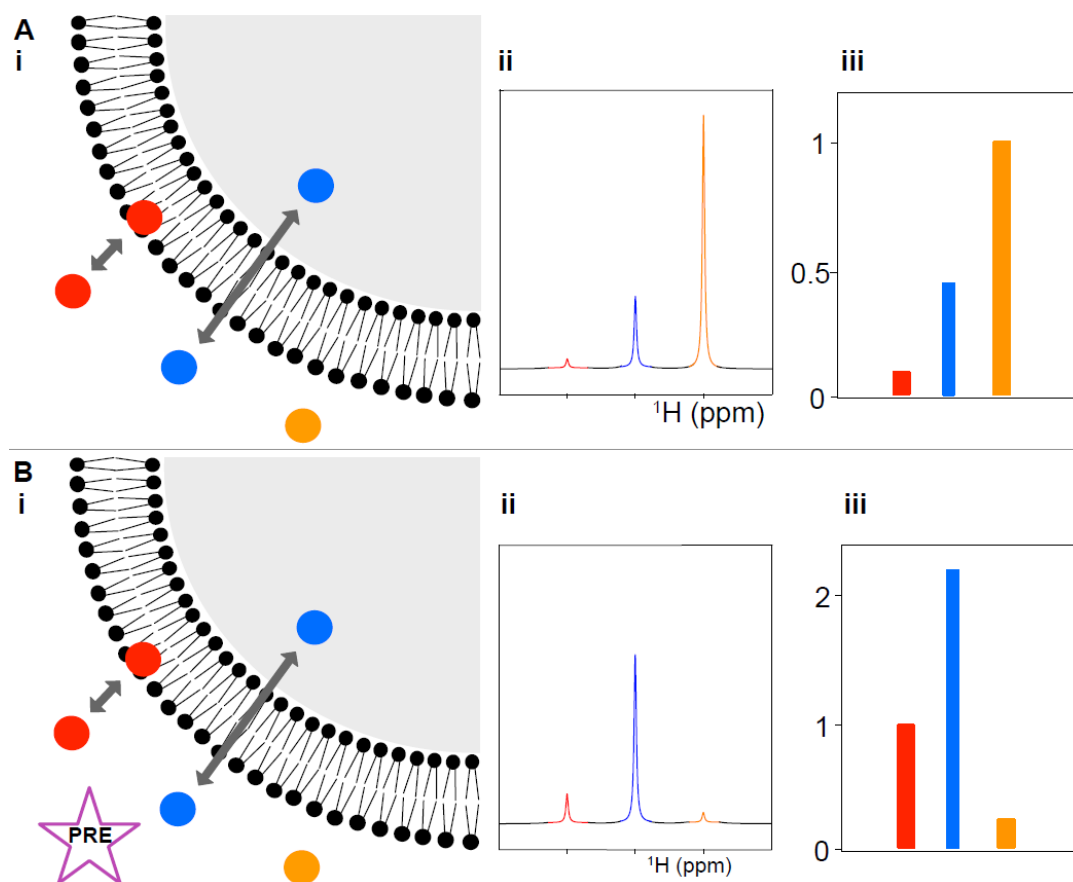


Figure 10. Schematic comparison between NMR permeation assays in presence or absence of a PRE agent. Three types of molecules are represented by a coloured sphere (red for a membrane interacting molecule, blue for a fully membrane-permeable molecule, and orange for a non-membrane permeable molecule). In a first experiment (A-i), drug(s) are mixed with vesicles, and 1D ^1H CPMG NMR spectra are collected. The expected spectrum is shown for each type of molecule (A-ii). A second experiment is collected with the same drug(s) and vesicle composition, but in the presence of a solvent PRE (B-i), with the expected spectra for each type of molecule shown in (B-middle). The ^1H intensities of each drug are normalised using a control experiment without vesicles. Finally, the membrane interaction (A-iii) and

permeation factors (B-iii) of each drug can be calculated using the ratio between the normalised intensities in the presence and absence of solvent PRE, with the expected factors shown in red (molecule attaching to the membrane), blue (membrane-permeable molecule) and orange (membrane impermeable molecule).

The controls used in this study have been selected because glucose cannot permeate the membrane in absence of carriers that facilitates their entrance into the cell while indol is a highly permeable molecule. When these two molecules are treated with manganese in absence of lipid vesicles, the PRE reagent does not produce a significant effect on them as can be observed in signals amplitude at the two smaller concentrations (0.5 mM and 2 mM) of this ion (Figure 11A).

The results showed in the Figure 11A and 11B display that glucose shows a significant drop of its ^1H intensities in the presence of Mn^{2+} independently on presence or absence of lipid vesicles. In addition, its signals are much broader when an increasing concentration of manganese is added. On the other hand, indol shows an opposite effect. While in the absence of vesicles, Mn^{2+} induced line broadening, we observed the converse effect in the presence of lipid vesicles showing an increase in the signal intensities.

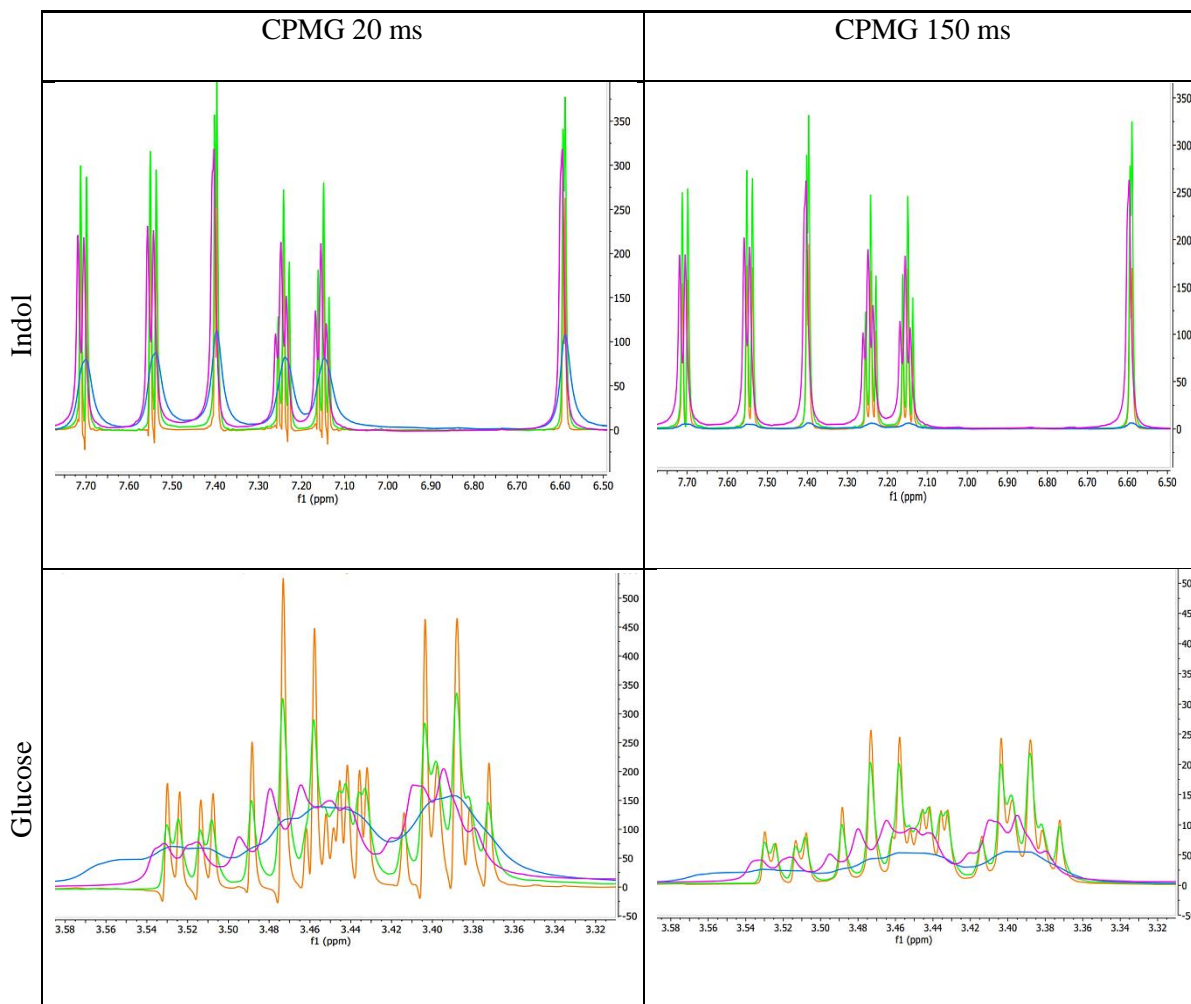
In terms of CPMG experiment, we employed different CPMG spin-lock times between 20 and 300 ms. After analysing the effect on controls, the CPMG spin-lock times selected were 20, 50 and 150 ms at which we observed the wanted results for both molecules: reduced or eliminated signals from vesicles and bound ligands. Figure 11A and 11B present

the shortest and longest collected CPMG times to evidence the great difference of the impact of CPMG pulse sequence between in glucose and indol.

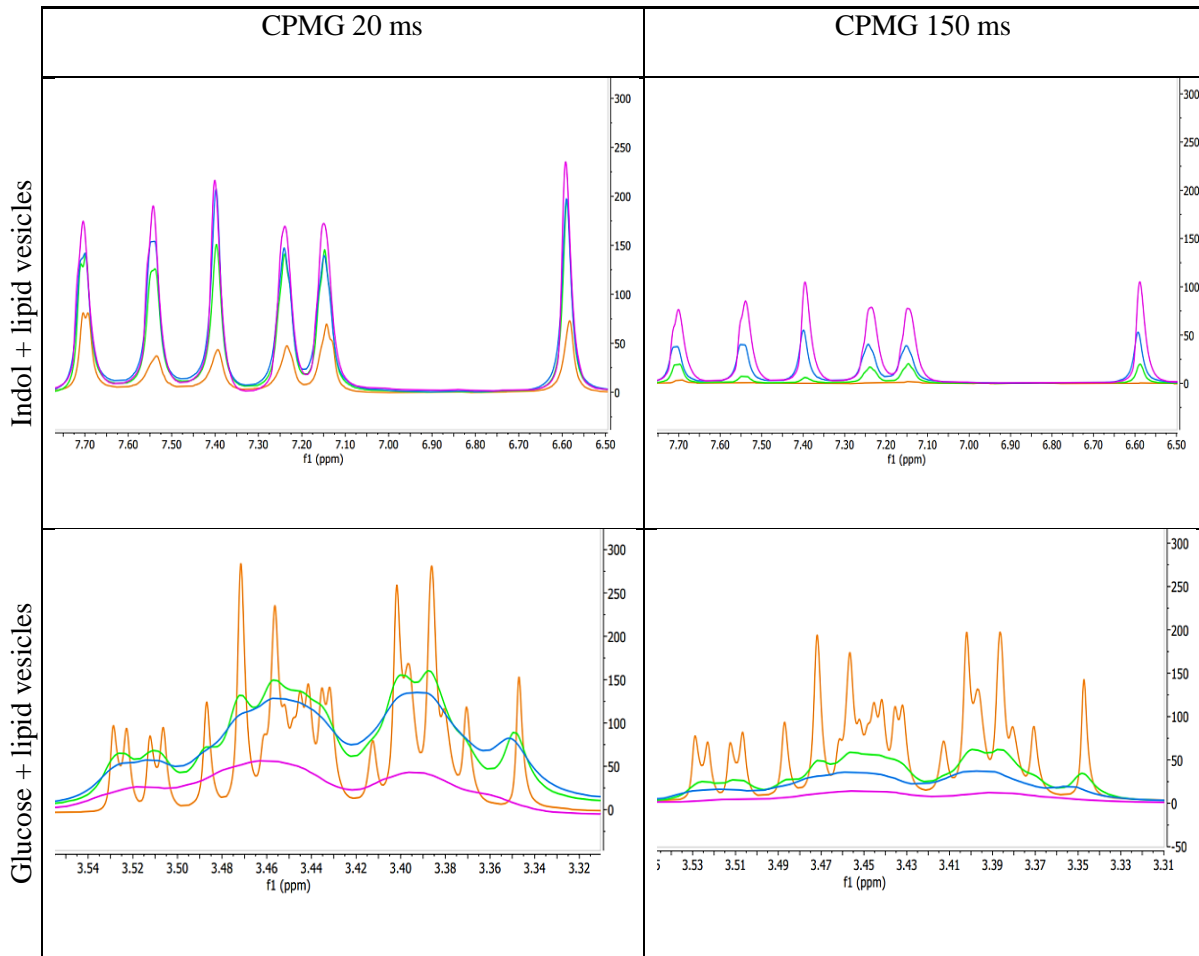
Moreover, Figure 11C illustrates the clear effect on permeability rate in presence of lipid vesicles at an increasing concentration of Mn^{2+} at the three CPMG spin-lock times: drop in signal intensity for glucose and the opposite effect for indol. Compellingly, a small amount of PRE reagent (0.5 mM) is sufficient to cause this significant effect on these two molecules.

All together, CPMG and PRE effects produce different results in indol and glucose, in other words, in permeable and non-permeable molecules. This distinction allows us to define the permeability of any molecule analysing its behaviour in presence or absence of lipid vesicles.

A)



B)



C)

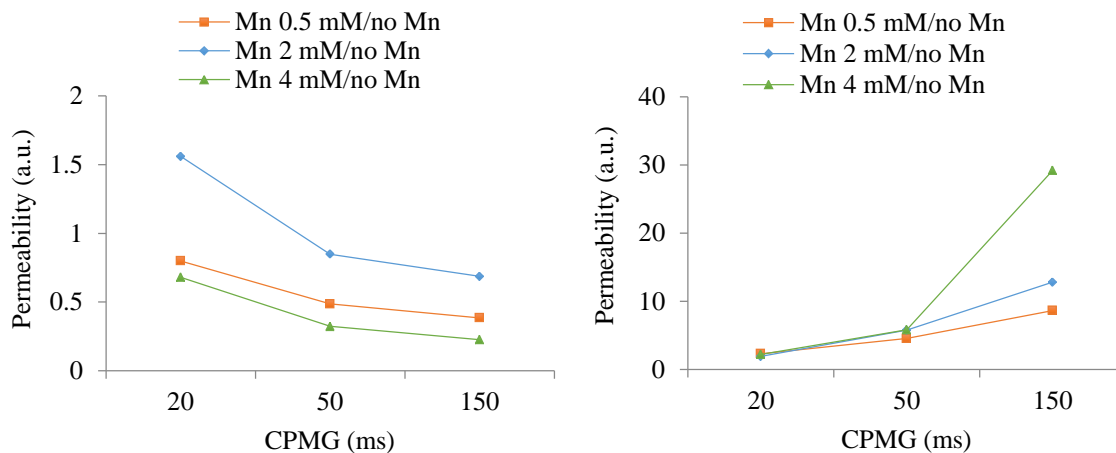


Figure 11. A) Spectra of controls samples (indol and glucose) treated with different concentrations of manganese: 0 mM (orange); 0.5 mM (green); 2 mM (blue); 4 mM (magenta). B) Spectra of samples containing lipid vesicles and controls treated with different concentrations of manganese: 0 mM (orange); 0.5 mM (green); 2 mM (blue); 4 mM (magenta). C) Permeability rate of glucose (right) and indol (left) tested in lipid vesicles at the three different concentrations of Mn^{2+} and spin-lock times. Units for permeability rate define as arbitrary units (a.u.).

5.2. Variation of T1 and T2 relaxation times in controls

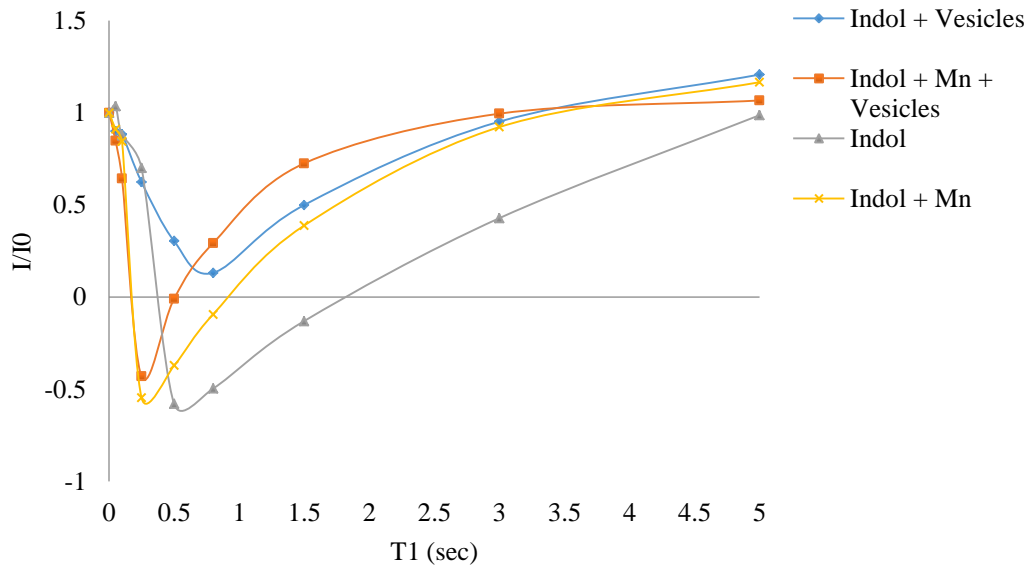
While the differences in broadening produced by Mn^{2+} between glucose and indol are the expected, we observed an increase of intensity of indol signals in the presence of vesicles that was unexpected. To understand in greater detail the PRE effect of Mn^{2+} in the relaxation properties of permeable and non-permeable compounds, T1 and T2 ^1H spin relaxation were measured for glucose and indol in the absence and presence of Mn^{2+} with and without vesicles.

Interestingly, Mn^{2+} produced a reduction in T1 in the presence of vesicles, thus resulting in more elevated signals when spectra were acquired with relaxation delays below 3 second, explaining the increase in intensity of indol signals in the presence of both Mn^{2+} and vesicles (Figure 12A). We found no change in the behaviour of glucose in presence and absence of vesicles and the same for glucose in presence and absence of Mn^{2+} which would indicate that the PRE reagent reduced T1 similarly in samples of glucose with and without vesicles because this molecule did not permeate into vesicles (Figure 12B).

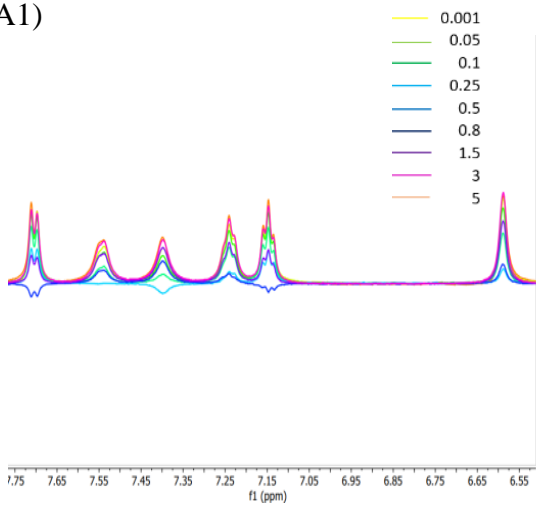
Regarding T2 relaxation, we observed that Mn^{2+} shortened T2 in indol (Figure 13A) while did the opposite effect in glucose (Figure 13B). In the presence of vesicles, the impact of Mn^{2+} on this transverse relaxation time constant was higher for indol than for glucose, but neglectable compared to the effects on T1.

In summary, we have found that the main action of Mn^{2+} as a PRE reagent in the presence of vesicles is to shorten 1H T1 rates, reducing the intensity of signals from non-permeable molecules and enhancing those from-highly permeable compounds.

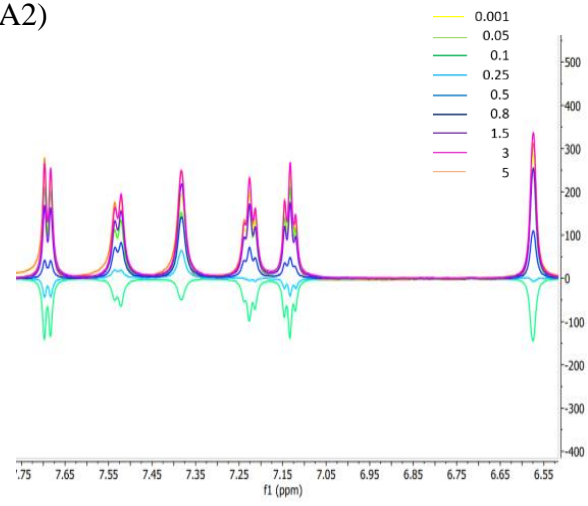
A)



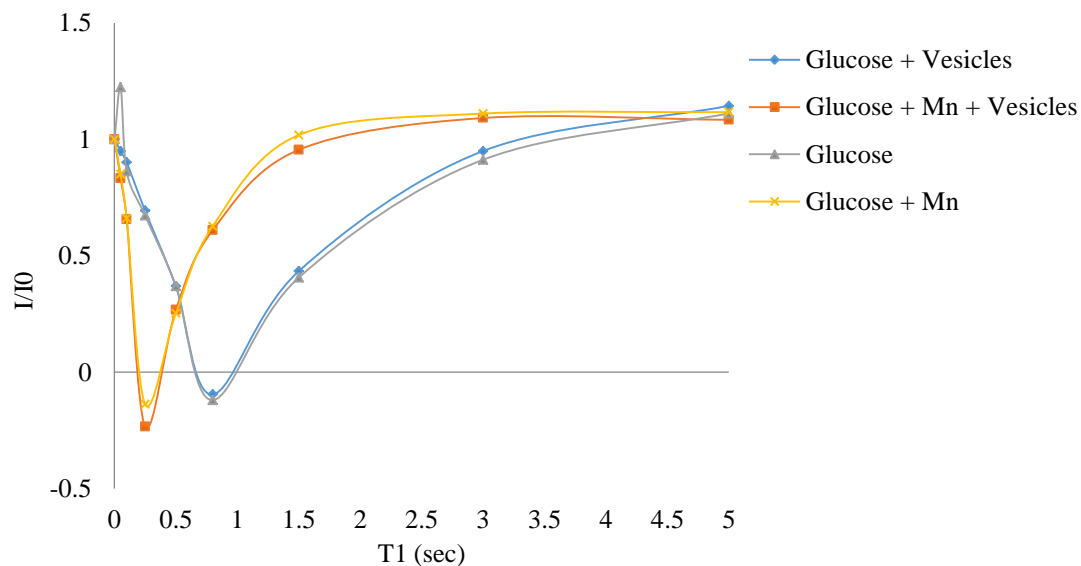
A1)



A2)



B)



B1)

B2)

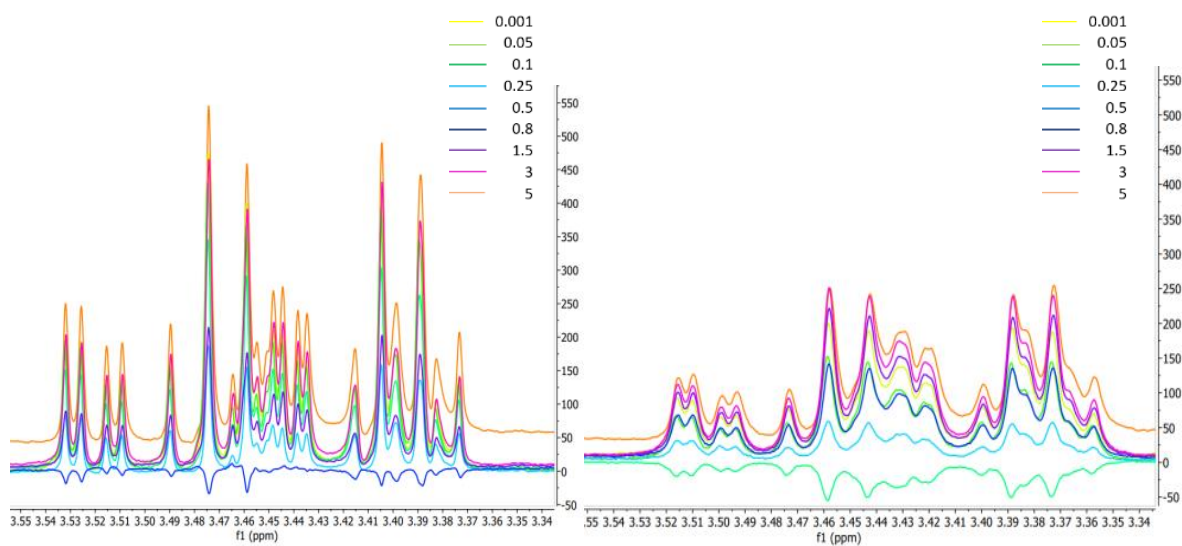
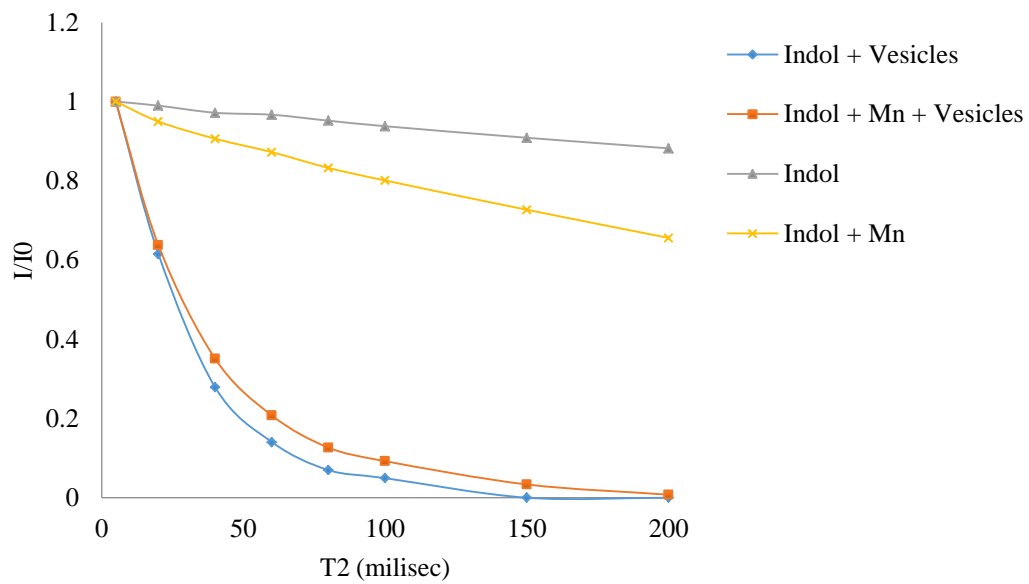
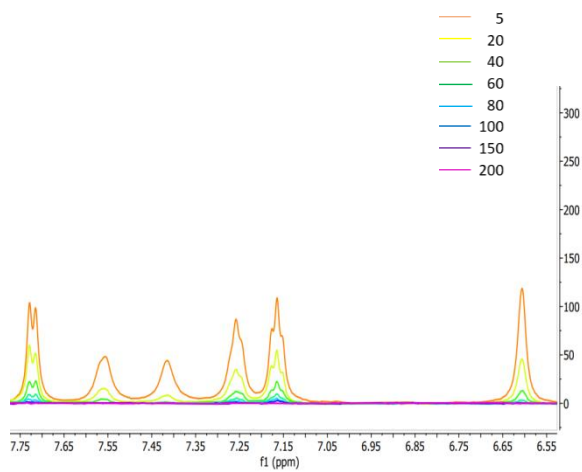


Figure 12. Variation of T1 in indol (A) and glucose (B) samples with their respective 1D ^1H NMR spectra (A1 and B1 from vesicles in absence of Mn^{2+} , A2 and B2 from vesicles treated with Mn^{2+}).

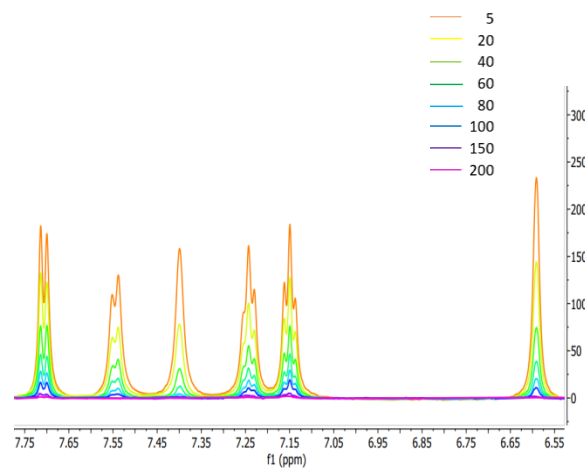
A)



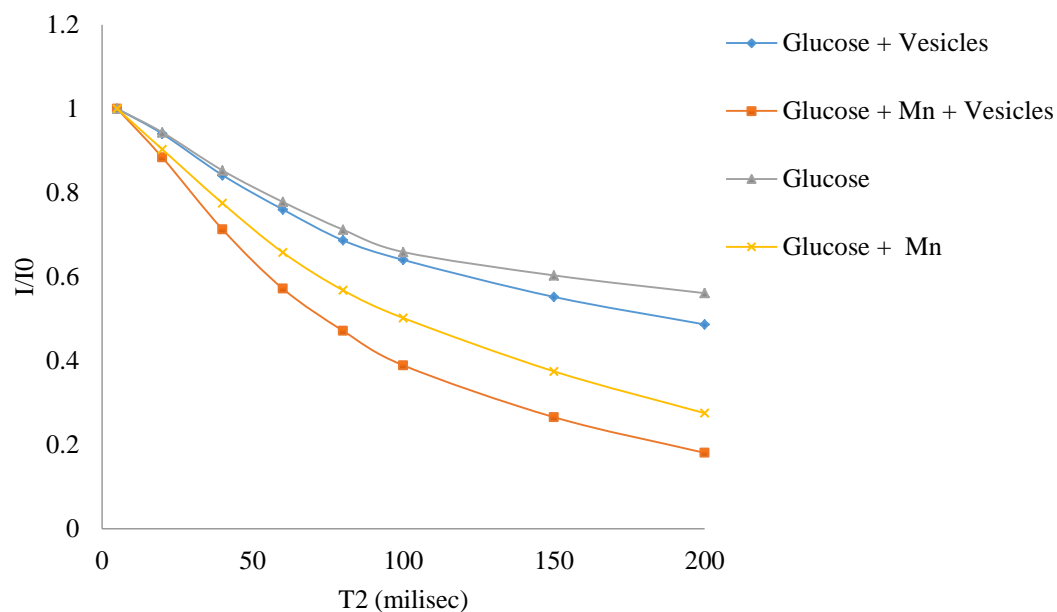
A1)



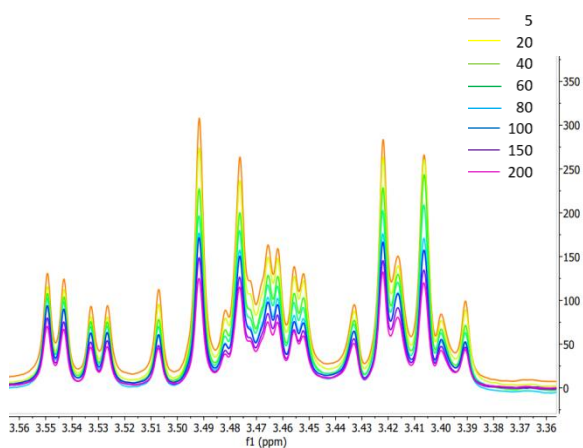
A2)



B)



B1)



B2)

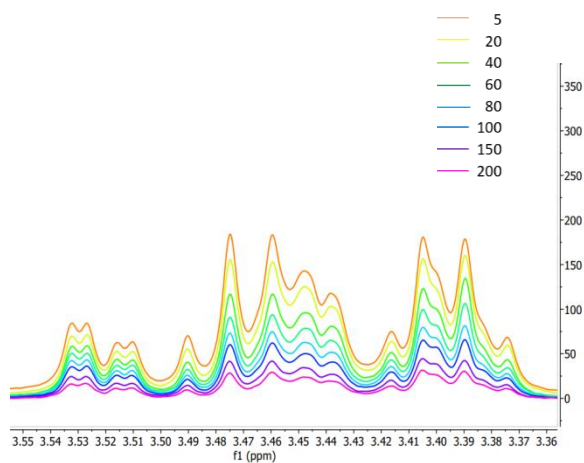


Figure 13. Variation of T2 in indol (A) and glucose (B) samples with their respective 1D ^1H NMR spectra (A1 and B1 from vesicles in absence of Mn^{2+} , A2 and B2 from vesicles treated with Mn^{2+}).

5.3. Quantification of permeability *in vitro*

Making use of the differences in intensity of signals from molecules of different permeability in the absence and presence of vesicles due to the addition of a soluble PRE reagent, we wanted to evaluate compound permeability in bacteria using a panel of antimicrobial agents. We initially assessed the permeability these compounds in membrane vesicles from *E. coli*.

The permeation rate on the PRE effect of ^1H intensities can be parametrised by comparing the intensity ratios of ^1H resonances in ^1H 1D CPMG experiments with the same CPMG spin-lock times with and without Mn^{2+} in the presence and absence of lipid vesicles. With that, a permeability value of 1 indicates no detectable permeation through the vesicles. This permeability factor and its variation at different spin-lock times can be used to compare the permeability of different compounds in vesicles with the same composition or to evaluate the permeation of a specific compound in vesicles with different lipid composition.

Using the measured experimental permeability values at the three CPMG spin-lock times (Table 1), we are able to divide our data into different categories: impermeable, hardly permeable, slightly permeable and highly permeable. The four impermeable compounds were glucose, SSA29, 48 and 57 at the lowest concentration of Mn^{2+} . However, together with indol, SSA60 was the antimicrobial with greatest permeability. SSA30 permeated lipid vesicles hardly while SSA32 showed more permeation. Following the selected analysis for indol and glucose, the spectra of SSAs in presence and absence of vesicles and Mn^{2+} were

employed to parametrised the permeation rate and interaction membrane (Appendix1, Figures 25-36).

Compound	Permeability			Permeation category
	CPMG 20 ms	CPMG 50 ms	CPMG 150 ms	
Glucose	0.520	0.488	0.385	No permeable
Indol	2.305	4.551	8.641	Highly permeable
SSA29	0.779	0.698	0.531	No permeable
SSA30	1.123	1.168	1.132	Hardly permeable
SSA32	1.386	1.744	1.558	Slightly permeable
SSA48	0.409	0.450	0	No permeable
SSA57	0.920	0.989	0.986	No permeable
SSA60	5.297	5.477	6.602	Highly permeable

Table 1. Predicted permeability for the set of control and SSA compounds at concentration of manganese 0.5 mM.

5.4. Quantification of membrane interaction *in vitro*

The modulation in the signal intensity of the spin-lock time in the CPMG sequences is related to the residence time of a small molecule with a large macromolecule, and thus with its affinity. The comparison of signal intensity of small molecules at different spin-lock times can therefore be used to quickly assess and compare the affinity of small molecules with lipid bilayers.

Hence, similar to permeation quantifications, the intensity ratio between ^1H resonances in ^1H 1D CPMG experiments with the same CPMG spin-lock times in the presence and absence of lipid vesicles report on the degree of interaction between small molecules and the lipid membrane, with a value of 1 implies no detectable membrane interaction whereas a value below 1 means detectable membrane interaction. Hence, The observation of the change of the membrane interaction parameter at each CPMG spin-lock time indicates the binding affinity of a compound to the membrane; this affinity is high at the CPMG spin-lock time deviated from 1 is observed (Table 2).

From the whole set of compounds tested; only indol, SSA48 and 60 presented significant interaction with the membrane. Moreover, indol and SSA60 exhibited great binding affinity even at the shortest CPMG spin-lock time (Table 2).

Compound	Membrane interaction (no Mn ²⁺)			Membrane Interaction category
	CPMG 20 ms	CPMG 50 ms	CPMG 150 ms	
Glucose	0.750	0.843	0.748	No interaction
Indol	0.334	0.119	0.021	Interaction
SSA29	1.017	0.997	0.911	No interaction
SSA30	1.070	1.063	1.015	No interaction
SSA32	1.566	1.529	1.466	No interaction
SSA48	1.211	0.978	0.304	Interaction
SSA57	0.920	0.900	0.753	No interaction
SSA60	0.631	0.425	0.186	Interaction

Table 2. Membrane interaction data for the set of control and SSA compounds.

The previous both parameters rely on intensities extracted from ¹H 1D CPMG spectra and therefore the molecules studies must not fully self-associate in solution at the concentrations used for the assay.

To ensure that the drop in CPMG spin-lock times was due to the interaction with the membrane, we evaluated the propensity of the SSA compounds to self-associate. The ratio between the longest (150 ms) and shortest (20 ms) CPMG spin-lock times can be used as a parameter to identify the self-association of the compounds since any loss of macromolecule signal at longest CPMG would arise from the compound tendency to self-associate, with parameter values close to 0. However, a value of 1 would discard the presence of self-association.

Firstly, we studied this self-association parameter in control samples, glucose and indol. The latter presented self-association as it was expected. However, glucose displayed a significant self-association which could come from chemical conformations. Although the results given in Table 3 report that SSA60 and SSA48 could present slight self-association, higher in SSA48, the expected interactions arise also from compound-vesicles.

Compound	Self-association Parameter
Glucose	0.707
Indol	0.954
SSA29	0.921
SSA30	0.886
SSA32	0.912
SSA48	0.306
SSA57	0.825
SSA60	0.516

Table 3. Self-association values for control and set of SSA compounds.

5.5. Permeability and membrane interaction of SSA compounds in cancer membrane vesicles

After measuring the membrane permeability of these compounds in lipid vesicles from *E. coli*, we tested them in membrane vesicles obtained from two distinct cancer cell lines:

non Cisplatin-resistant cells from the A2780 cell line and Cisplatin-resistant A2780 cell line.

As it shown in Table 4, the resulting data showed differences in the permeability of some compounds depending on the lipid composition of the membrane. SSA29 and 60 showed more interaction in lipid vesicles from resistant cells than non-resistant ones. However, SSA30, 32 and 57 performed the opposite action. We observed than SSA48 did not permeate any of type of lipid vesicles.

Compound	Permeability			Permeation category
	CPMG 20 ms	CPMG 50 ms	CPMG 150 ms	
SSA29	0.949	0.913	3.676	Highly permeable
	1.096	1.089	1.114	Hardly permeable
SSA30	1.186	1.289	1.419	Slightly permeable
	1.663	1.979	3.217	Highly permeable
SSA32	1.257	1.201	1.285	Slightly permeable
	1.367	1.479	1.929	Highly Permeable
SSA48	0.584	0.678	0.693	No permeable
	0.544	0.602	0.648	No permeable
SSA57	0.896	0.842	0.907	No permeable
	0.920	0.993	1.182	Hardly permeable
SSA60	6.545	8.157	10.585	Highly permeable
	4.212	4.162	3.441	Highly permeable

Table 4. Predicted permeability category for the set of SSA compounds at concentration of manganese 0.5 mM in two types of cancer membrane vesicles: resistant (green) and no resistant (yellow) cells.

Using the data in the absence of Mn^{2+} we determined the affinity of each compound towards the two different lipid compositions, reminding that more affinity to the membrane when lower value at that CPMG spin-lock time is observed.

We observed that SSA29 showed a very different affinity towards lipids from the Cis-resistant and non-resistant cell lines, presenting a higher affinity towards lipids from the non-resistant cells. SSA30, 32 and 57 also presented a stronger interaction with non Cis-resistant cells, while SSA60 showed very similar affinity to both lipid compositions. We found that SSA48 showed membrane interaction values considerably higher than 1 which could be related to the self-association that this compound presents (Table 5).

Compound	Membrane interaction (no Mn ²⁺)			Membrane interaction category
	CPMG 20 ms	CPMG 50 ms	CPMG 150 ms	
SSA29	1.112	1.111	0.247	Interaction
	0.434	0.436	0.435	Interaction
SSA30	0.813	0.824	0.873	No interaction
	0.550	0.554	0.565	No interaction
SSA32	1.346	1.378	1.391	No interaction
	0.754	0.763	0.768	No interaction
SSA48	2.677	3.091	4.645	No interaction
	2.076	2.250	3.031	No interaction
SSA57	1.124	1.292	1.311	No interaction
	0.540	0.550	0.532	No interaction
SSA60	0.669	0.497	0.335	Interaction
	0.410	0.368	0.326	Interaction

Table 5. Membrane interaction category for SSA compounds in two types of cancer membrane vesicles: resistant (green) and no resistant (yellow) cells.

6. Discussion

6.1. Measuring permeability, interaction and self-association of compounds

The permeability of small molecules across bacterial membranes remains poorly understood, and the development of novel methods to predict compound penetration is critically important to understand *in vivo* efficacy of candidate drugs. In this study, we introduce the use of a novel NMR strategy that employs 1D ^1H CPMG experiments and PRE effect for the determination of the permeability rate and binding affinity of a compound in different lipid membrane vesicles.

A CPMG pulse sequence is applied due to its sensitivity to elevated transverse relaxation resulting from the interaction of small molecules with larger macromolecules like lipid vesicles, and the solvent PRE effect, which further increases the transverse relaxation of molecules, is exploited to maximise the difference between compounds able to permeate through the membrane into the PRE-free interior of the vesicle and the PRE-loaded outside.

We have employed this approach to evaluate and classify the permeation rates and membrane interaction of a set of SSAs compounds. To date, compounds of SSA family have been shown to: (i) act as broad spectrum antimicrobial agents (ii) have the potential to act as drug delivery vehicles (iii) enhance the activity of currently used antimicrobial agents against both bacteria and (iv) enhance the activity of the anticancer agent cisplatin against ovarian cancer cells. The hypothesised basis for the therapeutic activity of this class of related compounds includes the ability of these agents to selectively coordinate with phospholipids of different head group composition and permeate into the cell.

Significant differences can be observed in the permeability of these compounds with SSA60 showing the highest permeability and membrane interaction affinity. SSA32 also shows very moderate permeability, although no detectable membrane interaction, an indication of its low affinity for *E. coli* lipid vesicles. SSA57 shows no detectable permeation, but noticeable membrane interaction. SSA29 and SSA30 show no detectable membrane permeation or interaction.

Recently, Boles and co-workers (Boles et al. 2022) reported that derivation of SSAs structures impacts on SSA molecular self-association, aggregation formation and biological efficacy properties which is consistent with our results. In this study, computational modelling methods were employed to understand the antibacterial activity of SSAs in distinct synthetic phospholipid vesicles by head group SSA interaction studies.

The findings of these simple computational studies indicated that SSAs with simplest structures have greater binding affinity towards bacterial membranes than those of normal mammalian cell (prevalent lipids PE and PG over PC, respectively). As we have shown in Tables 2 and 5, presenting SSA29, 30 and 32 a basic structure, these compounds exhibited more interaction and affinity towards lipid vesicles from ovarian cancer cells than those from *E. coli*. SSA48 did not show interaction with any type of lipid vesicles while Boles and co-workers (Boles et al. 2022) reported that this compound exhibited strong interaction with all phospholipid vesicles. However, SSA60 presented affinity preferably towards lipids from *E. coli* in both studies.

In addition to Boles group, Bennion *et al.* (Bennion et al. 2017) used also computational methodology as a strategy for the prediction of permeability. This group have focused on the development of a computation model that predicts the *in vitro* PAMPA-defined permeability level of a set of compounds across a physiological lipid membrane validating a model based on an umbrella sampling molecular dynamics. Furthermore, this study compares the semi-quantitative permeability prediction results to a high-throughput LogP calculation method which is extremely inaccurate in characterising the permeability of the compounds. LogP calculation method shows a large proportion of false negatives thereby excluding promising leads. As our study, Bennion group divided the permeability data into four categories: high, medium, low permeability and impermeable.

Although permeability of candidate compounds presents limitations that can divert the development process, computational model systems would become as a first filter for permeation. However, the computational time required in this type of studies is still less than the procedure period for novel compound design (Bennion et al. 2017).

Similar to our method, Ferreira and Kasson (Ferreira and Kasson 2019) developed an outer membrane vesicle swelling assay to measure small molecules (glycine, glucose, sucrose and known antibiotics) permeation across the bacterial outer membrane, specifically through OmpF from *E. coli*. It is evident that glucose showed also low permeability.

6.2. Relaxation modification for detection of ligand binding

Since ^1H T1 and T2 relaxation rates depend primarily on the molecular rotational correlation time, the addition of a PRE reagent to a sample offers a reduction in

experimental time by decreasing T1 much intensively than T2 values for small molecules. Nevertheless, the effect on T2 can be enlarged by employing different CPMG pulse sequences. Some studies have used gadolinium as a PRE reagent that accelerates the relaxation of small molecules such as metabolites, reducing T1 relaxation time from 2 to 10-fold depending on the concentration of this ion really reducing the T1 relaxation time (Honrao et al. 2021; Mulder, Tenori, and Luchinat 2019).

Hajduk *et al.* (Hajduk, Olejniczak, and Fesik 1997) described a NMR-based method for screening compounds that binds to proteins or other macromolecules without the need of isotopically labelled targets. This approach employs the change in the relaxation or diffusion rates of small molecules when upon binding to any biomolecule. For detection of ligand binding, ^1H NMR spectra were acquired with a CPMG spin-lock time of 400 ms to minimise or eliminate the signals of the protein or bound ligands without affecting the unbound molecules signals.

The previous described method mentions that an optimal strategy employing multiple spin-lock times would determine the affinity level of ligands. With this, long spin-lock times could be employed to find weak binding ligands while shorter spin-lock times would detect higher-affinity ligands (Hajduk, Olejniczak, and Fesik 1997). However, the experiments were carried out only with CPMG 400 ms. Since we have applied in our study a range of CPMG spin-lock times (20 ms, 50 ms and 150 ms) would offer a system to define precisely the affinity for those SSA compounds that have presented interaction with the lipid membrane vesicles. In this way, the result from analysing which minimal CPMG spin lock time is needed for each sample would determine the binding affinity of these compounds.

PART II: *IN VIVO* ASSAY TO MONITOR DRUG INTERNALISATION

7. Methods

7.1. Cultivation of *E. coli*

E. coli DH5 α used in this study were pre-cultivated in 5 mL Luria-Bertani broth (LB) with 10 μ L of kanamycin (50 mg/mL) at 37°C for 4 h and then this culture were transferred to 150 mL of LB medium and was incubated overnight to obtain viable cells. Afterwards, cells were recovered by centrifugation at 2500 rpm for 10 min and resuspended in 10 mL of LB medium containing 2 g/L sodium alginate previously autoclaved at 121 °C for 20 min, at pH 7.4, for the immobilization procedure.

7.2. Cultivation and encapsulation of *E. coli* cells in calcium alginate beads

Calcium alginate beads were prepared by gelation procedure using Ca²⁺ ions as a cross-linking agent (Bassani et al. 2019). The previous culture was incubated at 37 °C for 2 h. Beads formation was performed by dropping this mixture into a gently shaking solution of 150 mM CaCl₂ (100 mL) under magnetic stirring at room temperature. The cell solution was forced and streamed into the calcium chloride solution aided by a peristaltic pump (10 mL/min flow rate) via 1 mL syringe equipped with a 26-gauge needle (0.13 mm diameter). The beads were formed when the sodium alginate-cell suspension contacted a calcium chloride solution as the Ca²⁺ ions polymerize the alginate resulting in beads containing the cells (Figure 14). Immediately, the CaCl₂ solution was removed, and the beads were washed with the phosphate-free minimal medium [M9 buffer (50 mM HEPES, 5.3 mM

KCl and 0.5 g/L NaCl at pH 7.4) supplemented 0.8 mM $\text{MgSO}_4 \cdot 7\text{H}_2\text{O}$, 2 mM CaCl_2 , 1mg/mL NH_4Cl , 4g/L glucose, 1 mg/mL thiamine] three times. This medium was previously autoclaved at 121°C and degassed to avoid air bubbles in the NMR flow tube during the experiment. After washing, the encapsulated cells were left in latter solution and placed inside flow NMR tube using a Pasteur pipette (Sharaf et al. 2010).



Figure 14. Schematic of cells encapsulation device.

7.3. Viability assay of *E. coli* cells in calcium alginate beads

Viability of encapsulated *E. coli* cells was measured spectrophotometrically by using the MTT-type oxidoreductase reagent WST-8 as a qualitative and simple method. The viability was assessed at different points: immediately after casting and after a given amount of time (30 min, 1 h, 2 h and 4 h) both under flow conditions (in the NMR bioreactor at 37 °C, 0.2

mL/min flow). Few beads were recovered from the NMR tube with a Pasteur pipet and transferred to an Eppendorf tube and residual minimal medium was removed and beads were dissolved in 10 mL of PBS (pH 7.4) at room temperature under stirring conditions for 10 min. The suspension was centrifuged at 370 x g for 5 min.

A sterile stock solution of the MTT reagent at a concentration of 5 mg/mL was prepared in PBS (pH 7.4), mixed by vortexing and stored at 4 °C in the dark. PBS solution (1X, 500 mL) was composed of: 68 mM NaCl, 1.3 mM KCl, 5 mM Na₂HPO₄, 0.9 mM KH₂PO₄, 0.5 mM CaCl₂*2H₂O, 0.25 mM MgCl₂*6H₂O, dissolved in dH₂O. An aliquot of this MTT solution (20 uL) was added to the cell suspension and incubated at 37 °C, 5% CO₂ atmosphere for 24 h until the formation of formazan crystals after the action of cellular NADPH-dependent oxidoreductases. Afterwards, approximately 500 uL of beads suspension with the formazan crystals was centrifuged at rpm for 10 min. The formazan crystals produced in bacterial cells were dissolved in 1 mL of DMSO to get a complete dissolution and added into a cuvette. The absorbance of formazan products was determined by measuring absorbance at 570 nm using a Nanodrop Spectrophotometer. A blank containing medium only was used. The measurements of each sample were performed in triplicate and data were expressed as statistical mean in comparison with control cells. (Morais et al. 2020; Oh and Hong 2022; Benov 2019).

7.4. Cytotoxic activity of PRE reagent effects

The relative amount of bacteria was measured by OD600 to determine cytotoxic activity after PRE reagents treatment. OD measurements were performed in a Spectrostar Omega

microplate reader with a Costar Flat Bottom 96-well plate. Absorbance was measured at a wavelength of 600 nm and 37°C.

Previously, the cells were incubated overnight in LB medium with 2% Na-alginate at 37°C and 200 rpm. A sample of 200 µL was pipetted from the falcon tube and transferred to a flat-bottom 96-well plate. The samples performed were cells treated with different concentrations (200 µM, 500 µM, 1 mM, 2 mM and 4 mM) of two PRE reagents, manganese and gadolinium, a control of untreated cells as well as a blank of LB medium. Each sample was plated in triplicate.

Absorbance readings were taken for 5 hours at different points: 0 min, 15 min, 30 min, 1h, 2h and 4 h, while cells were incubated at 37°C with continuous shaking of 220 rpm. At every interval, the OD was measured at 600 nm to analyse the cell growth at different time periods.

7.5. Sample preparation for in-cell NMR

All samples performed were composed of beads contained in free-phosphate minimal medium. To prevent adverse effects of D₂O on cell growth and metabolism and make a constant uniform lock, 17 µL of deuterium solvent was placed into a thin glass capillary as well as 2.5 µL of DSS (chemical shift indicator). Each sample is approximately of 350 µL.

7.6. Sample preparation for drug screening

All the antimicrobial agents injected into the flow system were previously prepared at a concentration of 0.2 mM diluted in phosphate-free minimal medium. For manganese

treatment, 0.5 mM of this compound was also added to the sample. This concentration was chosen on the basis of do not affect cell viability as determined by rates of no significant effect on cell viability as determined these compounds in MTT assay.

7.7. Setting up the perfusion system

The NMR bioreactor employed in this study is based on the InsightMR system (Bruker) and consists of a flow NMR tube (o.d. = 5 mm, i.d. = 4.2 mm) connected to watertight sealing to form the total sample height of 38 mm for a total sample volume of 526 μ L. The inlet consists of capillary tubing inserted at the bottom of the NMR flow tube while the outlet is attached to the top of the tube holder (Figure 15). The transfer line was temperature-controlled using a thermostat at 37°C. (Luchinat et al. 2020)

For an uninterrupted flow of medium, the bioreactor system presents a standard screw cap NMR tube with a PTFE/silicone septum around the inlet and outlet tubes to maintain the flow. Around thirty minutes before each in-cell NMR experiment, medium was flowed to prime the system and eliminate air bubbles from the set-up that could obstruct the flow and allow the encapsulated cells to settle into the detection NMR region for accurate running/shimming (Breindel, Burz, and Shekhtman 2020). The free ends of the inlet and out lines were connected to a Waters HPLC system, with an inlet inserted into a reservoir of fresh minimal medium and the outlet inserted in a waste reservoir, respectively. The flow tube assembly was inserted carefully in the magnet until the glass tube seats on the probe, ready for starting NMR (Burz, Breindel, and Shekhtman 2019; Sharaf et al. 2010).

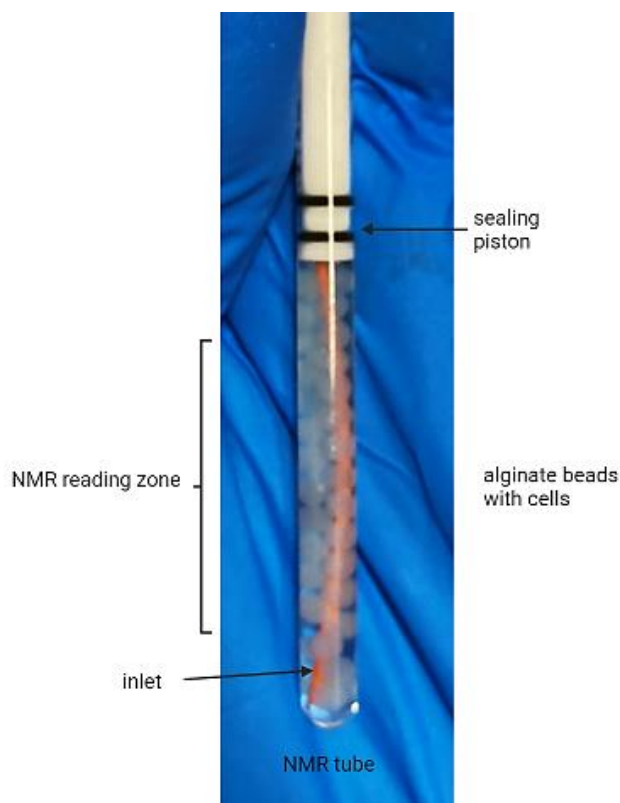


Figure 15. NMR tube filled with encapsulated cells in alginate beads.

During the in-cell NMR running, the HPLC maintains a continuous perfusion in the NMR tube in a single pass mode and at a constant flux rate, providing fresh medium with nutrients as well as removing the metabolic end-products. For that, 200 mL reservoir of phosphate-free minimal medium was supplied to the encapsulated cells in the NMR tube at a constant flow rate of 0.2 mL/min while *E. coli* was in LB medium inside the alginate beads.

The perfusion medium temperature is controlled by a thermostatic water bath along the bioreactor system and inside the magnet via the spectrometer temperature control device,

both maintained at 37°C. As *E. coli* bacteria do not need to be under an oxygenated atmosphere, this bioreactor set up does not present an oxygen pump.

Before and after each run, first ethanol 20% and then MilliQ water were flown at 1 mL/min through bioreactor lines for at least 30 min each, in order to remove any contaminant.

7.8. NMR acquisition

All spectra were collected at 310 K at a 600 MHz Bruker Avance III spectrometer equipped with a TCI CryoProbe. Each 1D ^1H NMR spectrum was acquired using a standard excitation sculpting water suppression pulse program (Bruker pulse sequence *zgesgp*) that provides good phase uniformity and flat baseline and optimal suppression of residual water to allow detection of resonances closed to water signal.

After loading the sample into the Bruker spectrometer, the sample was locked, tuned and matched. All 1D ^1H NMR spectra were acquired using the same parameters: a spectral width of 16042 ppm, a data size of 32768 points over 1.7 s acquisition time and a delay of 10 μs , receiver gain 80.6, 32 transients and 8 dummy scans (1 min 49 s each experiment).

For CPMG experiments, the same pulse sequence but with the addition of a CPMG pulse train after the initial 90-deg excitation pulse was employed (Bruker pulse sequence *zgprcpmg_mjh*). The spectra were collected with the same parameters as the 1D ^1H NMR except an acquisition time of 1.02 s and three different CPMG spin-lock times were applied: 20 ms (46 s), 50 ms (47 s) and 150 ms (52 s)

7.9. Processing of targeted metabolic profile

The Chenomx NMR Suite version 8.2 software was employed for metabolite identification and the determination of the concentration of individual metabolites. 1D ^1H NMR spectra were imported into this software which will overlay a 1D ^1H NMR reference spectrum for each metabolite identified in the experimental spectrum. The magnetic field strength of Chenomx was set to 600 MHz. Each reference metabolite was fit at pH 7.4 \pm 0.50 and peak centres recorded to DSS peak as a known reference signal. This calibration was stored in a field-dependant database and used for all spectra processed. Next, spectra were analysed in the Profile module which is linked to an existing library that includes over 300 metabolite entries with known reference signals. This list of metabolites was used to identify metabolites. Automatically, Chenomx enables obtaining the concentration of identified metabolites in all samples normalized by the concentration of the reference compound (DSS). In the fitted spectrum all metabolite concentrations and peak frequencies can be adjusted (Gowda and Raftery, n.d.; Weljie et al. 2006).

7.10. Analysis of metabolite concentration

Firstly, a study of the most representative metabolites of the super-pathways was carried out at different times (0, 30 min, 1 h and 2 h) in order to identify the biggest differences. Metabolic pathways were investigated using the KEGG PATHWAY Database-GenomeNet, free available online at: <https://www.genome.jp/kegg/pathway.html>. Each experiment was run in triplicate and expressed as a mean of all. Afterwards, the

concentration of each identified metabolite was calculated as a fold change log transformed at the different measured points.

For statistical analysis, all experiments were run in triplicate and uploaded to the MetaboAnalyst website version 5.0 available at <https://www.metaboanalyst.ca/>. Fold change analysis, one-way Analysis of Variance (ANOVA) and hierarchical clustering analysis were used to determine correlations among statistically significant metabolite changes in the same sample or between untreated and treated samples. Intrasample variability was assessed as standard deviation and reported in the bar plots as bar errors.

8. Results

Knowledge of *in vitro* and *in vivo* mechanisms improves the overall success rate in the drug design effort. However, understanding the mechanism of action of antimicrobial is still a challenge in drug discovery process. Herein, we have implemented the prior described NMR method to monitor the permeation and interaction membrane of several SSA in addition to the use of NMR metabolomics to analyse the metabolic response to a SSA compound in live *E. coli* encapsulated in alginate beads.

8.1. Measuring permeability and membrane interaction of SSA agents in live cells

After the analysis of the permeability of our set of compounds in vesicles, we selected three type of compounds depending on their ability of permeation into the lipid vesicles: SSA30 (slightly permeable), SSA48 (not permeable) and SSA60 (highly permeable). They were

injected into the flow system in presence and absence of Mn^{2+} and ^1H CPMG experiments were running for 30 min to see the effect of the flow of these compounds in the tube containing the beads. This experiment was carried out for samples containing cells encapsulated in beads and empty beads.

The analysis of spectra at different points after the injection of the antimicrobial agent determined the point of highest intensities of the signals from the compounds and highest effect of manganese as broadening of these peaks. Taking one of the samples as an example, Figure 16 evidences that the top peak was reached at 5 min. Hence, the addition of the compound at 0 min was not immediately unless the highest compound signal is after 5 min when was already in the NMR tube. We determined 5 min point as the accurate moment to measure the highest intensities for all the compounds tested.

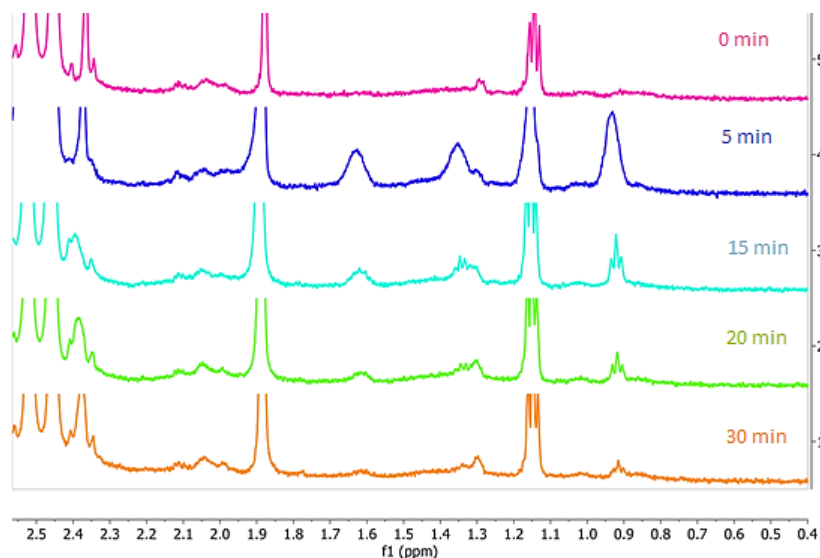


Figure 16. Stacked spectra showing the flow of 0.2 mM SSA48 + 0.5 mM Mn^{2+} at different points (0 min, 5 min, 15 min, 20 min and 30 min) after its injection in a sample containing cells encapsulated in beads.

The permeability values of the three SSA compounds analysed in this assay are given in Table 6. As can be observed, SSA30 and SSA60 displayed some permeability in comparison to SSA48 which was not permeable.

Compound	Permeability			Permeation category
	CPMG 20 ms	CPMG 50 ms	CPMG 150 ms	
SSA30	1.930	2.171	1.187	Slightly permeable
SSA48	1.393	0.961	0.895	No permeable
SSA60	1.733	1.2003	1.634	Slightly permeable

Table 6. Predicted permeability for SSA compounds at concentration of manganese 0.5 mM in live cells.

Despite the fact that live cells present a different composition of inner membrane compared to the inner membrane vesicles employed in *in vitro* assay and outer membrane due to the loss of channels and transport membrane protein in lipid vesicles, the membrane interaction of those compounds were also evaluated in live cells. Consequently, the interaction category of SSA compound could be expected not the same as we obtained in *in vitro* assay.

Our results presented in Table 7 suggest that only SSA60 presented interaction with the live cells encapsulated in alginate beads, even similar binding affinity at all CPMG spin-lock times. Similarly to the results obtained in lipid vesicles from *E. coli*, SSA30 did not interact with the membrane in live cells while SSA48 which showed interaction with lipid vesicles, did not showed binding in this *in vivo* assay.

Compound	Interaction (no Mn)			Membrane Interactin category
	CPMG 20 ms	CPMG 50 ms	CPMG 150 ms	
SSA30	1.023	1.116	1.501	No interaction
SSA48	0.762	0.865	1.184	No interaction
SSA60	0.543	0.660	0.500	Interaction

Table 7. Predicted membrane interaction for SSA compounds in live cells.

It is important to point out that self-association level depends on the solution where SSA compounds are diluted. As in *in vitro* assay these drugs were diluted in Hepes buffer, we needed to evaluate their self-association in minimal medium. This parameter was calculated as the ratio between the longest (150 ms) and shortest (20ms) CPMG spin-lock times in absence of Mn^{2+} . These results are presented in Table 8 and compared to the values obtained in *in vitro* assay. We can observe a lower self-association for the three compounds self-associate phosphate-free minimal medium compared to Hepes buffer.

Compound	Self-association Parameter	
	<i>In vitro</i> assay	<i>In vivo</i> assay
SSA30	0.886	0.731
SSA48	0.306	0.806
SSA60	0.516	0.761

Table 8. Comparison of self-association values of SSA compounds in *in vitro* and *in vivo* assays.

8.2. Cell viability of encapsulated cells

A major cellular function is the respiration and other NAD(P)H-dependant oxidoreductase activity. In order to evaluate this cellular function, encapsulated cells were conducted to the MTT assay. This test is based on the reduction of tetrazolium MTT by metabolically active cells, mainly by the action of dehydrogenase enzymes, to produce reducing equivalents (NAD(P)H). The product of this reaction is an intracellular violet formazan that can be solubilized and quantified spectrophotometrically. Therefore, the increasing formazan product is directly proportional to the amount of metabolically active cells (Morais et al. 2020; Uludag and Sefton 1990).

In this study, changes in formazan formation were evaluated after different bioreactor periods. Firstly, the bacterial culture media and media components were discarded by washing twice in PBS and bacterial MTT reduction was performed in this saline solution. After 24 h, formazan crystals were concentrated by centrifugation and dissolved in DMSO using sonication.

To verify the optimal absorbance for MTT formazan, different absorbances between 550 and 600 nm were also examined. The highest absorbance peak at 570 nm was chosen as the optimal one for each sample. An increasing absorbance value refers a rise in mitochondrial activity, number of viable cells and is likely to enhance cell proliferation. Otherwise, a reduction in absorbance suggests a decrease in cell viability which can be related to some factors (Morais et al. 2020).

Although, there were some subtle differences in our absorbance values over a period of 4 h, due to variations in the number of cells encapsulated in beads, the metabolic activity trend between different time points was very similar. Results shown in Figure 17 suggested that the alginate beads retained the metabolic activity of the encapsulated cells.

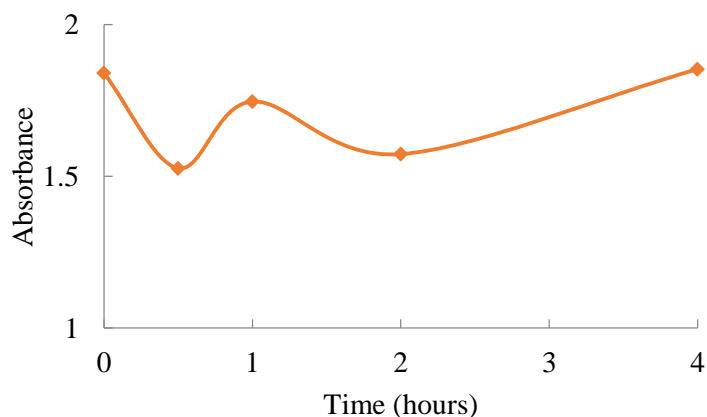


Figure 17. Change in the formation of bacterial MTT formazan by reduction time.

8.3. Cytotoxic activity of PRE reagent effects

In order to make use of the PRE effect in live cells we had to determine if PRE reagents would produce cytotoxicity in live cells.

Therefore, in order to determine whether this PRE reagent induced cell death or decrease cell growth, we measured the cytotoxic after the addition of Mn^{2+} to the cells in increasing concentrations. The assay was based on the comparison of cell growth using OD600 measurements at a chosen interval time between different conditions using a microplate.

Figure 18 shows the curves of *E. coli* treated with increasing concentrations of Mn^{2+} and a control growth with no Mn^{2+} . As can be seen from the curves, all concentrations tested allowed bacterial growth although lower Mn^{2+} concentrations achieved the highest OD600 values.

The measurements indicate that Mn^{2+} does not kill the cells and does not affect to bacterial growth. Thus, this metal ion was selected for the permeability study and at a preferred concentration of 0.5 mM.

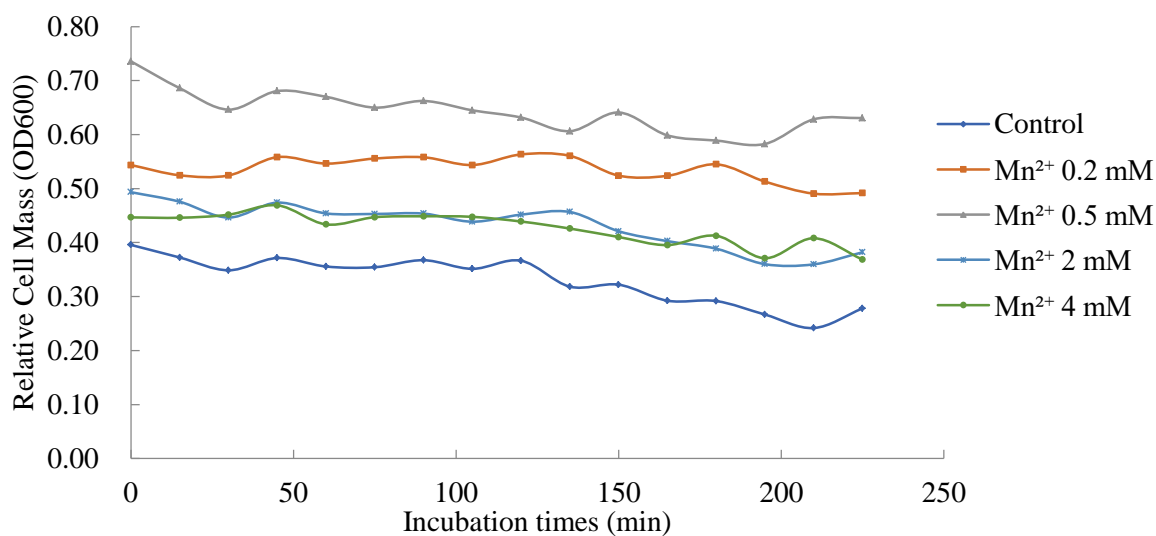


Figure 18. Optical density measurements of bacteria at a wavelength of 600 nm for *E. coli* at different concentrations of Mn^{2+} .

8.4. NMR profile and metabolic alterations in standard conditions

The 1D ^1H NMR spectrum of *E. coli* incubated in the bioreactor is shown in Figure 19 with the metabolites peaks identified by Chenomx NMR software and confirmed by the *E. coli* Metabolome Database (ECMDB). Around 32 metabolites were identified from the NMR spectra, with some of the most predominant and important ones corresponding to amino acids, nucleotides, carbohydrates and coenzymes.

The spectrum shows in the range between 0 and 4 ppm all the signal from organic acids and amino acids, and in the region between 5 and 8.5 ppm, aromatic compounds from nucleotides, coenzymes and few amino acids (Figure 19).

From all metabolites identified, only five were unambiguous because of the strong peak overlap in the spectrum (in particular with HEPES and glucose contained in the medium used) and the noise produced by significant solid particles in the flow tube (beads and cells).

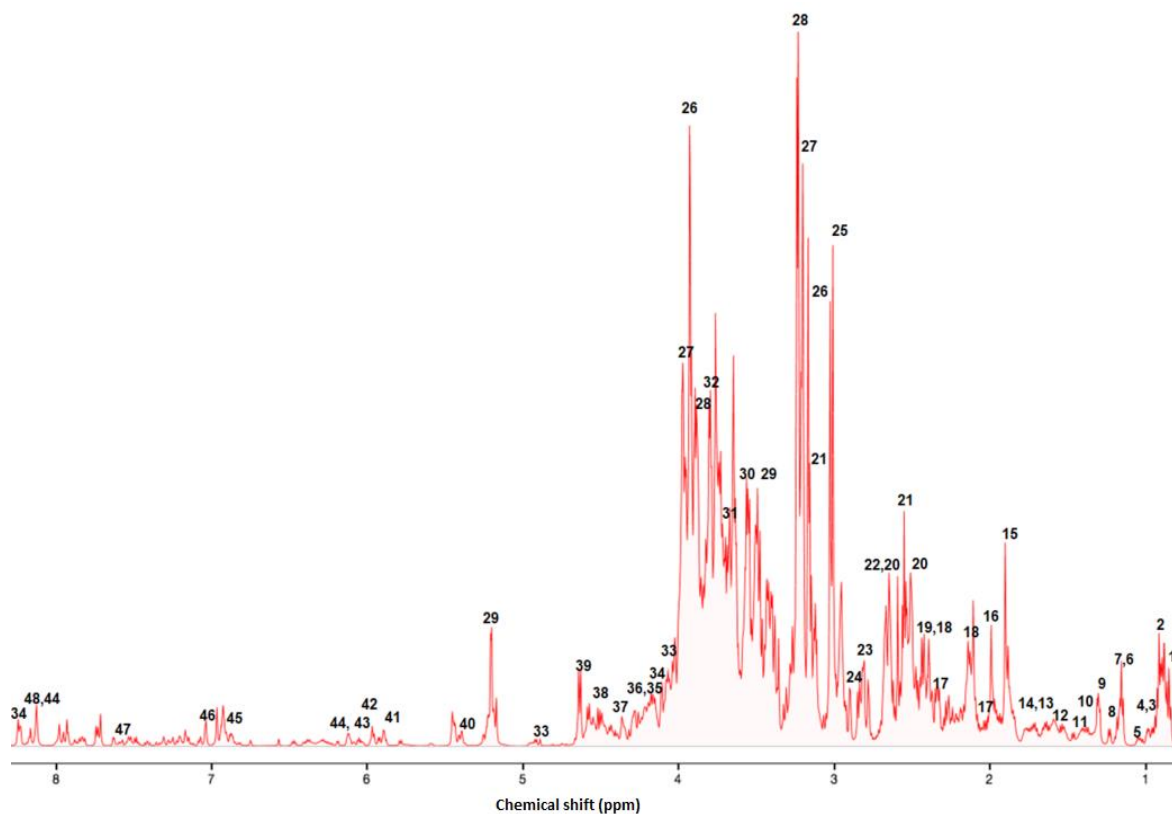
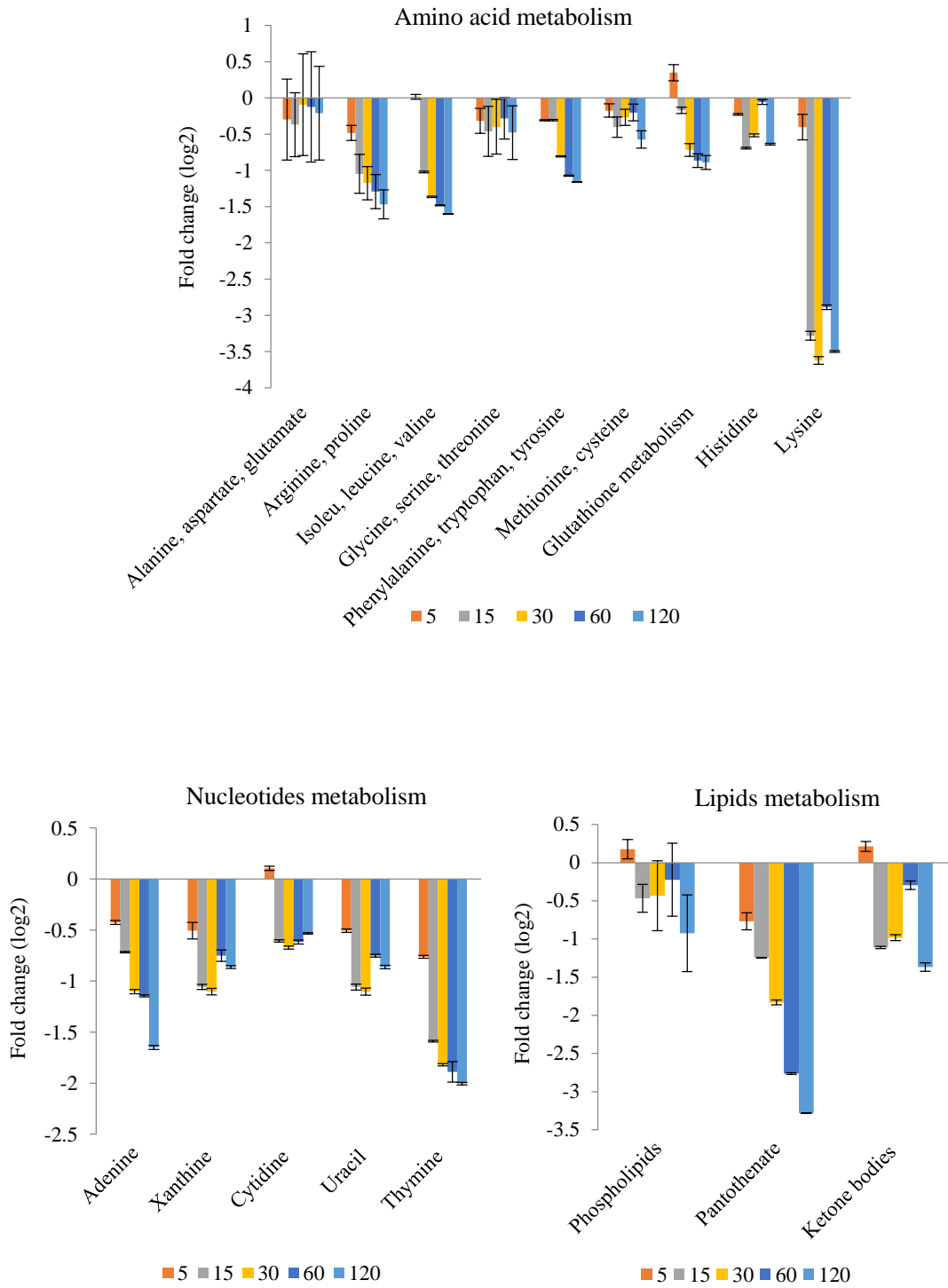


Figure 19. 1D ^1H NMR spectrum of *E. coli* used for metabolite quantification. Metabolites: 1. 2-hydroxybutyrate, 2.Pantothenate, 3.Leucine, 4.Isoleucine, 5.Valine, 6.Ethanol, 7.Thymol, 8.Fucose, 9.Threonine, 10.Lysine, 11.Alanine, 12.Biotin, 13.Arginine, 14.Putrescine, 15.Acetate, 16.Acetamide, 17.Glutamate, 18.Succinate, 19.Glutamine, 20.Citrate, 21. β -alanine, 22.Anserine, 23.Asparagine, 24.Glutathione, 25.Cysteine, 26.Creatine, 27.O-Phosphoethanolamine, 28.Betaine, 29.Glucose, 30.Glycerate, 31.Glycine, 32.Serine, 33.Ribose, 34.Adenosine, 35.Proline, 36.Uridine, 37.GTP, 38.Xylose, 39.Galactosa, 40.Sucrose, 41.Uridine, 42.Cytidine, 43.NADH, 44.ATP, 45.Tyrosine, 46.Histidine, 47.Niconitate, 48.Xanthine.

We performed the metabolomics analysis as a classification of most important metabolites included in the six main metabolic super pathways according to KEGG pathway Database. The concentrations of metabolites were quantified in the absence of antimicrobials to ensure that the cell metabolism reflects compensatory adaptations of *E. coli* due to the bioreactor. To this end, we monitored the short-term metabolic response of these bacteria in phosphate-free minimal medium for 2 h, defining the metabolic response as the relative change at each measured time respect to the initial time at which we began running experiments.

Firstly, we analysed each sample individually. Two metabolites, biotin and pantothenate were upregulated in the control sample (Appendix3, Figure 38).

All bar plots illustrated in Figure 20 evidence an overall drop in the levels of all metabolites, indicating that the optimization of the bioreactor experiment was not reliable enough. The change from 5 to 15 min suggests that the cells might not be adapted to the new conditions: being encapsulated in alginate beads and new medium. However, most of metabolites and sub-pathways from carbohydrates and energy metabolism did show an increase in their levels.



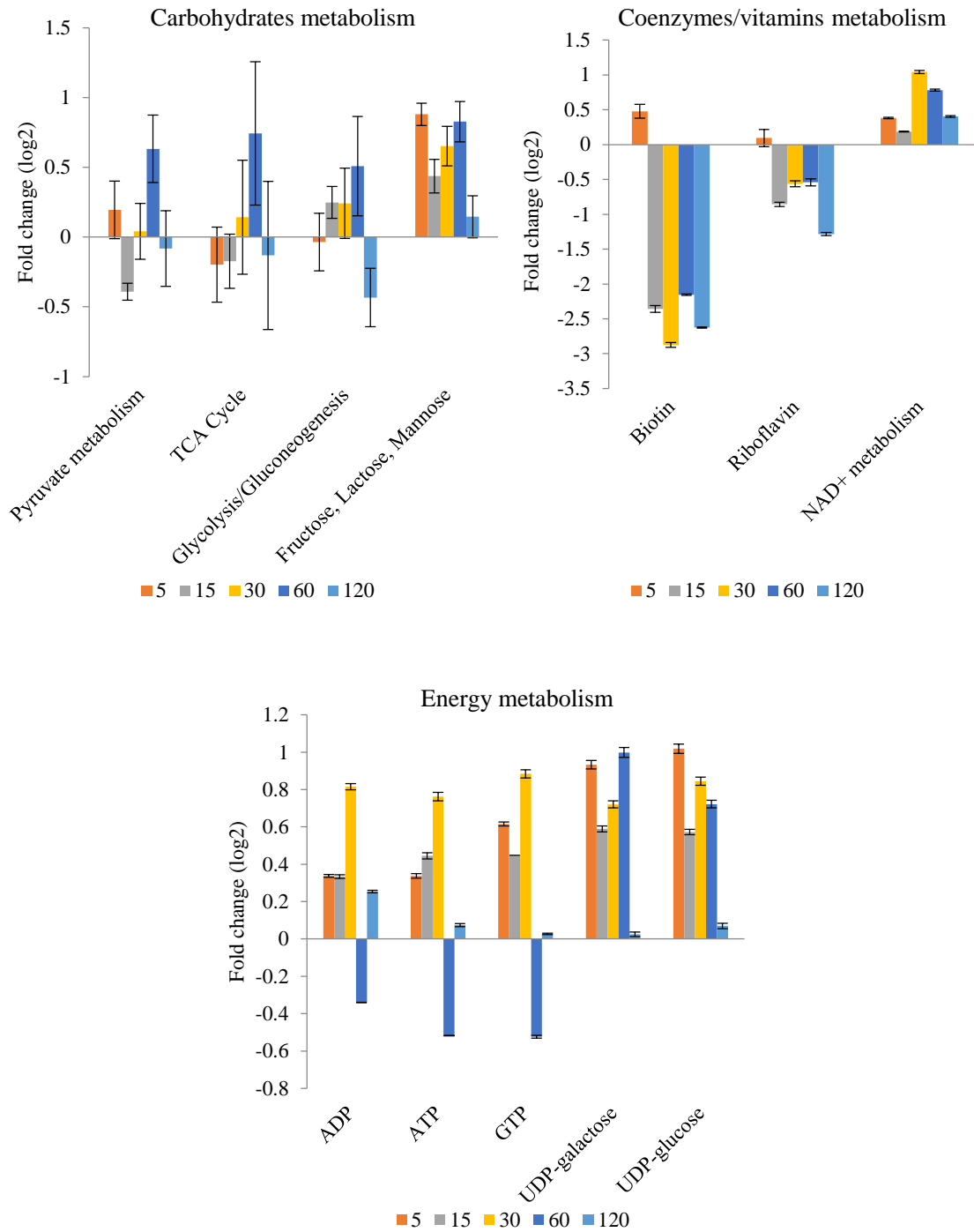


Figure 20. Bar plots illustrating fold change (log₂) in the relative concentration of individual metabolites and sub-pathways with respect to the t = 0 for *E. coli* at 5,

15, 30, 60 and 120. This control experiment was used to benchmark metabolite levels. The error bars represent the standard deviation.

8.5. SSA60 induces broad metabolic perturbations in *E. coli*

Once the bioreactor system was optimised and its efficiency for maintaining cell viability verified by MTT assay, the applicability of the system was evaluated in terms of energy level of cells when a drug was injected in the perfusion medium. NMR-based metabolomics was used to investigate cellular ATP levels as a measure of relative viability in the course of in-cell NMR experiments. With this, the cytotoxicity of that compound could be analysed along time.

The concentration of ATP for 6 hours was calculated and the results are shown in the Figure 21 showing that cells are metabolically active and alive during bioreactor experiments.

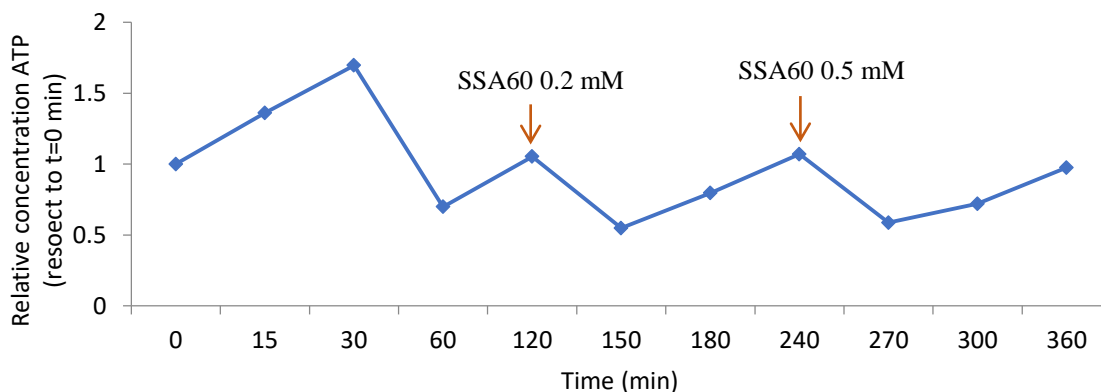


Figure 21. Time course of the relative concentration of ATP at time 0 min obtained treating cells encapsulated in alginate beads with increasing concentrations of SSA60.

Firstly, we monitored and profiled the *E. coli* metabolome to investigate important metabolic perturbations induced by the antimicrobial agent SSA60. We used nontargeted metabolomics to quantify the short-term metabolic response of these bacteria in free-phosphate minimal medium until 2 h after treatment. We analysed individually the two treated samples and did not find any significant change in the relative concentrations of the metabolites (Appendix 3, Figures 39 and 40).

The metabolic sub-pathways and super-pathways were analysed upon the addition of SSA60 at concentrations of 0.2 mM and 0.5 mM in order to observe firstly, any drug concentration-dependent metabolic effect and secondly, deduce the mechanism of action of SSA60 from the metabolic alterations.

Generally, for both concentration treatments, the relative concentration of carbohydrates and energy metabolites decreased whereas those of amino acids, nucleotides, lipids, coenzymes and vitamins increased (Figure 22).

In particular, upon an injection of 0.2 mM of SSA60, eight metabolites presented significant change respect to the untreated sample. In descending order of change in relative concentrations: arginine, pantothenate, lysine, leucine, alanine, biotin, acetone and 2-phosphoglycerate (Appendix 2, Table 9). In the case of 0.5 mM treatment, the same eight metabolites (arginine, leucine, lysine, pantothenate, acetone, alanine, biotin and 2-phosphoglycerate) displayed a significant alteration in their relative concentrations, although their degree of change was different respect to the prior treatment (Appendix 2, Table 10).

In terms of amino acid metabolism, an increase in amino acid levels was found after the first SSA treatment which might be a consequence of the activation of different protein synthesis pathways. However, some amino acids presented a drop in their level from 15 min post treatment such as the group of glycine, serine, threonine and histidine. The most marked change involves lysine at the two concentrations of SSA60. Moreover, we detected a substantial impact on the glutathione metabolism from the first 5 min post treatment which would be indicative of an antioxidant response to the antimicrobial agent.

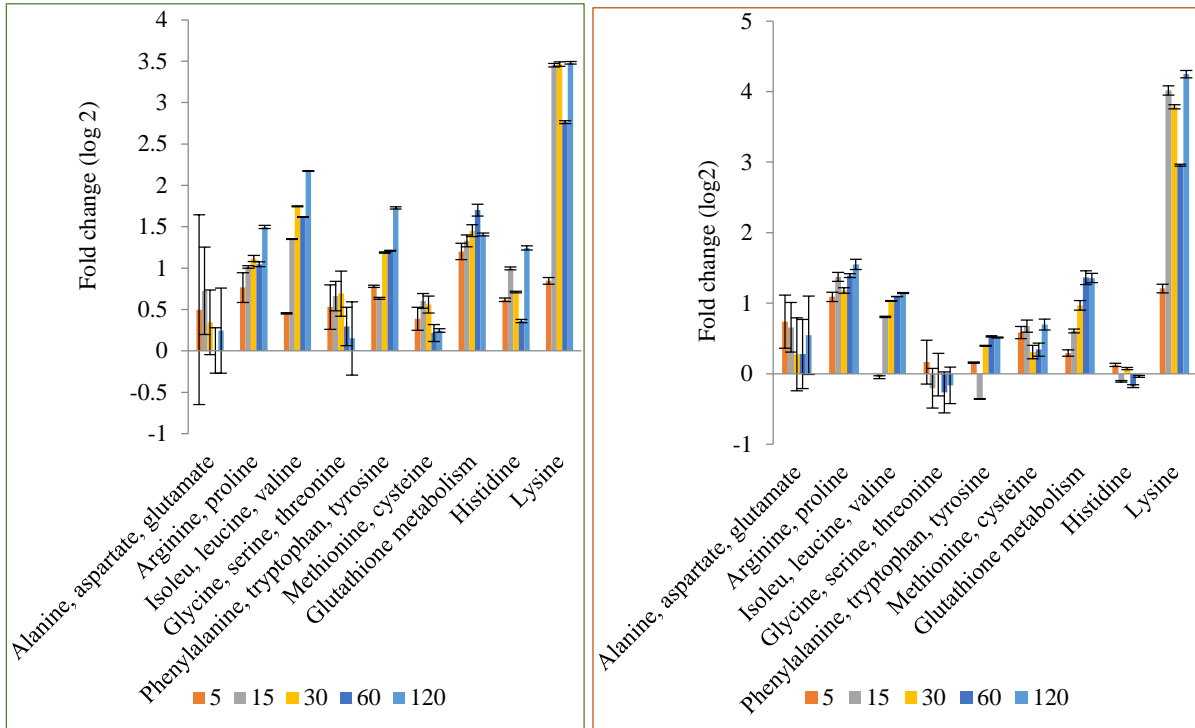
Our metabolomics dataset also identified a higher increase in the nucleotide pool upon SSA 0.2 mM compared to the next treatment. This difference could be in part related to a first major modification on RNA and DNA. In contrast to the rest of metabolic pathways, the fold change is more evident along time.

Among metabolites from lipid metabolism, phospholipids and pantothenate presented a considerably lower and higher increase in their levels, respectively. Ketone bodies were the only metabolites that did not showed any alteration at 5-min time point and their levels changed slightly along time.

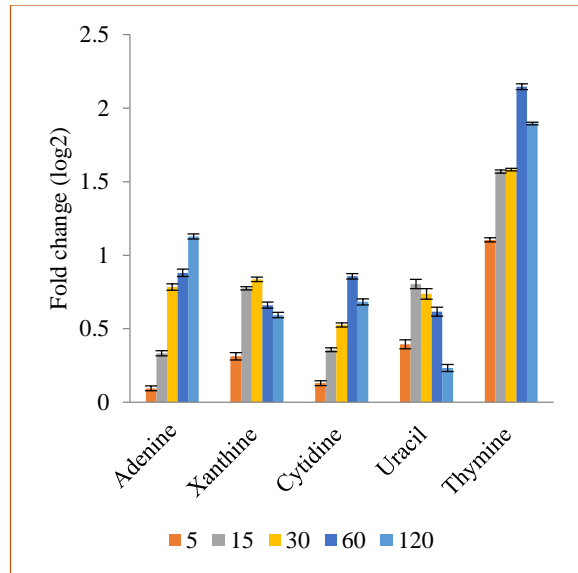
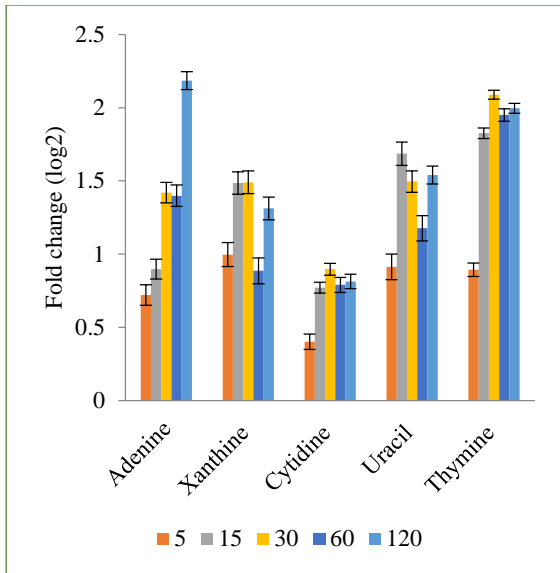
With respect to central carbon metabolism, we found lower levels of TCA cycle intermediated that together with an altered NAD⁺ metabolism indicate a perturbation of TCA cycle activity. We also detected marked changes on glycolysis/gluconeogenesis rate between the two SSA60 treatments, major in the second one. The pyruvate metabolism did not show big perturbations along time in both injections of SSA60.

At the 30-min time point, all of the energy metabolites levels except UDP-glucose were clearly decreased. Afterwards, we observed a significant improvement in their levels which could indicate cell recovery in the two SSA60 treatments.

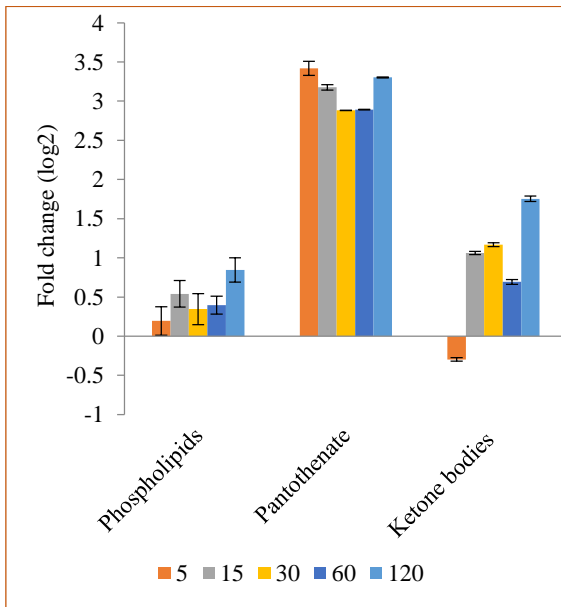
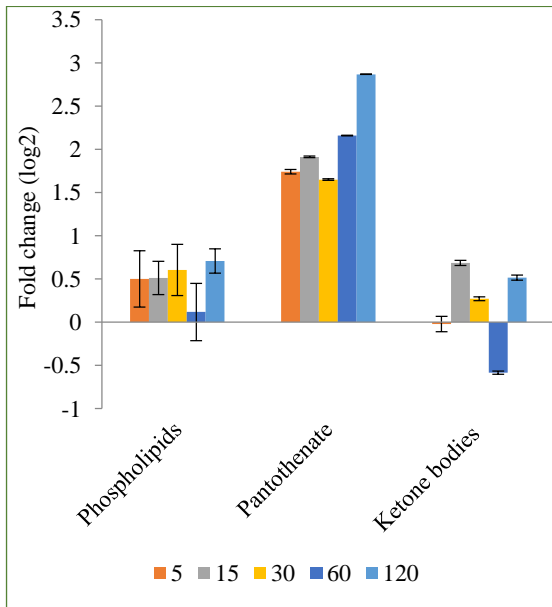
Amino acids metabolism



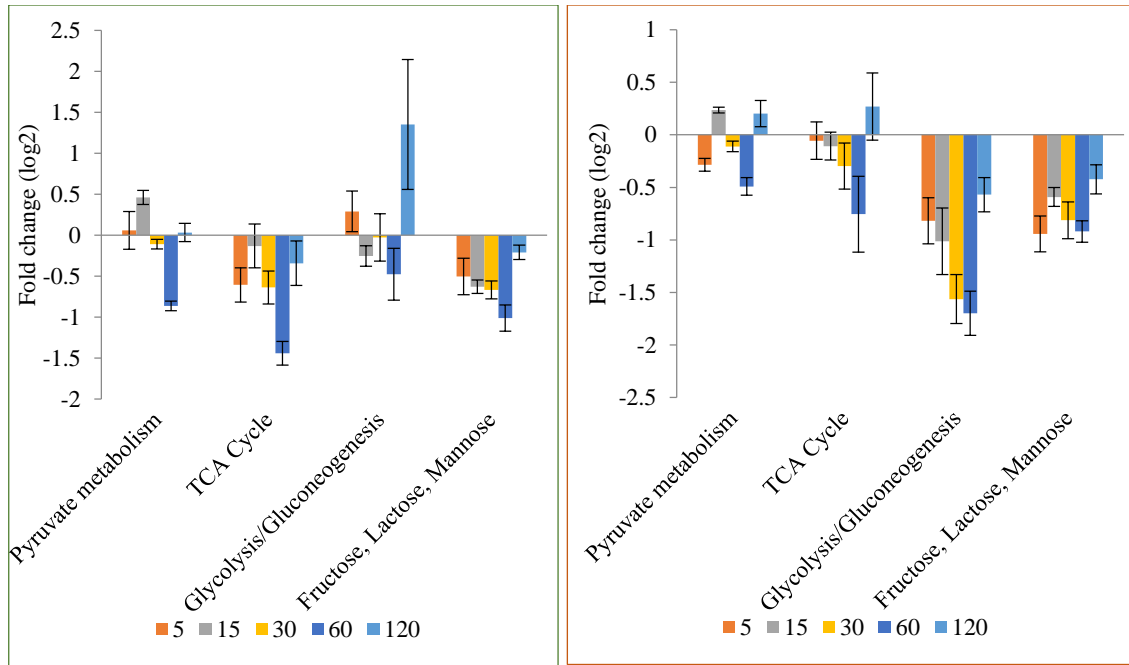
Nucleotides metabolism



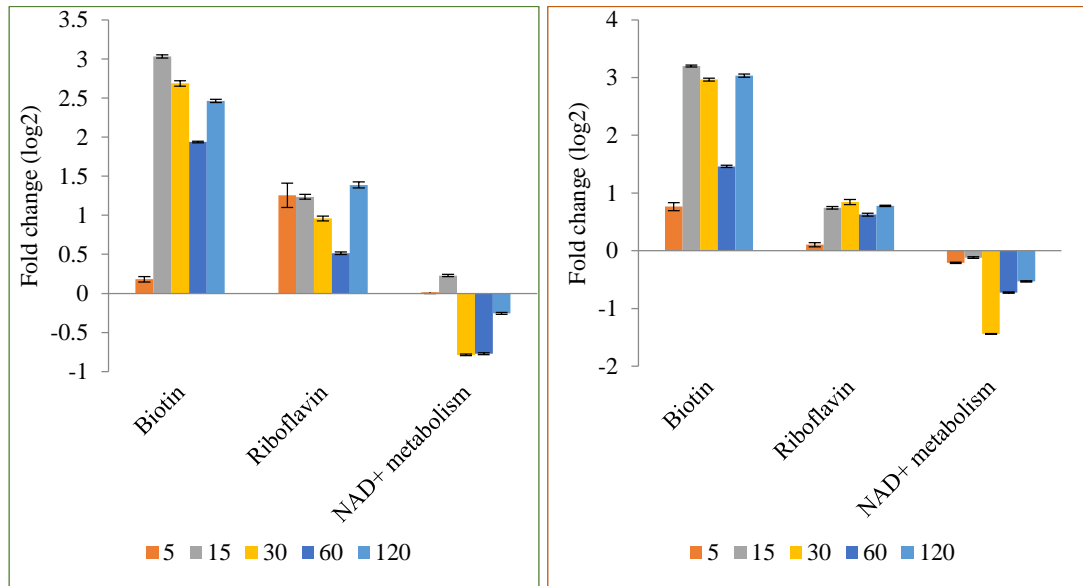
Lipids metabolism



Carbohydrates metabolism



Coenzymes/vitamins metabolism



Energy metabolism

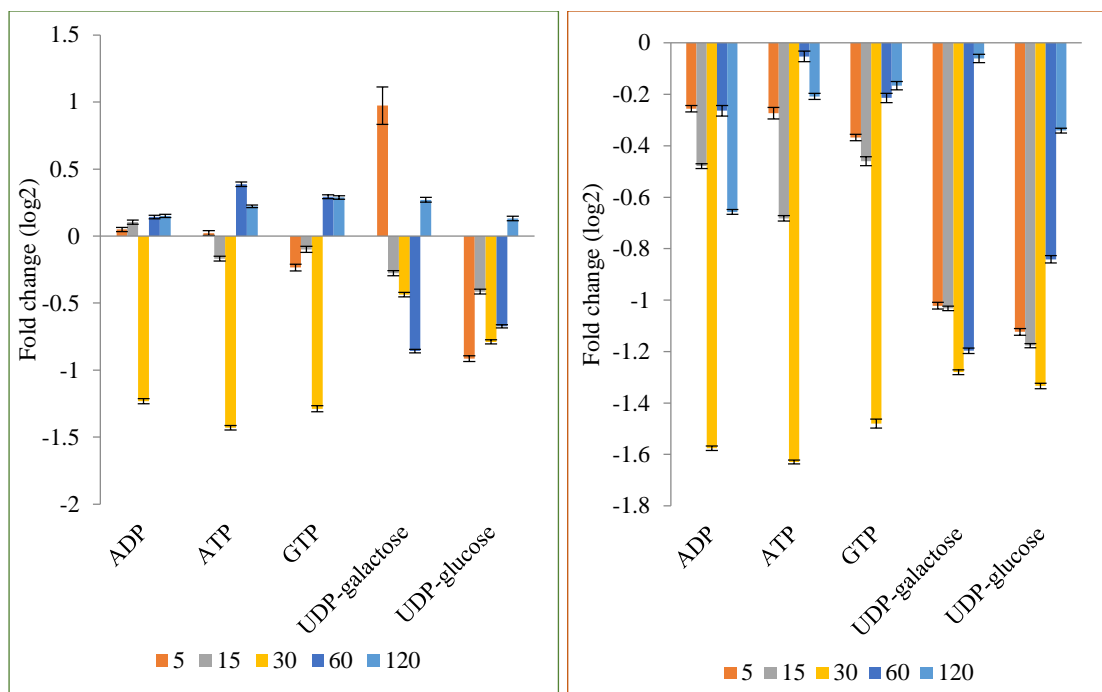


Figure 22. Bar plots illustrating fold change in the relative concentration of individual metabolites and sub-pathways with respect to the untreated sample for *E. coli* at 5, 15, 30, 60 and 120 min post antimicrobial SSA60 treatment at concentrations of 0.2 mM (green bar plots) and 0.5 mM (orange bar plots). The error bars represent the standard deviation.

To further illustrate the time-dependent impact on cell metabolism at the two concentrations of the drug tested, we performed hierarchical clustering on the relative concentration data from all treatment time points (Figure 23). At 5 min time point, metabolite concentrations at both SSA60 treatments became markedly elevated considering the majority of the differential clustering compared to the initial point. This point corresponds with the point at which we measured the highest peak of the compound

by NMR (Figure 16). Thus, we could report the rapid metabolic response of bacteria to the first SSA60 treatment.

At 120 min time point, the cells showed a metabolic recovering upon 0.2 mM treatment whereas at the same point upon the second addition of SSA60 the cells did not presented any change respect to the rest of the prior time. This could mean that the lowest concentration of SSA60 exerted a critical alteration of the metabolic profile without cell damage and a higher addition of the drug could have the opposite effect or the recovering time could be longer. Namely, the second addition of drug did not exert a significant impact on metabolic profile.

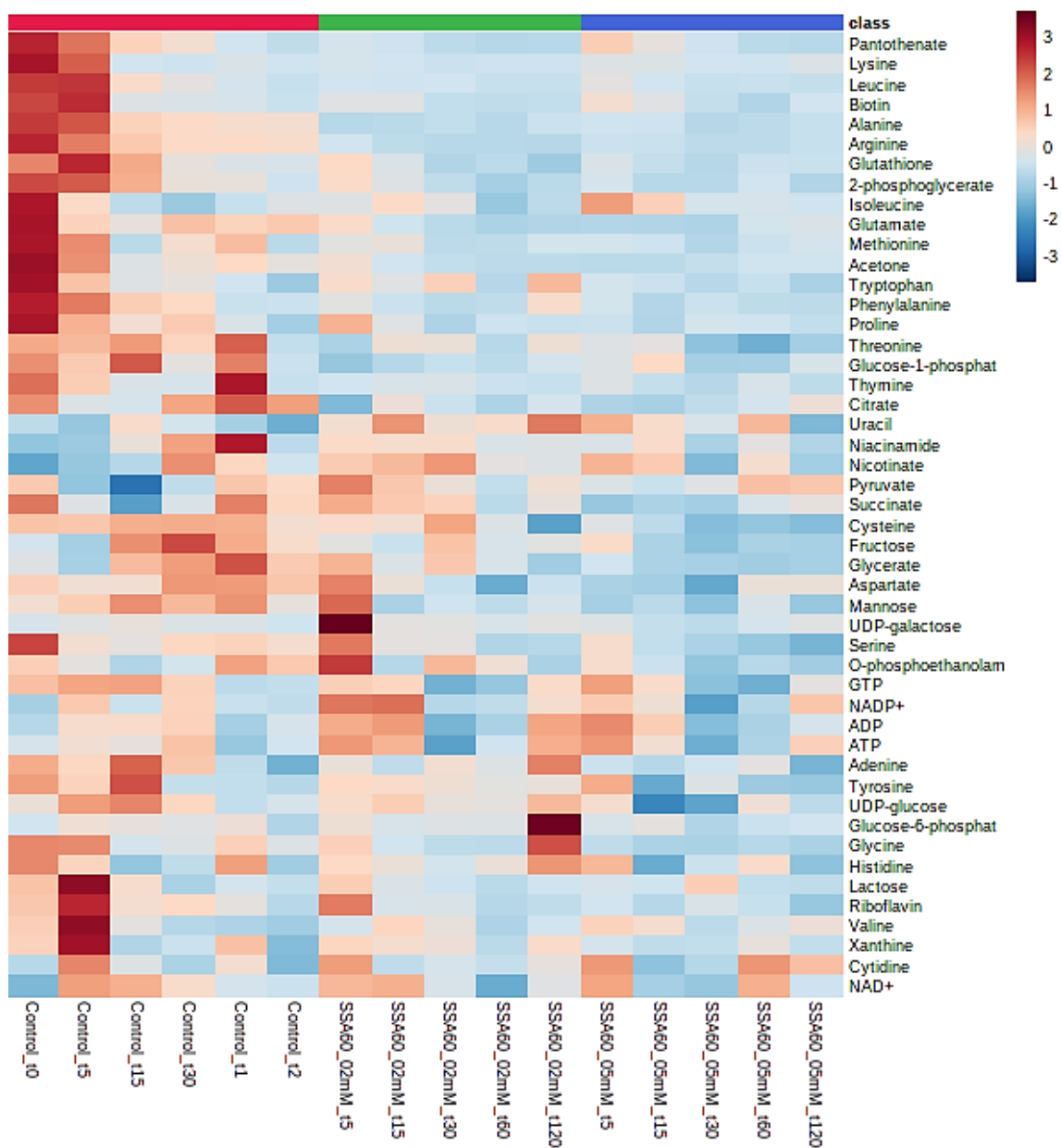


Figure 23. Hierarchical clustering of the metabolic profiling data at 0, 5, 15, 30, 60 and 120 min in controls and after SSA60 treatment at concentrations of 0.2 mM and 0.5 mM. Red and blue indicate increased and decreased concentrations of metabolites, respectively.

9. Discussion

9.1. Evaluating SSAs permeation and membrane interaction in live cells

It has previously been shown that several SSAs presented different binding affinity towards different membrane depending on their lipid composition (Boles et al. 2022), and our previous investigations in lipid vesicles have shown different permeation rates and membrane interaction affinities of a set of SSA compounds. Here we have focused on the comparison of SSAs permeation and membrane interaction between inner membrane vesicles prepared from *E. coli* and the live cells using an NMR bioreactor.

From the set of SSAs selected for the *in vivo* assay, none showed the same behaviour than in the *in vitro* assay. SSA30 exhibited slightly higher permeability in live *E. coli* than lipid vesicles while SSA60 presented considerably lower permeation compared to its permeability in vesicles. This could be due to the presence of outer membrane in whole bacteria or beads with a pore size hardly permeable. Conversely, SSA48 did not permeate either lipid vesicles or *E. coli* encapsulated. Regarding membrane binding, SSA30 and 60 exhibited similar results in the two assays, no interaction and interaction, respectively. However, SSA48 interacted with inner membrane vesicles whereas it did not exhibit interaction with the live cells, which indicate that SSA48 does not show binding affinity towards the outer membrane.

As Ferreira and Kasson (Ferreira and Kasson 2019) explained, whole-cell compound accumulation involves various other drug transport mechanisms such as porins, specific transporter and efflux pumps. In this study, computational predictions of small molecule

permeability against whole-cell permeability measurements was compared and evaluated, where the authors found similar differences as those between lipid vesicles and whole cell in our studies.

9.2. Efficacy and viability of encapsulated cells in a bioreactor system

As Bassani *et al.* (Bassani et al. 2019) demonstrated, the immobilization of *E. coli* cells within calcium alginate beads is a promising strategy for maintaining cell viability for long storage periods. The results of this assay indicated that the calcium alginate matrix method was very effective for the immobilization of *E. coli*, entrapping a high number of cells with success percentage of cell viability.

Other types of encapsulation have been developed to ensure the cell integrity. For instance, results of *Lactobacillus* encapsulated in genipin as a cross-linking agent to form novel alginate-chitosan microcapsules has demonstrated a favourable microenvironment for bacteria growth. This encouraging outcome is a result of successful intercellular communication (Chen et al 2007).

We used the well-established MTT assay to evaluate any cytotoxicity in the alginate beads, measuring cell metabolic activity after incubation in the bioreactor. Also, this procedure verifies the appropriate cell viability in encapsulated cells and nutrients reception through the percentage of alginate used (2%). The observed differences between the absorbance values at each time interval is due to the fact that MTT reduction is highly dependent on NAD(P)H, as a measure of the activity of mitochondrial oxidoreductases, and there are not the same amount of cells in each bead.

According to the obtained results by Morais *et al.* (Morais *et al.* 2020), 2% alginate presented a high viability and seemed to be a very promising encapsulation system to keep cellular metabolic activity and cell viability. The entrapment efficiency obtained in this study was similar to that described by (Bassani *et al.* 2019) who reported that the maintenance of cell viability could be associated to encapsulation method carried out. In fact, this better preservation in this study as well as ours is due the use of Luria-Bertani broth in the preparation of sodium alginate solution and the positive adaption of the cells for 2 h at 37°C before gelation with the Ca²⁺ ions.

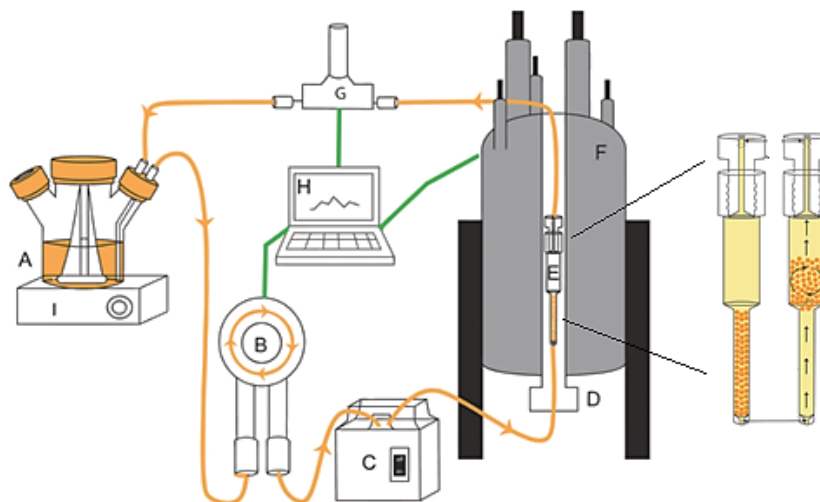
9.3. Challenges on cell viability and metabolic effect evaluation using in-cell NMR

A bioreactor offers the unique possibility of controlling and following cellular events in real time by NMR (Luchinat, Cremonini, and Banci 2021). The CEC bioreactor designed by Sharaf *et al.* (Sharaf *et al.* 2010) provide a controlled environment to deliver nutrients and remove waste products from the encapsulated cell contained in a circulation chamber. However, the data acquisition could only be completed when the flow media is stopped, as encapsulated cells settle on the bottom of the tube (Figure 24A). The set up developed and used in our study (Figure 24B) does not rely on the status of flow media the data acquisition, constituting a big improvement in its applicability.

The most used 5 mm wide bioreactors have been demonstrated ability to maintain a high number of alive and metabolically active cells for several hours or days while making possible the acquisition of in-cell NMR spectra (Luchinat, Cremonini, and Banci 2021).

Nevertheless, as our results reported, the future generation of bioreactor system should strengthen cell-growth conditions to achieve better results.

A)



B)

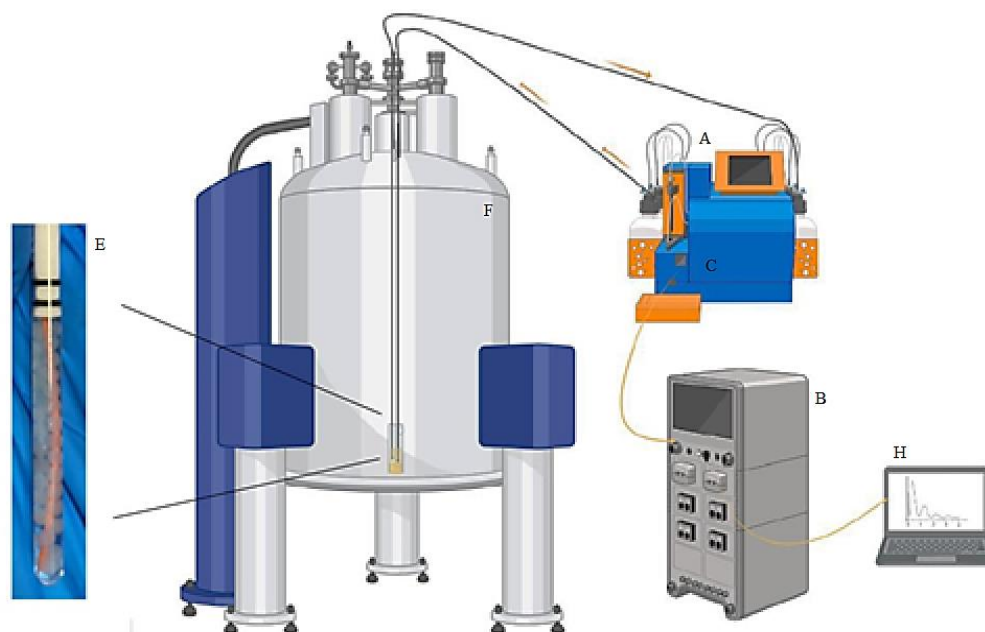


Figure 24. Comparison between the experimental set up of the CEC bioreactor (A) (Sharaf et al. 2010) and NMR-coupled bioreactor (B) used in this study. A: Flow

and waste media, B: peristaltic pump, C: water bath, D: 8 mm probe with heater removed, E: bioreactor flow tube, F: magnet, G: pH probe, H: computer, I: stir plate.

Moreover, further complexity monitoring live-cell metabolism arises from materials used for sample preparation such as agarose or alginate gels which can be cell-unfriendly. Consequently, reduced metabolite diffusion rates and additional induced stress can conceal real metabolic profile (Alshamleh et al. 2020).

For more reliable metabolite identification and quantification, the standard 1D ^1H NMR approach is based on the superposition of 1D ^1H NMR spectra of pure metabolites with the experimental NMR spectrum. Peak overlap and high S/N due to solid particles (beads and cells) in the samples tested are one of the factors that can complicate the analysis of biomolecules. However, overlap is not a critical issue when a metabolite presents more than one peak, mostly in other region that can be resolved (Q. Liu et al. 2017).

Somes studies in the literature have reported that the use of ^{31}P NMR experiments is able to monitor physiological conditions of cell. Additionally, ^{31}P NMR spectroscopy allows the study of the energetic status of cell as well as provide useful information about cytotoxicity of drugs in live cells by observing metabolic effects (Carvalho et al. 2019; Lohmeier-Vogel, Ung, and Turner 2004) . In our case, these experiments presented very low signal to noise and didn't yield any information about the energetic state of the cells (Data not shown).

9.4. Antimicrobial agents induce metabolic alterations in *E. coli*

Herein, we employed NMR-based metabolomics to monitor the immediate metabolic response of *E. coli*. This approach can be applied to the study of a wide variety of antibiotic perturbations. The aim of employing quantitative NMR metabolomics is to estimate metabolite concentrations at different points in a fast and automated way during a run of the bioreactor since the measured samples are likely to change metabolite profiles along the experiment. Furthermore, not only the concentration of metabolites is being altered but also new metabolites could appear.

It is important to note that a high increase or drop of specific metabolites levels indicates that these metabolites may play an important role in antimicrobial resistance or tolerance. Hence, we evaluated the impact of drug treatment using statistical analysis that describes the influence of various metabolites. We only chose SSA60 for metabolite analysis since this compound showed both membrane interaction and slightly permeation compared to the other two SSA compounds tested in encapsulated cells. Our results suggest that the metabolic changes directly induced upon SSA60 treatment indicate the rapid metabolic adaptation to the drug target. However, the low permeability of SSA60 would result on just a slight impact on the metabolism of *E. coli*, even if this compound interacts with the membrane, indicating that the changes in several metabolite levels are exacerbated in the presence of SSA60 compared to the control experiment.

The bacterial metabolic finger and footprinting analysis by Hoerr group reported that antibiotics with intracellular targets presented alterations in levels of alanine, glutamate,

acetamide and energy metabolites such as ethanol, citrate and formate whilst antibiotics with effect on cell wall showed fewer changes on the metabolic fingerprint. For those latter profiles, most of energy metabolites derived from TCA pathway were decreased while metabolites derived from anaerobic energy pathways (formate, acetate and acetone were increased (Hoerr et al. 2016). Assuming their hypothesis, our results suggest that SSA60 could have an effect on the cell wall as TCA cycle metabolites and ketone bodies were decreased and increased, respectively.

9.5. Prediction of mechanism of action using NMR metabolomics

Our results showed that metabolomics analysis describe how an antimicrobial agent affects cell metabolism making it possible to predict their mode of action. Compounds sharing the same mechanism of action would be expected to have similar effects on the cell metabolome. Overall, NMR metabolomics is a powerful tool that offers a strategy of classifying antimicrobials in distinct classes depending on their targets.

In this study, we demonstrated that by monitoring the cellular metabolome during the first exposure to different antibiotics, we could identify pathways and biological processes contributing to the global cell response to antimicrobial treatments. Several studies has demonstrated that rapid metabolic changes can reflect drug modes of action and reveal the active role of metabolism in mediating the first stress response to antimicrobials exposure (Halouska et al. 2012; Zampieri et al. 2017, 2018).

Taking our prior permeation study, since SSA60 presents affinity to the membrane, cell wall perturbation might result in intracellular metabolites outflow. To confirm out premise

it would be necessary the visualization of cell membrane shape and integrity by scanning electron microscope analysis or fluorescence microscopy (Al-Kandari et al. 2019; Hoerr et al. 2016). Boles and co-workers (Boles et al. 2022) explored the mode of antimicrobial action of these compound for lysis activity by using sample of phospholipid vesicles containing a fluorescent molecule. The results of this study reported that SSA60 exhibited a great degree of vesicle lysis activity at concentrations lower than 1.5 mM, hence confirming our hypothesis.

In recent years, the number of strategies to assign the mechanism of action of novel drugs has increased and driven drug discovery processes. These approaches are based on quantification and interpretation of dynamic metabolic responses at high throughput. Halouska *et al.* (Halouska et al. 2012) have demonstrated a general approach to predict *in vivo* modes of action from NMR metabolomics data by clustering novel chemical leads to known antibiotics. Another recent example of this is given by Zampieri group who have design a rapid systematic metabolome profiling strategy to classify the mechanism of action of uncharacterized antimicrobial compounds. For that, metabolome-based screening analysis was applied directly to resolve different dynamic metabolome responses that were exerted by a drug with a known mechanism of action and used to identify new compounds (Zampieri et al. 2018).

We can determine if the SSA60 presents a bactericidal or bacteriostatic effect. Unlike Belenky and co-workers (Belenky et al. 2015), we detected a general reduction in concentration of carbohydrates, coenzymes/vitamins and energy metabolites which indicate that SSA60 may not behave as a bactericidal antibiotics. This class of antibiotics

includes for instance β -lactams and ampicillin which activate the metabolic state that correlates with cell death.

On the other hand, previous work reported that bacteriostatic compounds downregulate glycolysis and gluconeogenesis, pyruvate metabolism and TCA cycle (X. Lin et al. 2014) whereas another work has revealed that bacteriostatic antibiotics such as chloramphenicol cause accumulation of metabolites from energy and central carbon metabolism (Lobritz et al. 2015). Our data shared only the same results than the first studies which would suggest that SSA60 acts as a bacteriostatic antibiotic. To corroborate this finding, future work should carry out a hydroxyl radical production assay where bacteriostatic drugs do not produce these radicals in bacteria (Kohanski et al. 2007).

Hoerr *et al.* (Hoerr et al. 2016) revealed that bacteria treated with doxycycline, a bacteriostatic compound, might release active metabolites to the extracellular medium which would confirm the significant changes in finger- and footprint profiles even if this drug did not exhibit altered membrane permeability. As we previously discussed, SSA60 interacted with the bacterial membrane but did not show a high permeability and thus our compound tested could share the mode of action of the doxycycline.

10. General discussion

NMR spectroscopy is a powerful tool that can offer essential information at early stages of drug discovery process. Our simple quantitative NMR approach allows to rapidly determine the type of permeation and binding membrane of thousands of compounds. This is achieved by assessing the permeability and membrane interaction parameters at different CPMG spin-lock times in presence and absence of a PRE reagent. This method can be implemented in any laboratory that has a NMR spectrometer available for liquid sample analysis. Also, we have demonstrated that it is feasible to assess these two properties, permeation and membrane interaction, in-cell, which provide a new strategy to understand and predict the efficacy of candidate drugs. As a result, we believe that the differences in the selective permeation and interaction of SSAs could be associated to the distinct lipid composition of bacterial membranes.

Additionally, we have verified that NMR metabolomics is a reliable and quantitative method to examine the impact of drugs on cell metabolism pathways and thus determine their mode of action. Our results corroborate that the action of an antimicrobial cannot be explained regarding an individual target; on the contrary, the whole induced response network must be examined. The application of these predictive methods would facilitate faster detection or improvement of existing lead compounds with intended biochemical target.

SSAs are amphiphilic compounds and thus present surfactant properties. To explore the interaction of SSAs with all types of lipid membranes, Boles and co-workers explored the

relation between membrane lysis/permeation and interaction values to support the hypothesis that the increase in antimicrobial efficacy depends on the general surfactant properties of the SSA compound. Herein, we could also analyse the relation between permeation and membrane interaction with the lysis of lipid vesicles obtained by the previous study. Their results revealed that SSA48 could not disrupt the lipid membrane from *E. coli* which supports our finding that this compound did not permeate either the lipid vesicles or cell membrane in our experimental assays. SSA30 presented slight permeability while SSA60 presented very high lipid permeability in lipid vesicles formed with bacterial and mammalian cells lipids. Both presented lysis properties against all the phospholipid membranes, markedly higher in SSA60, showing a good correlation between the permeability values obtained in our NMR-based assay and the efficacy of these antimicrobials due to their ability to disrupt cell membranes.

In summary, we have developed a simple NMR-based assay to measure the permeability and membrane interaction affinity of small molecules, both in lipid vesicles of controlled composition or in live cells. Our results revealed a good agreement between permeability values obtained by our new methodology and efficacy of compounds from the SSA family, indicating that this simple, high-throughput assay can be used for the development of new families of antimicrobials.

11. Future work and limitations

The application of the permeability approach described in this study is appropriate for any type of membrane or cell. Herein, we have developed the differences or similarities of permeability and interaction membrane parameters between two distinct assays: inner membrane vesicles and live cells. Nevertheless, this method presents several challenges that limited the accurate analysis.

Firstly, as it has been described previously, Gram-negative bacteria presents a complex cell envelope that should be simultaneously studied in order to optimise the permeability category of each compound. For this reason, future improvement would be addressed to select outer membrane vesicles of these bacteria and investigate the ability of SSA compounds to interact and go through the membrane.

Secondly, compound permeation involves several other drug transport mechanisms, including specific transporters and efflux pumps actions. Thus, these mechanisms should be taken into account in in-cell NMR experiments where the permeation or interaction of a compound could be due to transporters. In this way, a major detailed study of metabolite profile and protein-ligand binding investigations could determine how they are involved or if, conversely, compounds passively diffuse into the bacteria.

To make possible an accurate classification of compounds depending on permeability and membrane interaction, new CPMG spin-lock times should be measured as the affinity to the membrane is determined by them.

In terms of metabolomics and patho-mechanism investigations, the effect of different antibiotics with known modes of action (for instance, ampicillin and kanamycin) should be examined in the same conditions for the study of SSA60. This way, we would infer the degree of reliability of our metabolomics investigation and the deduction of the mechanism of action of SSA60.

12. Conclusions

In this study, we have designed a novel, simple methodology to assess membrane permeability of drugs making use of the PRE effect in lipid vesicles that is applicable to any type of cell/bacterial membrane. We have found important differences in the permeability of new families of antimicrobial compounds providing unique information for the further development of this family of compounds.

Furthermore, we have developed a live-cell NMR assay that allows the measurement of NMR-based metabolomics to monitor the immediate response of *E. coli* to antimicrobial perturbations. Upon addition of SSA60 we observe rapid changes along time on the six metabolic super-pathways that can reveal its mechanisms of action.

In summary, we present here a novel method reporting on drug permeability in lipid vesicles and live cells that will allow the design of more efficacious drugs and antimicrobial agents.

13. References

- Al-Kandari, Fatemah, Rabeah Al-Temaimi, Arnoud H.M. Van Vliet, and Martin J. Woodward. 2019. "Thymol Tolerance in *Escherichia Coli* Induces Morphological, Metabolic and Genetic Changes." *BMC Microbiology* 19 (1). <https://doi.org/10.1186/s12866-019-1663-8>.
- Alanis, Alfonso J. 2005. "Resistance to Antibiotics: Are We in the Post-Antibiotic Era?" *Archives of Medical Research* 36 (6): 697–705. <https://doi.org/10.1016/j.arcmed.2005.06.009>.
- Allen, Nyasha, Lisa J. White, Jessica E. Boles, George T. Williams, Dominique F. Chu, Rebecca J. Ellaby, Helena J. Shepherd, et al. 2020. "Towards the Prediction of Antimicrobial Efficacy for Hydrogen Bonded, Self-Associating Amphiphiles." *ChemMedChem* 15 (22): 2193–2205. <https://doi.org/10.1002/cmdc.202000533>.
- Alshamleh, Islam, Nina Krause, Christian Richter, Nina Kurrle, Hubert Serve, Ulrich L. Günther, and Harald Schwalbe. 2020. "Real-Time NMR Spectroscopy for Studying Metabolism." *Angewandte Chemie* 132 (6): 2324–28. <https://doi.org/10.1002/ange.201912919>.
- Aries, Michelle L., and Mary J. Cloninger. 2020. "NMR Metabolomic Analysis of Bacterial Resistance Pathways Using Multivalent Quaternary Ammonium Functionalized Macromolecules." *Metabolomics* 16 (8). <https://doi.org/10.1007/s11306-020-01702-1>.

- Bassani, Joseane C., Vidianny A. Queiroz Santos, Aneli M. Barbosa-Dekker, Robert F.H. Dekker, Mário Antônio A. da Cunha, and Edimir A. Pereira. 2019. "Microbial Cell Encapsulation as a Strategy for the Maintenance of Stock Cultures." *LWT* 102 (March): 411–17. <https://doi.org/10.1016/j.lwt.2018.12.058>.
- Belenky, Peter, Jonathan D. Ye, Caroline B.M. Porter, Nadia R. Cohen, Michael A. Lobritz, Thomas Ferrante, Saloni Jain, et al. 2015. "Bactericidal Antibiotics Induce Toxic Metabolic Perturbations That Lead to Cellular Damage." *Cell Reports* 13 (5): 968–80. <https://doi.org/10.1016/j.celrep.2015.09.059>.
- Benedetto Tiz, Davide, Danijel Kikelj, and Nace Zidar. 2018. "Overcoming Problems of Poor Drug Penetration into Bacteria: Challenges and Strategies for Medicinal Chemists." *Expert Opinion on Drug Discovery*. Taylor and Francis Ltd. <https://doi.org/10.1080/17460441.2018.1455660>.
- Bennion, Brian J., Nicholas A. Be, M. Windy McNerney, Victoria Lao, Emma M. Carlson, Carlos A. Valdez, Michael A. Malfatti, et al. 2017. "Predicting a Drug's Membrane Permeability: A Computational Model Validated with in Vitro Permeability Assay Data." *Journal of Physical Chemistry B* 121 (20): 5228–37. <https://doi.org/10.1021/acs.jpcc.7b02914>.
- Benov, Ludmil. 2019. "Effect of Growth Media on the MTT Colorimetric Assay in Bacteria." *PLoS ONE* 14 (8). <https://doi.org/10.1371/journal.pone.0219713>.
- Bhinderwala, Fatema, and Robert Powers. 2019. "NMR Metabolomics Protocols for Drug Discovery." In *Methods in Molecular Biology*, 2037:265–311. Humana Press Inc.

https://doi.org/10.1007/978-1-4939-9690-2_16.

Blair, Jessica M.A., Grace E. Richmond, and Laura J.V. Piddock. 2014. “Multidrug Efflux Pumps in Gram-Negative Bacteria and Their Role in Antibiotic Resistance.” *Future Microbiology* 9 (10): 1165–77. <https://doi.org/10.2217/FMB.14.66>.

Bloch, F. 1946. “Nuclear Induction.” *Physical Review* 70 (7–8): 460–74. <https://doi.org/10.1103/PhysRev.70.460>.

Boles, Jessica E, Charlotte Bennett, Jennifer Baker, Kira L F Hilton, Hiral A Kotak, Ewan R Clark, Yifan Long, et al. 2022. “Chemical Science Coordination , Permeation and Lysis Properties for ‘Druggable’ Supramolecular Self- Associating Antimicrobial Amphiphiles†.” <https://doi.org/10.1039/d2sc02630a>.

Bolla, Jean Michel, Sandrine Alibert-Franco, Jadwiga Handzlik, Jacqueline Chevalier, Abdallah Mahamoud, Gérard Boyer, Katarzyna Kieć-Kononowicz, and Jean Marie Pags. 2011. “Strategies for Bypassing the Membrane Barrier in Multidrug Resistant Gram-Negative Bacteria.” *FEBS Letters* 585 (11): 1682–90. <https://doi.org/10.1016/j.febslet.2011.04.054>.

Breindel, Leonard, David S. Burz, and Alexander Shekhtman. 2020. “Active Metabolism Unmasks Functional Protein–Protein Interactions in Real Time in-Cell NMR.” *Communications Biology* 3 (1). <https://doi.org/10.1038/s42003-020-0976-3>.

Burz, David S., Leonard Breindel, and Alexander Shekhtman. 2019. “Improved Sensitivity and Resolution of In-Cell NMR Spectra.” In *Methods in Enzymology*, 621:305–28.

Academic Press Inc. <https://doi.org/10.1016/bs.mie.2019.02.029>.

Cabrera-Pérez, Miguel Ángel, Marival Bermejo Sanz, Victor Mangas Sanjuan, Marta González-Álvarez, and Isabel González Álvarez. 2016. “Importance and Applications of Cell-and Tissue-Based in Vitro Models for Drug Permeability Screening in Early Stages of Drug Development.” In *Concepts and Models for Drug Permeability Studies: Cell and Tissue Based In Vitro Culture Models*, 3–29. Elsevier Inc. <https://doi.org/10.1016/B978-0-08-100094-6.00002-X>.

Cai, Sheng, Candace Seu, Zoltan Kovacs, A. Dean Sherry, and Yuan Chen. 2006. “Sensitivity Enhancement of Multidimensional NMR Experiments by Paramagnetic Relaxation Effects.” *Journal of the American Chemical Society* 128 (41): 13474–78. <https://doi.org/10.1021/ja0634526>.

Carneiro, Marta G., A. B. Eiso, Stephan Theisgen, and Gregg Siegal. 2017. “NMR in Structure-Based Drug Design.” *Essays in Biochemistry*. Portland Press Ltd. <https://doi.org/10.1042/EBC20170037>.

Carr, H Y, and E M Purcell. 1954. “Effects of Diffusion on Free Precession in Nuclear Magnetic Resonance Experiments.” *Journal of the American Physical Society* 94(3). <https://doi.org/10.1103/PhysRev.94.630>

Carvalho, Josué, Sara Alves, M. Margarida C.A. Castro, Carlos F.G.C. Geraldes, João A. Queiroz, Carla P. Fonseca, and Carla Cruz. 2019. “Development of a Bioreactor System for Cytotoxic Evaluation of Pharmacological Compounds in Living Cells Using NMR Spectroscopy.” *Journal of Pharmacological and Toxicological Methods*

95 (January): 70–78. <https://doi.org/10.1016/j.vascn.2018.11.004>.

Chen, H., Ouyang, W., Jones, M. et al. 2007. “Preparation and Characterization of Novel Polymeric Microcapsules for Live Cell Encapsulation and Therapy.” *Cell Biochemistry and Biophysics* 47: 159–67. <https://doi.org/https://doi.org/10.1385/CBB:47:1:159>.

Chopra, I. 1988. “Molecular Mechanisms Involved in the Transport of Antibiotics into Bacteria.” *Parasitology* 96 (S1): S25–44. <https://doi.org/10.1017/S0031182000085966>.

Cox, Georgina, and Gerard D. Wright. 2013. “Intrinsic Antibiotic Resistance: Mechanisms, Origins, Challenges and Solutions.” *International Journal of Medical Microbiology* 303 (6–7): 287–92. <https://doi.org/10.1016/j.ijmm.2013.02.009>.

Dhingra, Sameer, Nor Azlina A. Rahman, Ed Peile, Motiur Rahman, Massimo Sartelli, Mohamed Azmi Hassali, Tariqul Islam, Salequl Islam, and Mainul Haque. 2020. “Microbial Resistance Movements: An Overview of Global Public Health Threats Posed by Antimicrobial Resistance, and How Best to Counter.” *Frontiers in Public Health*. Frontiers Media S.A. <https://doi.org/10.3389/fpubh.2020.535668>.

Emwas, Abdul Hamid, Raja Roy, Ryan T. McKay, Leonardo Tenori, Edoardo Saccenti, G. A. Nagana Gowda, Daniel Raftery, et al. 2019. “NMR Spectroscopy for Metabolomics Research.” *Metabolites*. MDPI AG. <https://doi.org/10.3390/metabo9070123>.

Emwas, Abdul Hamid, Kacper Szczepski, Benjamin Gabriel Poulson, Kousik Chandra,

Ryan T. McKay, Manel Dhahri, Fatimah Alahmari, Lukasz Jaremko, Joanna Izabela Lachowicz, and Mariusz Jaremko. 2020. “NMR as a ‘Gold Standard’ Method in Drug Design and Discovery.” *Molecules*. MDPI AG. <https://doi.org/10.3390/molecules25204597>.

Ferreira, Ricardo J., and Peter M. Kasson. 2019. “Antibiotic Uptake across Gram-Negative Outer Membranes: Better Predictions towards Better Antibiotics.” *ACS Infectious Diseases* 5 (12): 2096–2104. <https://doi.org/10.1021/acsinfecdis.9b00201>.

Ferri, Maurizio, Elena Ranucci, Paola Romagnoli, and Valerio Giaccone. 2017. “Antimicrobial Resistance: A Global Emerging Threat to Public Health Systems.” *Critical Reviews in Food Science and Nutrition* 57 (13): 2857–76. <https://doi.org/10.1080/10408398.2015.1077192>.

Folch, J., M. Lees, and G. H. Sloane Stanely. 1957. “A Simple Method for the Isolation and Purification of Total Lipides from Animal Tissues.” *The Journal of Biological Chemistry* 226 (1): 497–509. [https://doi.org/10.1016/s0021-9258\(18\)64849-5](https://doi.org/10.1016/s0021-9258(18)64849-5).

Freyer, James P, Nancy H Fiak, Patricia L Schor, James R Coulter, Michal Neemans, and Laurel O Sillemdb. 1990. “A System for Viably Maintaining a Stirred Suspension of Multicellular Spheroids during NMR Spectroscopy.” *NMR Biomedicine* 3 (5):195-205. <https://doi.org/10.1002/nbm.1940030502>

Gowda, G A Nagana, and Daniel Raftery. 2019. “NMR-Based Metabolomics: Methods and Protocols.” *Humana Press*. <http://www.springer.com/series/7651>.

Hajduk, Philip J., Edward T. Olejniczak, and Stephen W. Fesik. 1997. "One-Dimensional Relaxation- and Diffusion-Edited NMR Methods for Screening Compounds That Bind to Macromolecules." *Journal of the American Chemical Society* 119 (50): 12257–61. <https://doi.org/10.1021/ja9715962>.

Halouska, Steven, Robert J. Fenton, Raúl G. Barletta, and Robert Powers. 2012. "Predicting the in Vivo Mechanism of Action for Drug Leads Using NMR Metabolomics." *ACS Chemical Biology* 7 (1): 166–71. <https://doi.org/10.1021/cb200348m>.

Hertig, Damian, Sally Maddah, Roman Memedovski, Sandra Kurth, Aitor Moreno, Matteo Pennestri, Andrea Felser, Jean Marc Nuoffer, and Peter Vermathen. 2021. "Live Monitoring of Cellular Metabolism and Mitochondrial Respiration in 3D Cell Culture System Using NMR Spectroscopy." *Analyst* 146 (13): 4326–39. <https://doi.org/10.1039/d1an00041a>.

Hibberd, and Leedale. 1970. "Multiple Antibiotic Resistance in a Bacterium with Suppressed Atuolytic System." *Nature Publishing Group* 228: 138-140. <https://doi.org/10.1038/227138a0>

Hoerr, Verena, Gavin E. Duggan, Lori Zbytnuik, Karen K.H. Poon, Christina Große, Ute Neugebauer, Karen Methling, Bettina Löffler, and Hans J. Vogel. 2016. "Characterization and Prediction of the Mechanism of Action of Antibiotics through NMR Metabolomics." *BMC Microbiology* 16 (1). <https://doi.org/10.1186/s12866-016-0696-5>.

- Honrao, Chandrashekar, Nathalie Teissier, Bo Zhang, Robert Powers, and Elizabeth M. O'Day. 2021. "Gadolinium-Based Paramagnetic Relaxation Enhancement Agent Enhances Sensitivity for NUS Multidimensional NMR-Based Metabolomics." *Molecules* 26 (17). <https://doi.org/10.3390/molecules26175115>.
- Kang, Congbao. 2019. "Applications of In-Cell NMR in Structural Biology and Drug Discovery." *International Journal of Molecular Sciences*. MDPI AG. <https://doi.org/10.3390/ijms20010139>.
- Kansy, Manfred, Frank Senner, and Klaus Gubernator. 1998. "Screening: Parallel Artificial Membrane Permeation Assay in the Description Of" 41 (7): 0–3.
- Kocman, Vojč, Giacomo M. Di Mauro, Gianluigi Veglia, and Ayyalusamy Ramamoorthy. 2019. "Use of Paramagnetic Systems to Speed-up NMR Data Acquisition and for Structural and Dynamic Studies." *Solid State Nuclear Magnetic Resonance*. Elsevier B.V. <https://doi.org/10.1016/j.ssnmr.2019.07.002>.
- Kohanski, Michael A., Daniel J. Dwyer, Boris Hayete, Carolyn A. Lawrence, and James J. Collins. 2007. "A Common Mechanism of Cellular Death Induced by Bactericidal Antibiotics." *Cell* 130 (5): 797–810. <https://doi.org/10.1016/j.cell.2007.06.049>.
- Lin, Xiangmin, Liqun Kang, Hui Li, and Xuanxian Peng. 2014. "Fluctuation of Multiple Metabolic Pathways Is Required for *Escherichia Coli* in Response to Chlortetracycline Stress." *Molecular BioSystems* 10 (4): 901–8. <https://doi.org/10.1039/c3mb70522f>.
- Lin, Yuexu, Wanxin Li, Lina Sun, Zhenping Lin, Yuhang Jiang, Yueming Ling, and

- Xiangmin Lin. 2019. “Comparative Metabolomics Shows the Metabolic Profiles Fluctuate in Multi-Drug Resistant *Escherichia Coli* Strains.” *Journal of Proteomics* 207 (September). <https://doi.org/10.1016/j.jprot.2019.103468>.
- Lippens, G., E. Cahoreau, P. Millard, C. Charlier, J. Lopez, X. Hanouille, and J. C. Portais. 2018. “In-Cell NMR: From Metabolites to Macromolecules.” *Analyst*. Royal Society of Chemistry. <https://doi.org/10.1039/c7an01635b>.
- Liu, Qin, Ji'en Wu, Zhi Yang Lim, Arushi Aggarwal, Hongshun Yang, and Shifei Wang. 2017. “Evaluation of the Metabolic Response of *Escherichia Coli* to Electrolysed Water by ^1H NMR Spectroscopy.” *LWT* 79: 428–36. <https://doi.org/10.1016/j.lwt.2017.01.066>.
- Liu, Yuan, Kangni Yang, Haijie Zhang, Yuqian Jia, and Zhiqiang Wang. 2020. “Combating Antibiotic Tolerance Through Activating Bacterial Metabolism.” *Frontiers in Microbiology*. <https://doi.org/10.3389/fmicb.2020.577564>.
- Lobritz, Michael A., Peter Belenky, Caroline B.M. Porter, Arnaud Gutierrez, Jason H. Yang, Eric G. Schwarz, Daniel J. Dwyer, Ahmad S. Khalil, and James J. Collins. 2015. “Antibiotic Efficacy Is Linked to Bacterial Cellular Respiration.” *Proceedings of the National Academy of Sciences of the United States of America* 112 (27): 8173–80. <https://doi.org/10.1073/pnas.1509743112>.
- Lohmeier-Vogel, Elke M., Shiela Ung, and Raymond J. Turner. 2004. “In Vivo ^{31}P Nuclear Magnetic Resonance Investigation of Tellurite Toxicity in *Escherichia Coli*.” *Applied and Environmental Microbiology* 70 (12): 7342–47.

<https://doi.org/10.1128/AEM.70.12.7342-7347.2004>.

Luchinat, Enrico, and Lucia Banci. 2017. “In-Cell NMR: A Topical Review.” *IUCrJ*. International Union of Crystallography. <https://doi.org/10.1107/S2052252516020625>.

Luchinat, Enrico, Letizia Barbieri, Timothy F. Campbell, and Lucia Banci. 2020. “Real-Time Quantitative In-Cell NMR: Ligand Binding and Protein Oxidation Monitored in Human Cells Using Multivariate Curve Resolution.” *Analytical Chemistry* 92 (14): 9997–10006. <https://doi.org/10.1021/acs.analchem.0c01677>.

Luchinat, Enrico, Matteo Cremonini, and Lucia Banci. 2021. “Radio Signals from Live Cells: The Coming of Age of In-Cell Solution NMR.” *Chemical Reviews*. American Chemical Society. <https://doi.org/10.1021/acs.chemrev.1c00790>.

Majors, Paul D., Jeffrey S. McLean, and Johannes C.M. Scholten. 2008. “NMR Bioreactor Development for Live In-Situ Microbial Functional Analysis.” *Journal of Magnetic Resonance* 192 (1): 159–66. <https://doi.org/10.1016/j.jmr.2008.02.014>.

Makowski, Marcin, Mário R. Felício, Isabel C.M. Fensterseifer, Octávio L. Franco, Nuno C. Santos, and Sónia Gonçalves. 2020. “EcDBS1R4, an Antimicrobial Peptide Effective against *Escherichia Coli* with in Vitro Fusogenic Ability.” *International Journal of Molecular Sciences* 21 (23): 1–19. <https://doi.org/10.3390/ijms21239104>.

Maldonado, Andres Y., David S. Burz, and Alexander Shekhtman. 2011. “In-Cell NMR Spectroscopy.” *Progress in Nuclear Magnetic Resonance Spectroscopy*. Elsevier B.V. <https://doi.org/10.1016/j.pnmrs.2010.11.002>.

- Mlynárik, Vladimír. 2017. "Introduction to Nuclear Magnetic Resonance." *Analytical Biochemistry*. Academic Press Inc. <https://doi.org/10.1016/j.ab.2016.05.006>.
- Morais, Everton C., Helena T. Schroeder, Cristina S. Souza, Silvia R. Rodrigues, Maria Ines L. Rodrigues, Paulo Ivo Homem De Bittencourt, and João Henrique Z. Dos Santos. 2020. "Comparative Study on the Influence of the Content and Functionalization of Alginate Matrices on K-562 Cell Viability and Differentiation." *Journal of Materials Research* 35 (10): 1249–61. <https://doi.org/10.1557/jmr.2020.96>.
- Morrison, Lindsay, and Teresa R. Zembower. 2020. "Antimicrobial Resistance." *Gastrointestinal Endoscopy Clinics of North America*. W.B. Saunders. <https://doi.org/10.1016/j.giec.2020.06.004>.
- Mulder, Frans A.A., Leonardo Tenori, and Claudio Luchinat. 2019. "Fast and Quantitative NMR Metabolite Analysis Afforded by a Paramagnetic Co-Solute." *Angewandte Chemie - International Edition* 58 (43): 15283–86. <https://doi.org/10.1002/anie.201908006>.
- Nalbantoglu, Sinem. 2019. "Metabolomics: Basic Principles and Strategies." In *Molecular Medicine*. IntechOpen. <https://doi.org/10.5772/intechopen.88563>.
- Oh, Yeong Ji, and Jungil Hong. 2022. "Application of the MTT-Based Colorimetric Method for Evaluating Bacterial Growth Using Different Solvent Systems." *LWT* 153. <https://doi.org/10.1016/j.lwt.2021.112565>.
- Parigi, Giacomo, Enrico Ravera, and Claudio Luchinat. 2019. "Magnetic Susceptibility and

Paramagnetism-Based NMR.” *Progress in Nuclear Magnetic Resonance Spectroscopy*. Elsevier B.V. <https://doi.org/10.1016/j.pnmrs.2019.06.003>.

Penchovsky, Robert, and Martina Traykovska. 2015. “Designing Drugs That Overcome Antibacterial Resistance: Where Do We Stand and What Should We Do?” *Expert Opinion on Drug Discovery*. Informa Healthcare. <https://doi.org/10.1517/17460441.2015.1048219>.

Powers, Robert. 2014. “The Current State of Drug Discovery and a Potential Role for NMR Metabolomics.” *Journal of Medicinal Chemistry* 57 (14): 5860–70. <https://doi.org/10.1021/jm401803b>.

Projan, Steven J., and D. M. Shlaes. 2004. “Antibacterial Drug Discovery: Is It All Downhill from Here?” *Clinical Microbiology and Infection, Supplement* 10 (4): 18–22. <https://doi.org/10.1111/j.1465-0691.2004.1006.x>.

Serber, Z., and V. Dötsch. 2001. “In-Cell NMR Spectroscopy.” *Biochemistry* 40 (48): 14317–23. <https://doi.org/10.1021/bi011751w>.

Sharaf, Naima G., Christopher O. Barnes, Lisa M. Charlton, Gregory B. Young, and Gary J. Pielak. 2010. “A Bioreactor for In-Cell Protein NMR.” *Journal of Magnetic Resonance* 202 (2): 140–46. <https://doi.org/10.1016/j.jmr.2009.10.008>.

Shi, Li, and Naixia Zhang. 2021. “Applications of Solution Nmr in Drug Discovery.” *Molecules*. MDPI AG. <https://doi.org/10.3390/molecules26030576>.

Siegal, G., and Philipp Selenko. 2019. “Cells, Drugs and NMR.” *Journal of Magnetic*

Resonance 306 (September): 202–12. <https://doi.org/10.1016/j.jmr.2019.07.018>.

Smeraldo, Alessio, Paolo A. Netti, and Enza Torino. 2020. “New Strategies in the Design of Paramagnetic CAs.” *Contrast Media and Molecular Imaging*. Hindawi Limited. <https://doi.org/10.1155/2020/4327479>.

Softley, Charlotte A., Mark J. Bostock, Grzegorz M. Popowicz, and Michael Sattler. 2020. “Paramagnetic NMR in Drug Discovery.” *Journal of Biomolecular NMR* 74 (6–7): 287–309. <https://doi.org/10.1007/s10858-020-00322-0>.

Stokes, Jonathan M., Allison J. Lopatkin, Michael A. Lobritz, and James J. Collins. 2019. “Bacterial Metabolism and Antibiotic Efficacy.” *Cell Metabolism*. Cell Press. <https://doi.org/10.1016/j.cmet.2019.06.009>.

Sugiki, Toshihiko, Kyoko Furuita, Toshimichi Fujiwara, and Chojiro Kojima. 2018. “Current NMR Techniques for Structure-Based Drug Discovery.” *Molecules*. MDPI AG. <https://doi.org/10.3390/molecules23010148>.

Uludag, Hasan, and Michael V Sefton. 1990. “Calorimetric Assay for Cellular Activity in Microcapsules Cell Culture” 11: 708–12.

Wang, Roy Chih Chung, David A. Campbell, James R. Green, and Miroslava Čuperlović-Culf. 2021. “Automatic 1D ^1H NMR Metabolite Quantification for Bioreactor Monitoring.” *Metabolites*. MDPI AG. <https://doi.org/10.3390/metabo11030157>.

Weljie, Aalim M., Jack Newton, Pascal Mercier, Erin Carlson, and Carolyn M. Slupsky. 2006. “Targeted Profiling: Quantitative Analysis Of ^1H NMR Metabolomics Data.”

Analytical Chemistry 78 (13): 4430–42. <https://doi.org/10.1021/ac060209g>.

White, Lisa J., Jessica E. Boles, Melanie Clifford, Bethany L. Patenall, Kira H.L.F. Hilton, Kendrick K.L. Ng, Rebecca J. Ellaby, Charlotte K. Hind, Daniel P. Mulvihill, and Jennifer R. Hiscock. 2021. “Di-Anionic Self-Associating Supramolecular Amphiphiles (SSAs) as Antimicrobial Agents against *MRSA* and *Escherichia Coli*.” *Chemical Communications* 57 (89): 11839–42. <https://doi.org/10.1039/d1cc05455d>.

Zampieri, Mattia, Balazs Szappanos, Maria Virginia Buchieri, Andrej Trauner, Ilaria Piazza, Paola Picotti, Sébastien Gagneux, et al. 2018. “High-Throughput Metabolomic Analysis Predicts Mode of Action of Uncharacterized Antimicrobial Compounds.” *Science Translational Medicine* 10 (429): 1–13. <https://doi.org/10.1126/scitranslmed.aal3973>.

Zampieri, Mattia, Michael Zimmermann, Manfred Claassen, and Uwe Sauer. 2017. “Nontargeted Metabolomics Reveals the Multilevel Response to Antibiotic Perturbations.” *Cell Reports* 19 (6): 1214–28. <https://doi.org/10.1016/j.celrep.2017.04.002>.

14. Appendices

Appendix1. List of spectra of SSA agents in NMR conventional employing CPMG pulse sequence.

SSA29 400 μ M

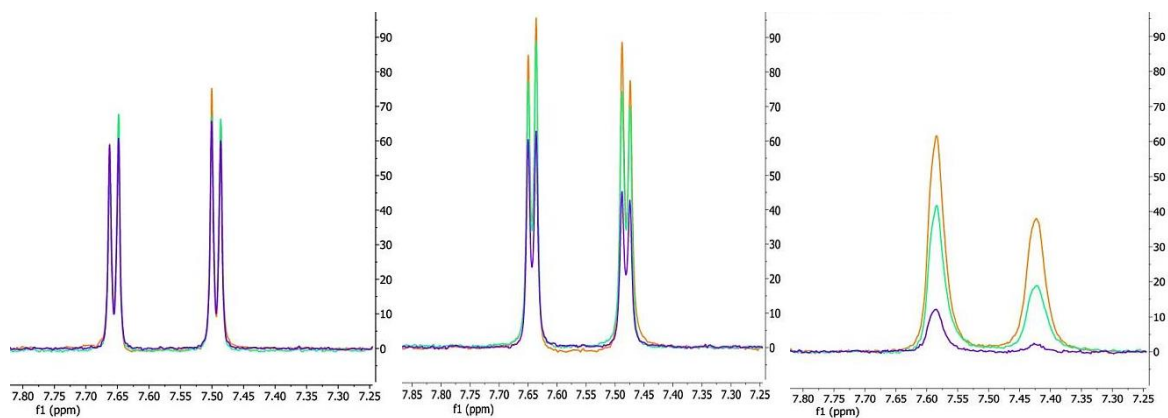


Figure 25. Increasing concentrations of manganese from left to right (0 mM, 0.5 mM, and 4 mM) at different CPMG spin-lock times: 20 ms (orange), 50 ms (green) and 150 ms (purple).

SSA29 200 μ M + lipid vesicles

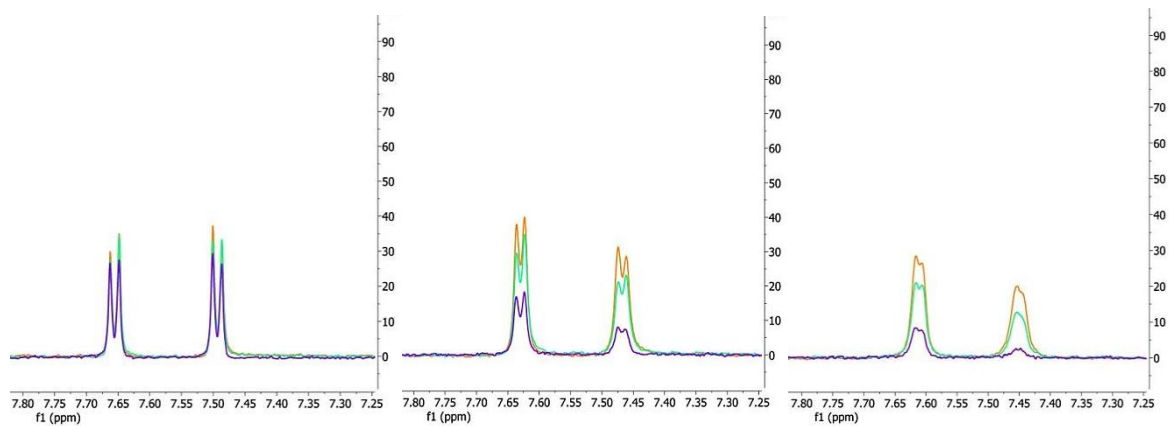


Figure 26. Increasing concentrations of manganese from left to right (0 mM, 0.5 mM, and 2 mM) at different CPMG spin-lock times: 20 ms (orange), 50 ms (green) and 150 ms (purple).

SSA30 400 μ M

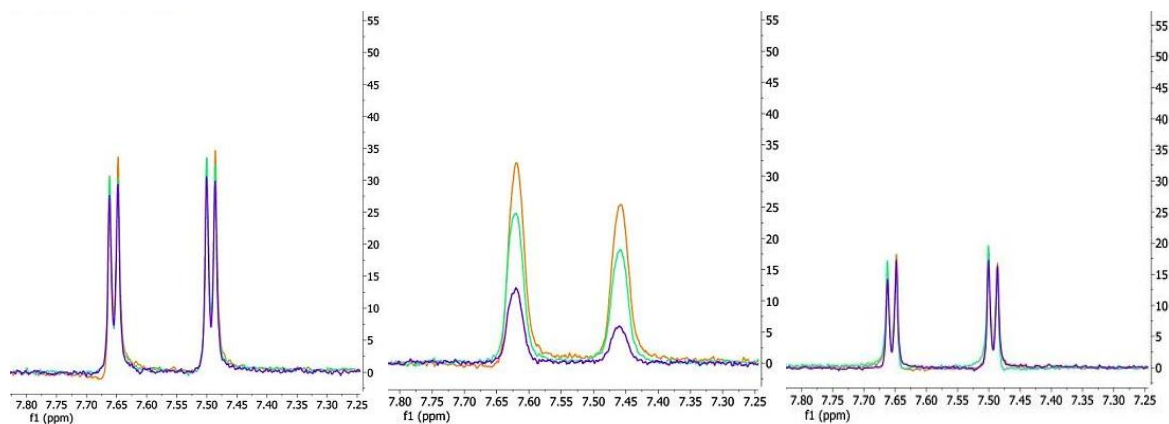


Figure 27. Increasing concentrations of manganese from left to right (0 mM, 0.5 mM, and 4 mM) at different CPMG spin-lock times: 20 ms (orange), 50 ms (green) and 150 ms (purple).

SSA30 200 μ M + lipid vesicles

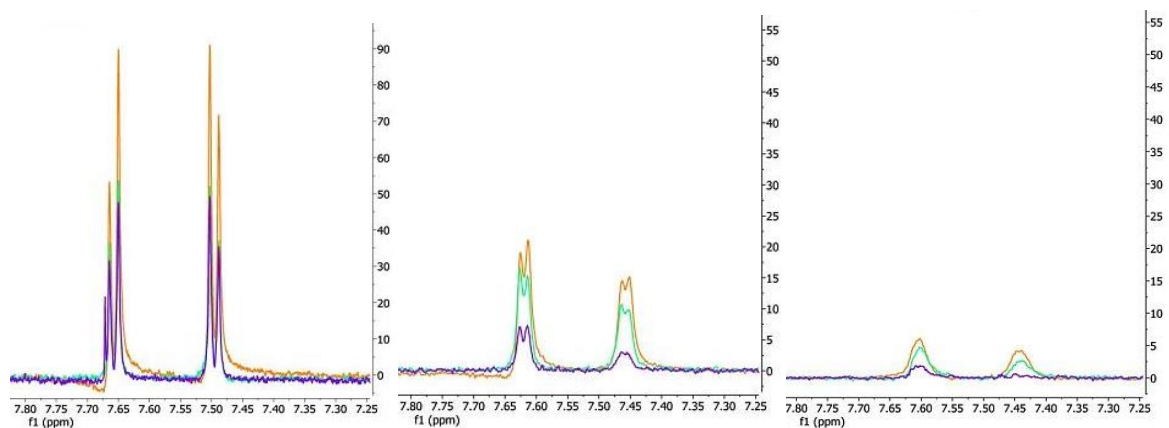


Figure 28. Increasing concentrations of manganese from left to right (0 mM, 0.5 mM, and 2 mM) at different CPMG spin-lock times: 20 ms (orange), 50 ms (green) and 150 ms (purple).

SSA32 400 μ M

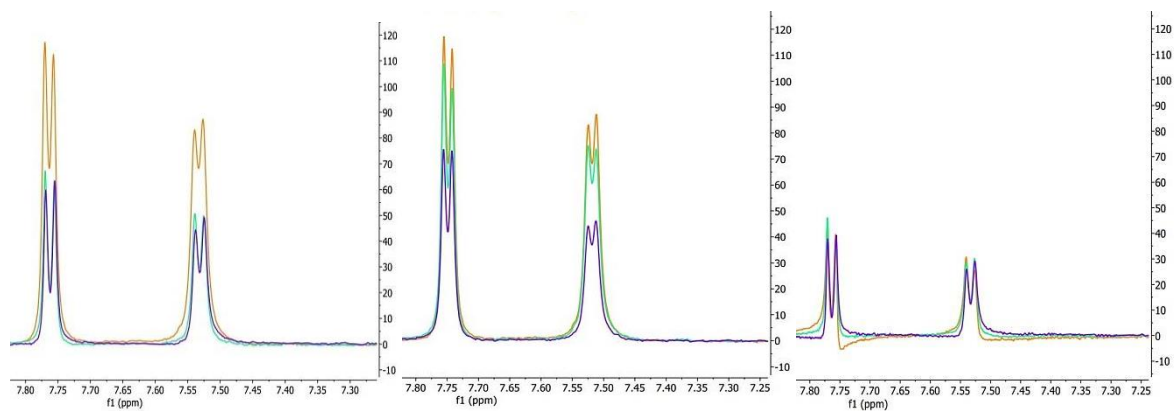


Figure 29. Increasing concentrations of manganese from left to right (0 mM, 0.5 mM, and 4 mM) at different CPMG spin-lock times: 20 ms (orange), 50 ms (green) and 150 ms (purple).

SSA32 200 μ M + lipid vesicles

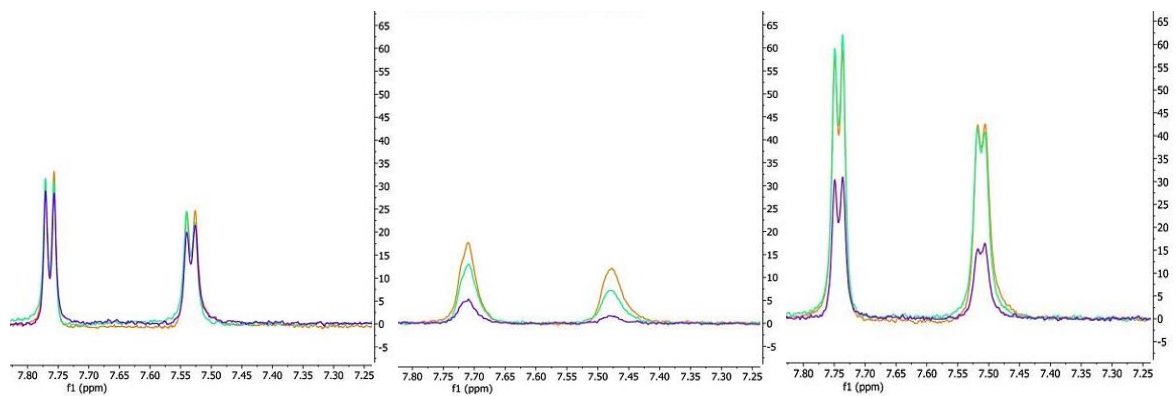


Figure 30. Increasing concentrations of manganese from left to right (0 mM, 0.5 mM, and 2 mM) at different CPMG spin-lock times: 20 ms (orange), 50 ms (green) and 150 ms (purple).

SSA48 400 μ M

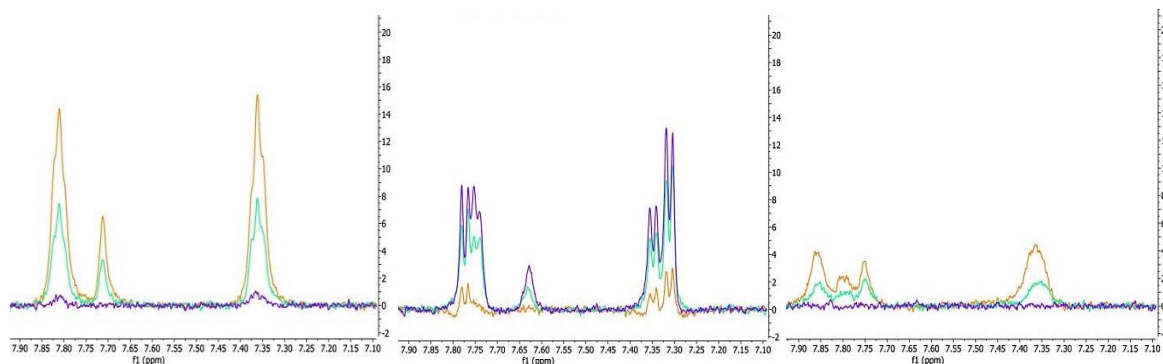


Figure 31. Increasing concentrations of manganese from left to right (0 mM, 0.5 mM, and 4 mM) at different CPMG spin-lock times: 20 ms (orange), 50 ms (green) and 150 ms (purple).

SSA48 200 μ M + lipid vesicles

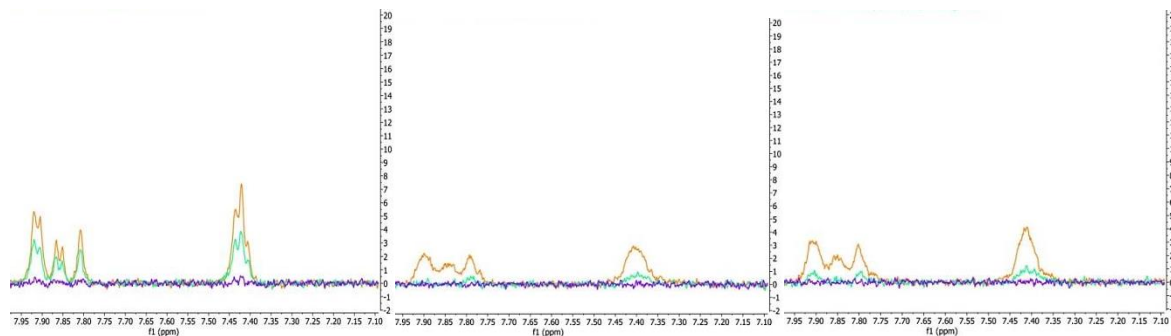


Figure 32. Increasing concentrations of manganese from left to right (0 mM, 0.5 mM, and 2 mM) at different CPMG spin-lock times: 20 ms (orange), 50 ms (green) and 150 ms (purple).

SSA57 400 μ M

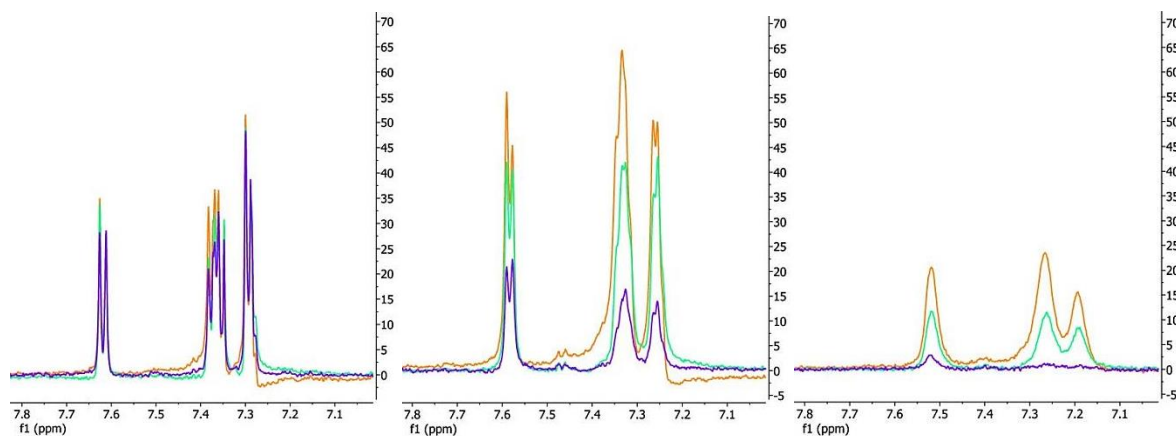


Figure 33. Increasing concentrations of manganese from left to right (0 mM, 0.5 mM, and 4 mM) at different CPMG spin-lock times: 20 ms (orange), 50 ms (green) and 150 ms (purple).

SSA57 200 μ M + lipid vesicles

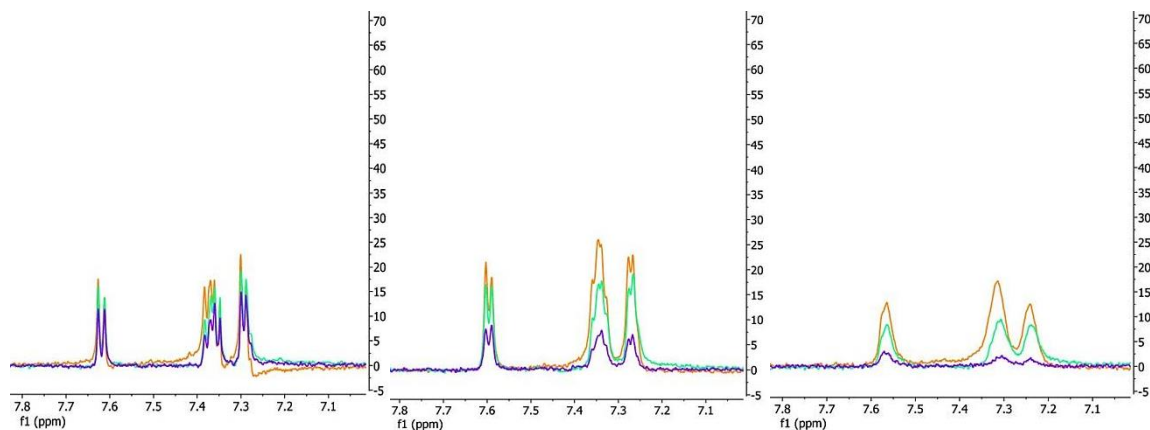


Figure 34. Increasing concentrations of manganese from left to right (0 mM, 0.5 mM, and 2 mM) at different CPMG spin-lock times: 20 ms (orange), 50 ms (green) and 150 ms (purple).

SSA60 400 μ M

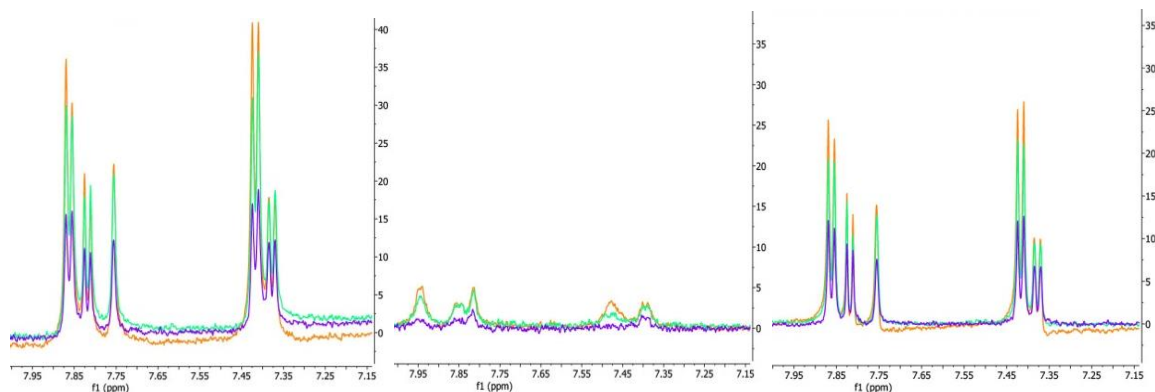


Figure 35. Increasing concentrations of manganese from left to right (0 mM, 0.5 mM, and 4 mM) at different CPMG spin-lock times: 20 ms (orange), 50 ms (green) and 150 ms (purple).

SSA60 200 μ M + lipid vesicles

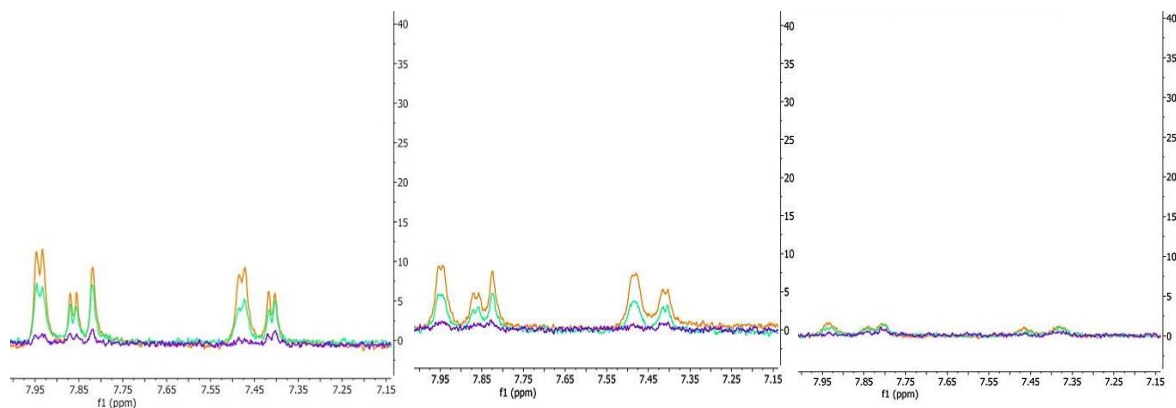


Figure 36. Increasing concentrations of manganese from left to right (0 mM, 0.5 mM, and 2 mM) at different CPMG spin-lock times: 20 ms (orange), 50 ms (green) and 150 ms (purple).

Appendix2. Quantification of lipid composition of membrane vesicles from *E. coli*.

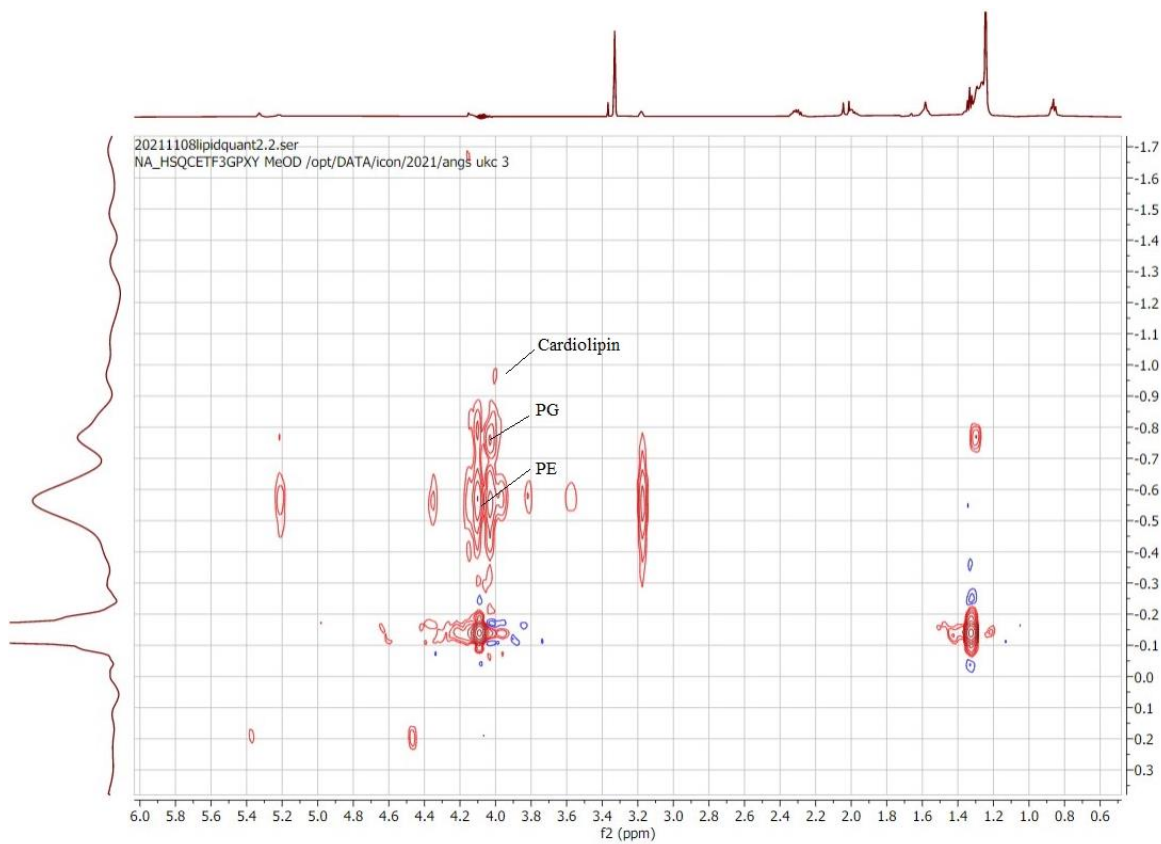


Figure 37. ^1H - ^{31}P HSQC spectrum for quantification of lipid composition of membrane vesicles prepared from *E. coli*. Integration of the lipid peaks gave rise to a PE:PG ratio of 3:1.

Appendix3. Metabolomics analysis in control sample and sample including SSA60 at concentrations of 0.2 mM and 0.5 mM in in-cell NMR experiments.

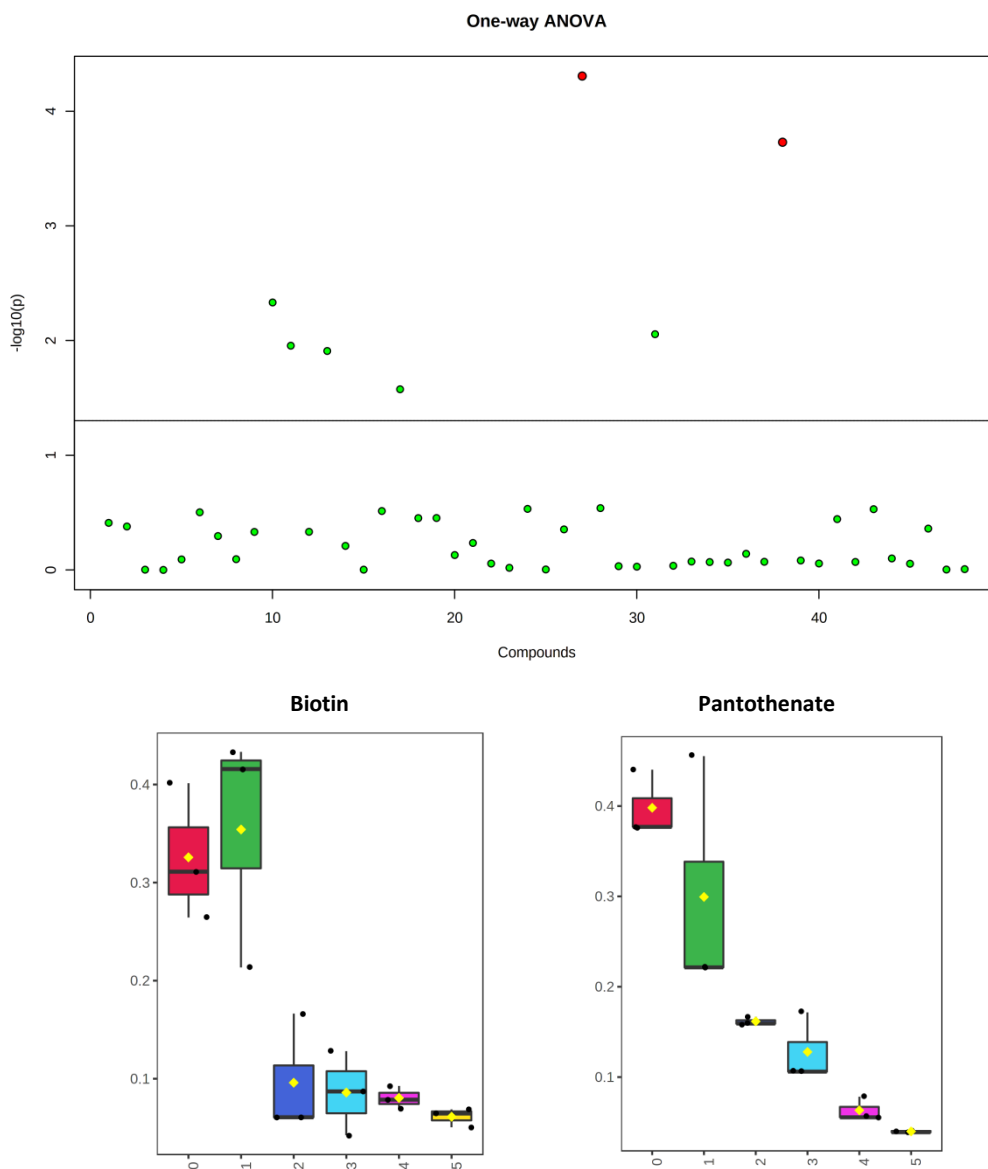


Figure 38. At the top a diagram of one-way ANOVA analysis of control sample with a significant change of 2. At the bottom the two up-regulated significant metabolites: biotin and panthothenate.

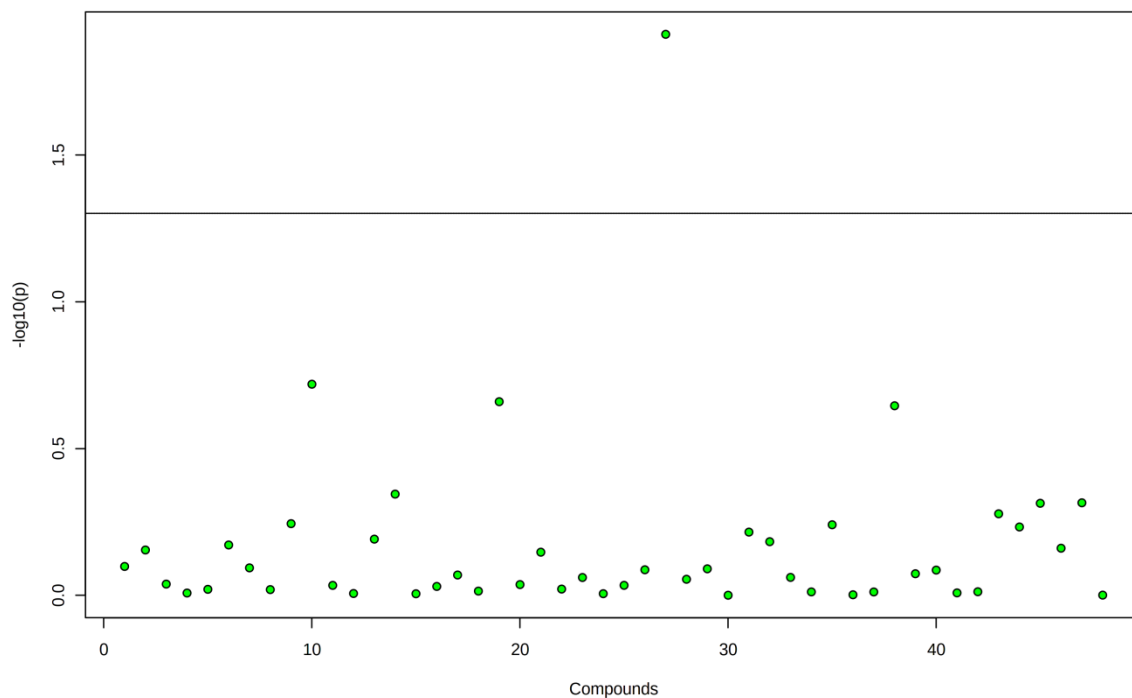


Figure 39. Diagram of one-way ANOVA analysis of sample containing SSA60 0.2 mM with a significant change of 2.

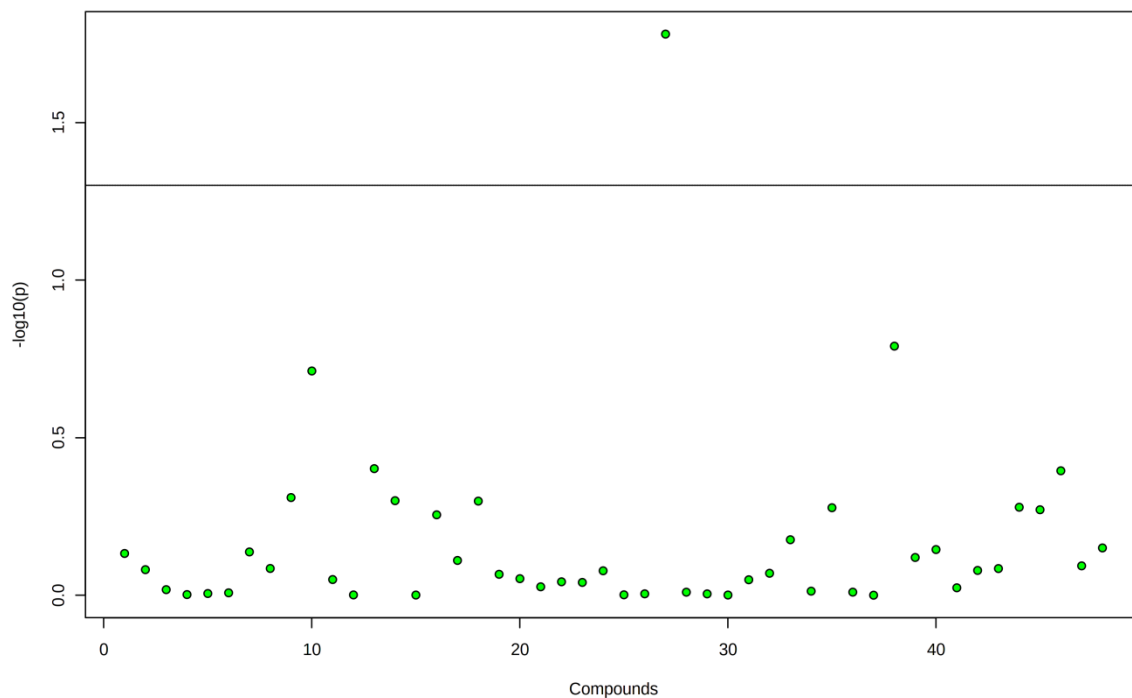


Figure 40. Diagram of one-way ANOVA analysis of sample containing SSA60 0.5 mM with a significant change of 2.

Metabolite	Fold change (log2)
Arginine	2.4155
Pantothenate	2.1303
Lysine	1.9592
Leucine	1.8306
Alanine	1.4328
Biotin	1.2674
Acetone	1.0327
2-phosphoglycerate	1.01

Table 9. Fold change values log transformed for metabolites of cells treated with SSA60 0.2 mM.

Metabolite	Fold change (log2)
Arginine	2.2447
Leucine	1.7104
Lysine	1.5843
Pantothenate	1.3851
Acetone	1.3468
Alanine	1.2764
Biotin	1.1675
2-phosphoglycerate	1.1375

Table 10. Fold change values log transformed for metabolites of cells treated with SSA60 0.5 mM.